**Lakehead University**

# Hydraulic and Dynamic Assessment of Triangular Labyrinth Weirs and Weir-Pool type Fishways

by

**Shahram Dizabadi**

A thesis submitted to the

Faculty of Engineering

In partial fulfillment of the requirements for degree of

Master of Science

In

Environmental Engineering

Department of Civil Engineering

Thunder Bay, Ontario, Canada

April 2019

# Table of Contents

## List of Figures

**Abstract**

The hydraulic performance of traditional labyrinth weirs has been extensively studied in the literature. The research outcomes indicated that labyrinth weirs have many hydraulic advantages to pass more flow with a constant water head which reduces the construction cost and improve flood prevention. In this study, a series of laboratory experiments was conducted to test a new weir design based on a classical triangular labyrinth weir. A square pool was added to the vertex of a triangular labyrinth weir in two different directions to form two new designs named as labyrinth weirs with upstream and downstream pools. Detailed velocity and turbulence measurements were conducted using an Acoustic Doppler Velocimetry (ADV) probe to investigate the flow dynamics and turbulence characteristics of the new design in both free and submerged flow conditions. The ability of using a series of the newly design weirs as a fish passage was tested by constructing a series of weirs with different weir spacing. The upstream flow velocities in three directions and the mean and the turbulent kinetic energies (TKE) were measured with the ADV probe. The mean velocity and the turbulent kinetic energy distribution indicated that the maximum range occurred in the corner of the main sidewall of the weir and the pool's sidewalls. The maximum longitudinal and vertical velocities and TKE for the weir with the upstream pool occurred inside the pool, whereas the maximum lateral velocity located in the vicinity of the main sidewall of the weir. In addition, the lateral velocity in the labyrinth weir with the upstream pool changed to the elevation equal to 70% of the upstream water level.

Furthermore, experimental results on the weir-pool fishway with labyrinth sharp crested weir with downstream pool and upstream pool induced hydraulic and flow field and its relation to fish behavior are presented. A wooden ramp with 3% slope was built along a 12 *m* x 0.61 *m* x 0.5 *m* laboratory flume and the Acoustic Doppler Velocity measurements were taken in a grid with 659

points for low, medium, and high flow discharges. The flow characterized applying spatial and point analysis techniques. Point analysis indicated that the weir to weir distance in the fishway with 0.75 *m* and 1 *m* distance was small enough to disrupt turbulent coherent structures. The areas which sweep and ejection events were not observed evidencing an appropriate resting place for fish during their migration. The flow field indicated a high spatial variability controlled by the geometry of the weir arrangement that might allow a variety of fish to develop their preferred paths characterized by flow properties with different magnitudes depending on the particular species. The obtained results were compared well with similar outcomes reported for other standard fishways. It was found that the newly designed fishway has higher performance in comparison with other fishway structures.

# Chapter 1

## 1.1. Introduction

A need for constructing hydraulic structures is inevitable in order to enhance, preserve, and effectively employ the water resources and manage the most efficient use of water. Weirs are one of the most common and functional hydraulic structures which are employed as the flow control structures in order to control and regulate upstream water depths as well as flow discharge measurements (Sitompul, 1993 and Ackers et al. 1978). Increasing the discharge capacity by increasing the crest length in a limited width of a channel is another advantage of labyrinth weirs. Increasing hydraulic capacity of weirs can prevent reservoir over flow (Paxson et al. 2011). Weirs are generally categorized into sharp-crested weirs and weirs of finite crest length (Ackers et al., 1978). Weirs of finite crest length have been further subdivided into, long-crested, broad-crested and narrow-crested weirs (Azimi and Rajaratnam, 2009). Weirs also, can be categorized to different types related to the shape of the opening. The most common types of weirs are rectangular, triangular, trapezoidal, labyrinth, and circular weirs (Tingey, 2011).

In lakes, rivers, and streams fish migrations requires completing a cycle of upstream and downstream movements. This chain is related to the fish's life stage, its location, and the type of migration. Generally, downstream migration is a feature of early life stages, while upstream migration is a feature of adult life (Chris Katopodis, 1992). Fish migrate to spawn, to feed, and to seek refuge from predators or harmful environmental conditions, such as the complete freeze-up of a stream or lake. Presence of a natural (e.g. a waterfall) or man-made (e.g. a dam, weir, or culvert) obstruction blocks the stream, slows or even stopes the fish migration. A fishway is a waterway designed to create the passage of a species or a number of different species of fish pass a particular obstruction (Chris Katopodis, 1992). In most cases fishways are built for adult

spawners, whereas, in some cases migrating juveniles are the target species (Chris Katopodis, 1992). For adult fish spawning migrations are usually intricate and delays are critical to reproductive success. For juveniles feeding migrations are usually intricate too but delays are not as critical. Fishway over damns and weirs or through hanging culverts is a key consideration in fish bearing stream (Chris Katopodis, 1992). Fishways allow fish to maintain migrations past new hydraulic structures, re-establish migrations after years of blockage at man-made barriers and extend migrations upstream of natural barriers.

### 1.2. General Terms Related to the Weirs

**1.2.1 Crest:** The top edge of the weir is called the crest and its shape has a crucial influence on the capacity of weirs and their performance. As it is depicted in Figure 1-1, weirs has been categorized based on their crest shape to sharp crested, half-round, quarter-round, and flat round weir (Falvey, 2003).

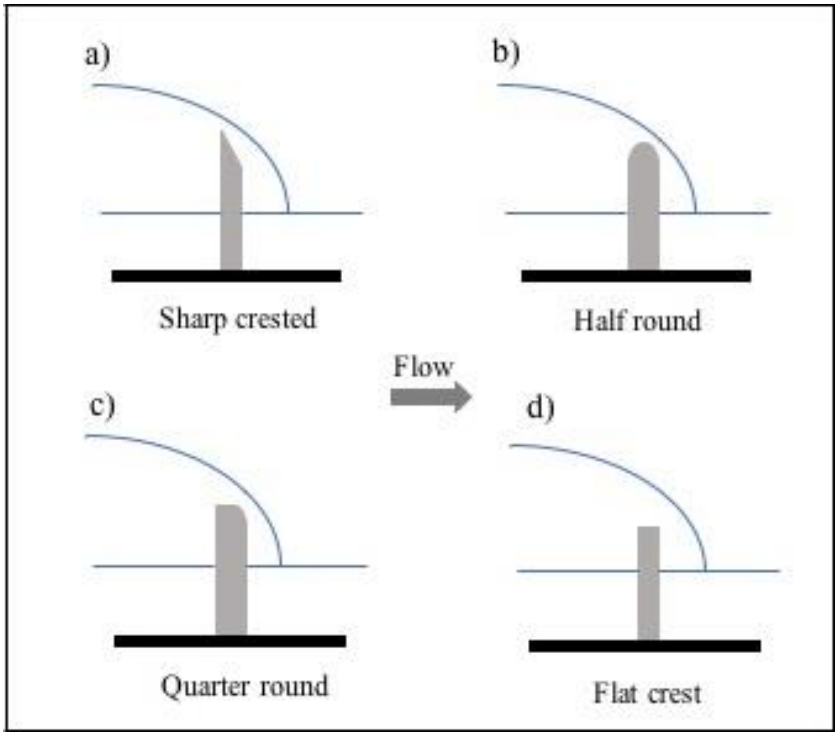


**Figure 1-1:** Side view sketch of (a) Sharp- crested weir; (b) Half-round weir; (c) Quarter-round weir; (d) Flat crest weir.

**1.2.2 Weir Height (*P*):** The weir height, *P*, is the difference between the crest elevation and the elevation of the upstream bed.

**1.2.3 Head Water ($h_o$):** The height of water over the crest is called water head $h_o$.

**1.2.4 Nappe:** Overflowing sheet of water over the weir is called nappe. Nappe is classified into aerated, non-aerated, and drowned nappe (Figure 1-2). In a non-aerated nappe condition, water clings to the downstream side of the weir plate and no air gets behind the nappe. In an aerated nappe condition, air cavity is developed between the weir wall and free-falling water and water separate from the downstream face of the weir plate. Drowned nappe happens when air hole is saturated with flow and nappe is thick (Tingey, 2011).

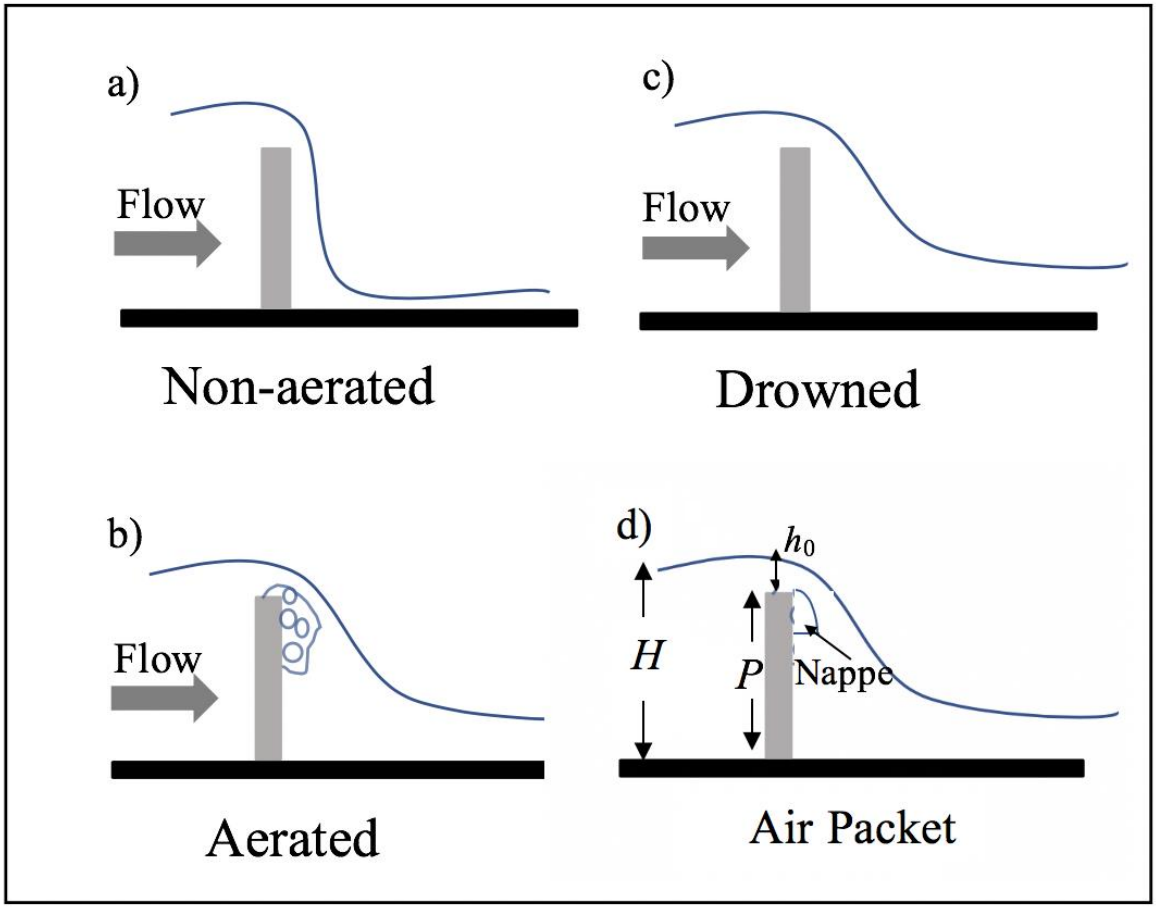


**Figure 1-2:** Different nappe condition (a) Non-aerated; (b) Aerated; and (c) Drowned.

**1.2.5 Total Head (*H*):** Total energy available in a flow that define as sum of pressure head, potential head, and velocity head.

$$H = \frac{P}{\rho g} + \frac{V^2}{2g} + z \tag{1-1}$$

where, $P/\rho g$ is the pressure head, $V^2/2g$ is the kenetic head, and $z$ is the potential head. Eq. (1-1) can be simplify in Eq. (1-2) based on the assumption that the datum line locates on the weir's crest.

$$H = h_0 + \frac{V^2}{2g} \tag{1-2}$$

**1.2.6 Free Flow:** Free flow happens when the discharge of the weir is not limited by the downstream conditions. In free flow condition, the lowest point of the weir is higher than water level at the downstream. In the other word, whenever the upstream level does not change by increasing the discharge, the flow is called free.

**1.2.7 Submerge Flow:** Submerged flow occurs when the downstream water level is more than the height of the weir. In submerged flow condition, the downstream level start affecting the upstream level and it changes the flow regime. In this condition, the downstream standing water push back the overflow resulting in flow reduction over the weir relative to the free flow condition (Ackers et al., 1978 and Villemonte, 1947).

## 1.3 Types of Sharp-Crested Weirs

### 1.3.1 Linear weir

Weirs can be classified in many different geometrical configurations; the most basic of these weirs are the linear weirs, a sketch of a linear weir is shown in Fig 1-3a. Linear weir is an obstacle directed perpendicular to the direction of the flow and the length of the weir, $L$, is equal to the width of the channel, $B$.

### 1.3.2 Oblique weir

Oblique weir is a linear weir but installed at an angle smaller than 90$^{o}$ to the channel centerline to obtain an additional crest length for a given channel width (Figure 1-3b).

### 1.3.3 Labyrinth weir

Labyrinth weir is an effective hydraulic structure and an essential device for increasing the capacity of weir when the channel width is limited. Labyrinth weir is fabricated as a series of cycles having trapezoidal, rectangular, triangular or circular shapes to obtain additional crest length, thus causing an increase in flow discharge capacity and also results in decreae of the free board requirement in the upstream reservoir compared to linear weirs with the same channel width (Sitompul, 1993). This advantage of labyrinth wires allows for reducing the upstream water head in comparison to the use of linear weirs. Figure 1-3c shows different types of labyrinth weirs. Labyrinth weirs with triangular and trapezoidal cycle shape have been reported by Sitompul, (1993) to be more effective than labyrinth weir with rectangular cycle shape on the basis of discharge capacity.

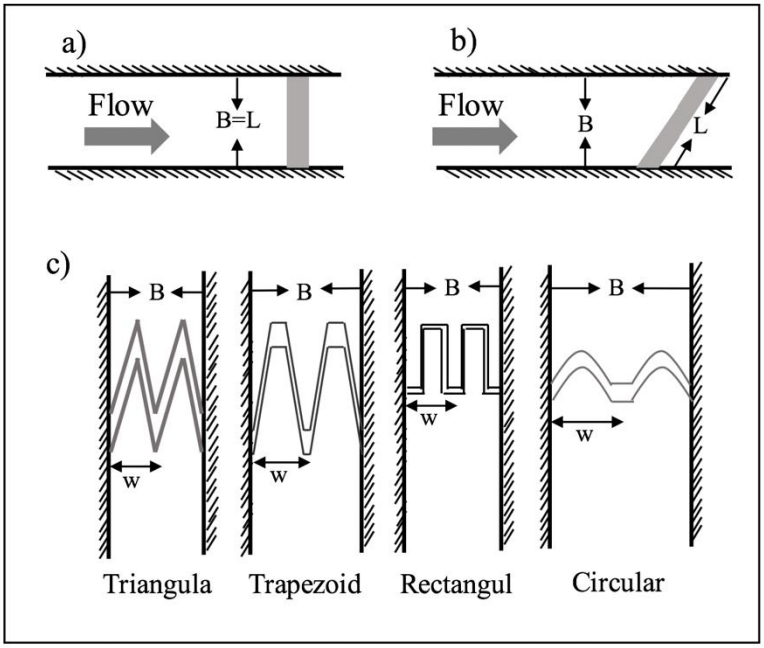


**Figure 1-3:** Plan view of (a) Linear weir; (b) Oblique weir; and (c) Labyrinth weir.

## 1.4 Types of Fishways

### 1.4.1 Vertical slot fishways

In the vertical slot fishway, baffles are placed at regular intervals along the length to create a series of pools (Figure 1-4). Fish easily retain their location within each pool. However, travel between pools need a burst effort through each slot. Water velocities are mostly constant at the slots from top to bottom. The main advantage of the vertical slot fishway is in its ability to cover large variations in water levels. Usually the difference between water levels in successive pools is 300 mm for adult salmon and 200 mm for adult freshwater fish (Chris Katopodis, 1992). In this kind of fishway usually the slope is 10%.

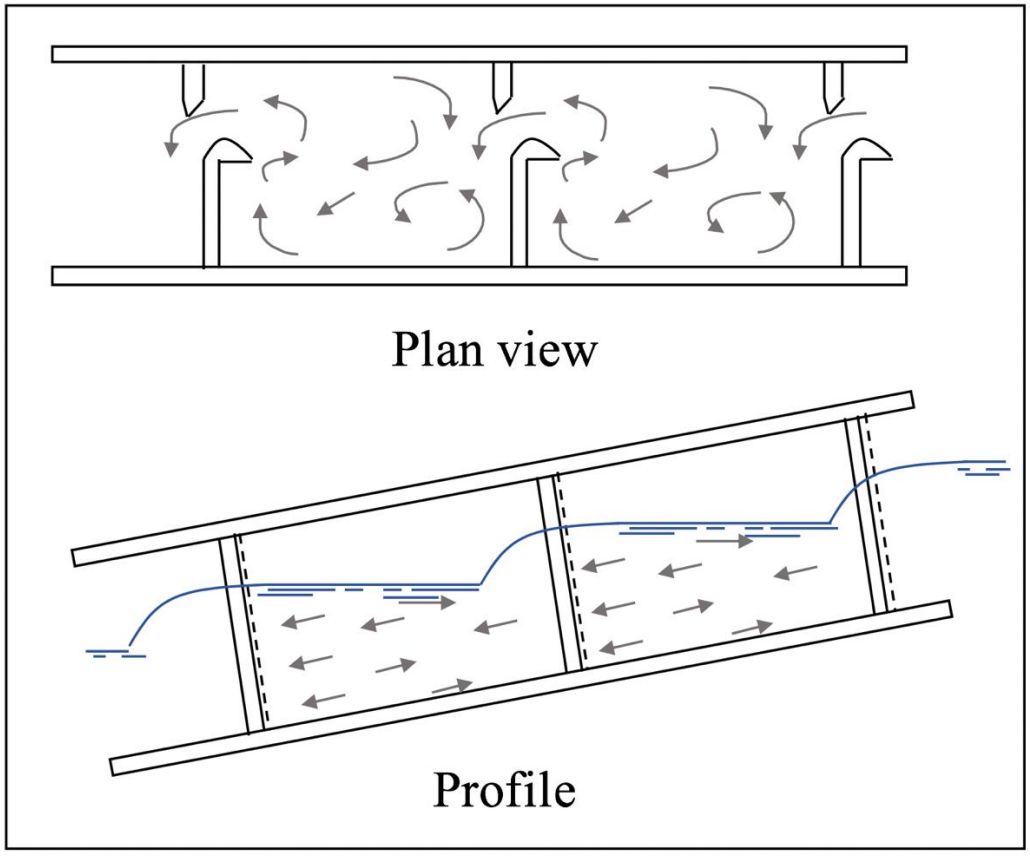


**Figure 1-4:** Vertical slot fishway; (a) plan view; and (b) profile view.

### 1.4.2 Denil fishway

It has been named after its inventor and the Denil fishway has been made up of a rectangular chute with closely spaced baffles or vanes placed along the sides and bottom. The Denil fishway have been expanded over the years and employed for fish passage (Chris Katopodis, 1992). One of the more common Denil fishway type employed today is shown in Figure 1-5. The plain Denil fishway includes a series of planar baffles pointing upstream, at an angle of 45 degrees with the fishway bed. Baffles in the steep pass Denil also aim to the upstream direction but are angled away from the walls of the chute. Flow through Denil fishways is highly turbulent, with large momentum exchange and high energy dissipation. In the plain Denil, the water in the chute flows at a relatively low velocity near the bed with a faster velocity near the top.

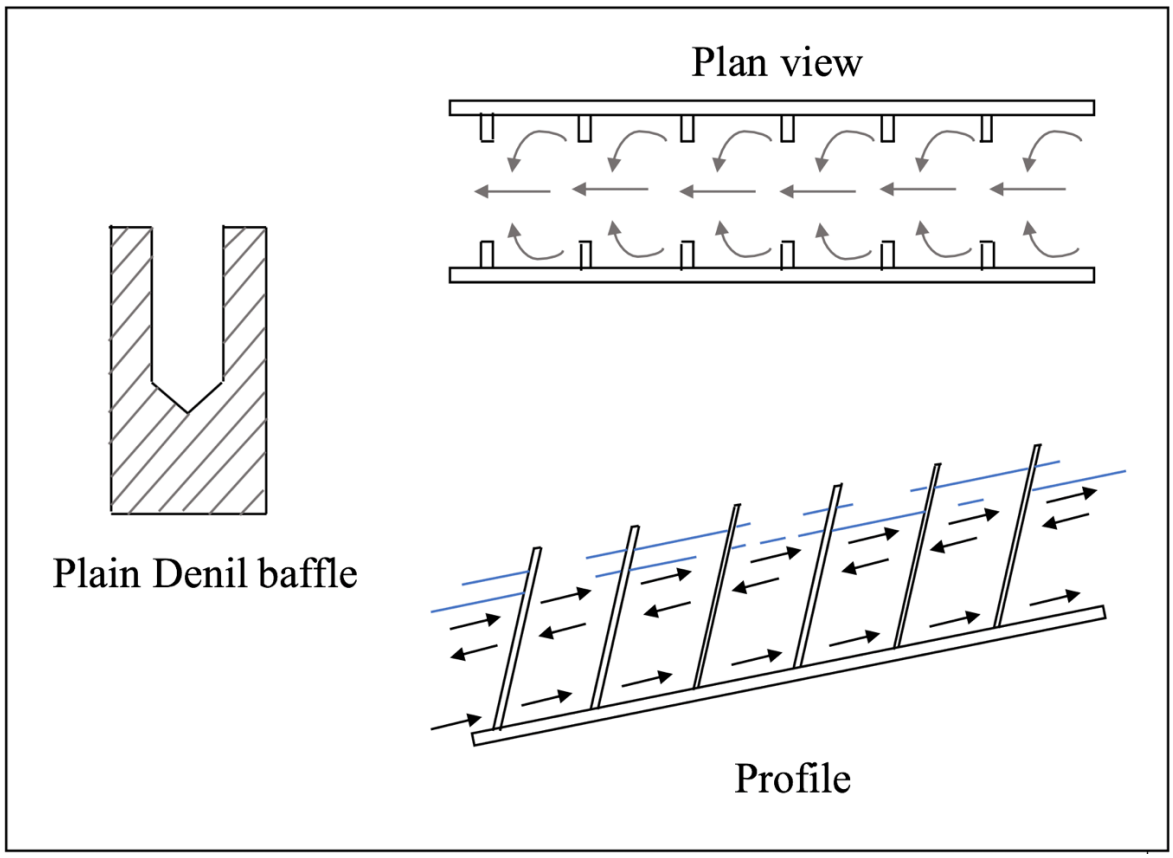


**Figure 1-5:** Plan and side views of the Denil fishway.

In the steep pass and at low depths, velocities tend to be higher near the bed of the fishway and reduce towards the water surface.

In deep water, flow divides into an upper and a lower layer, and velocity profiles become approximately symmetrical with the maximum velocities located at the mid-depth (Chris Katopodis, 1992). The flow with high velocity in the Denil designs decreases the sediment deposition through the fishway, also, prepare the well attraction helping fish to find the fishway. In the chute, the resting pools are located every 10 m to 15 m for adult salmon and 5 m to 10 m for adult freshwater species along the fishway as fish needs to swim constantly while they are in the chute. The slopes for Denil fishways are usually ranging from 10% to 15% for adult freshwater fish and 15% to 25% for adult salmon (Chris Katopodis, 1992).

### 1.4.3 Weir fishway

The weir fishway is made up of a different number of pools located in a stepped pattern separated by weirs (Figure 1-6). The fish attracted by the flowing water, move from pool to pool by either jumping or swimming, depending on the water depth, until they pass the fishway. Swimming or jumping between pools usually requires burst speeds (Chris Katopodis, 1992). An orifice may also be located to the submerged portion of the weir allowing the fish to swim through the orifice instead of jumping over the weir. This kind of fishways are simple to construct, whereas, the pool and weir fishways are sensitive to the water fluctuations. The water level drop between the pools is usually set at 300 mm for adult salmon and 200 mm for adult freshwater fish. The weir fishways usually performs well for a slope of 10% or less (Chris Katopodis, 1992).

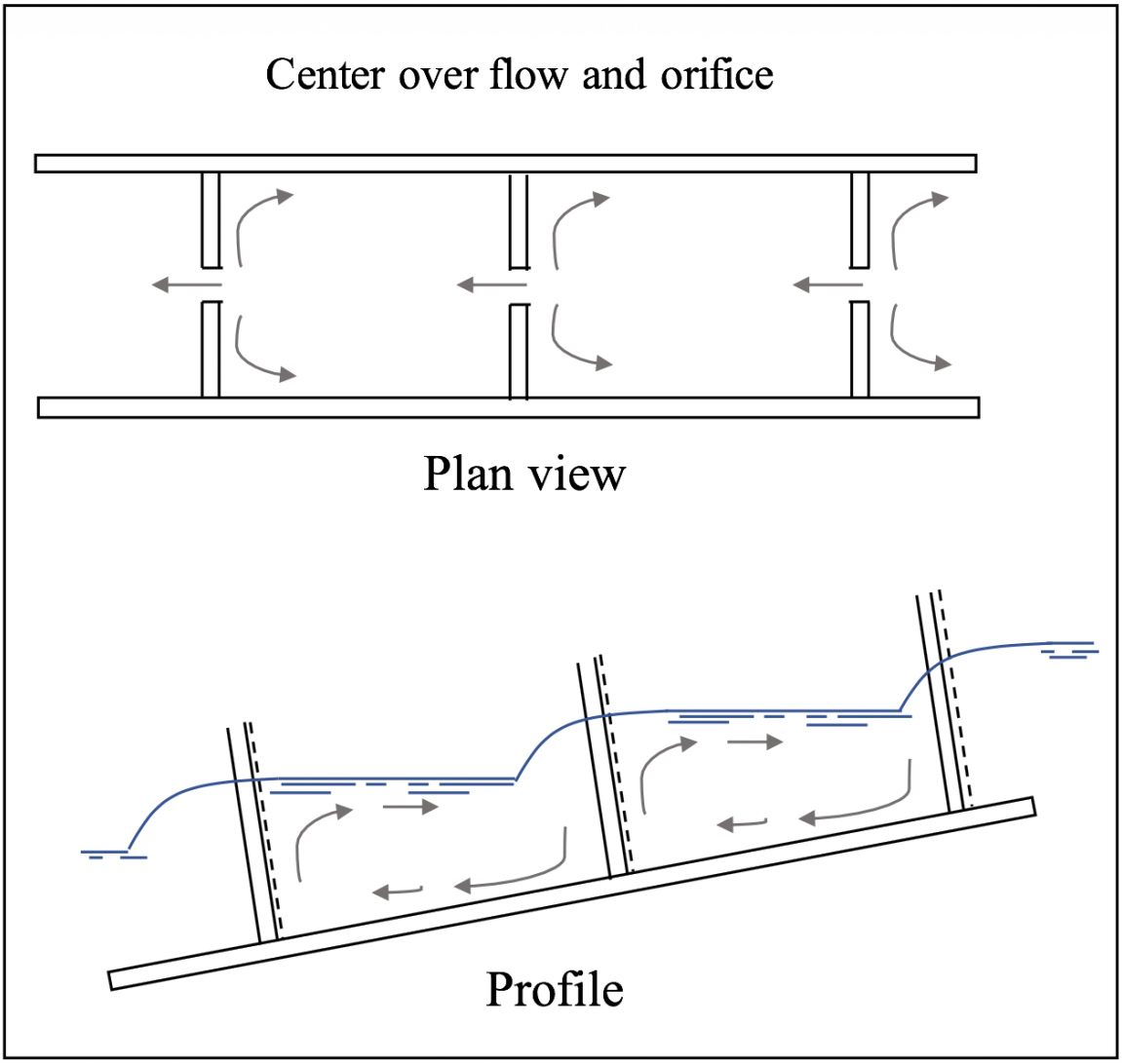


**Figure 1-6:** Weir fishway; (a) plan view; and (b) profile view

### 1.4.4 Culvert fishway

Culverts are used to transport water from one side of a roadway embankment to the other side. Culverts are built with circular, elliptic, pipe-arch, rectangular, and square cross-sections. Special considerations are needed to use culverts as fishway structures. For example, the culvert dimensions should be large enough to ensure that fish can enter, pass through, and exit the culvert without undue or harmful delay.

In many cases culverts are placed below the stream bed and special devices such as riprap, baffles, weirs, blocks or plates are used to form a culvert fishway (Figure 1-7) (Chris Katopodis, 1992). Mainly associated with roadway construction, culvert fishways usually have longitudinal slopes of between 0.5% and 5% (Chris Katopodis, 1992).

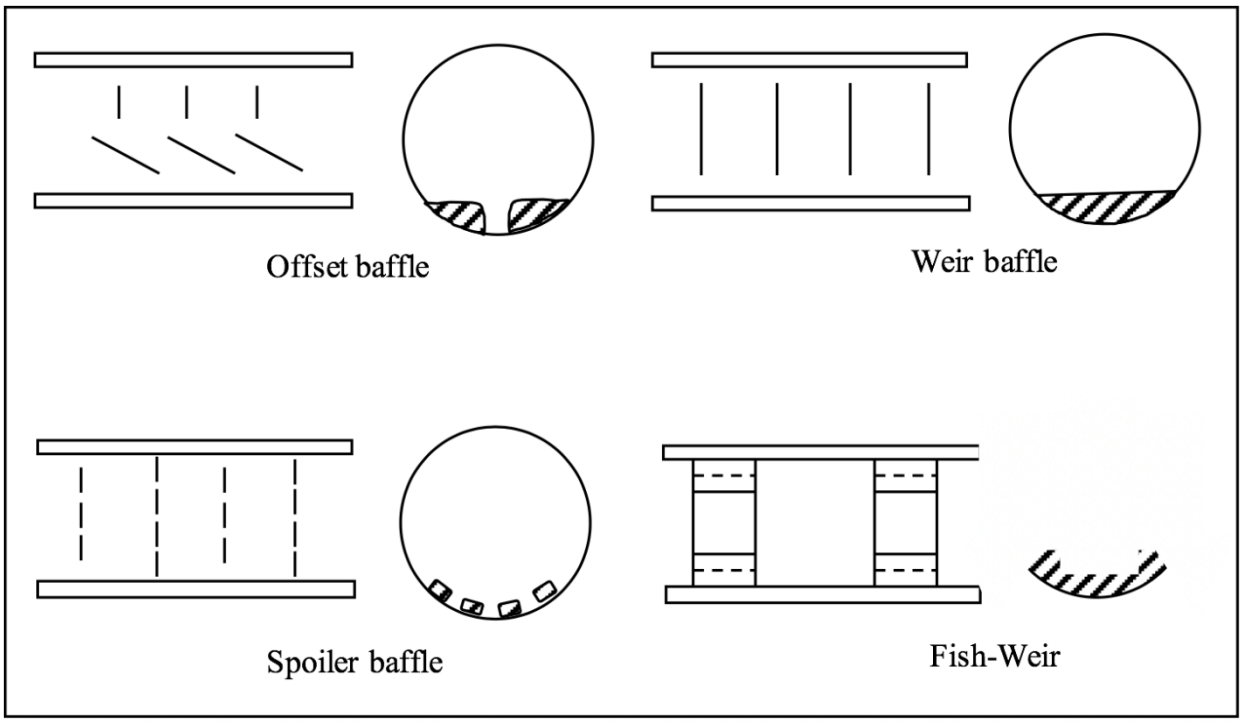


**Figure 1-7:** Culvert fishway; (a) offset baffle; (b) weir baffle; (c) spoiler baffle; and (d) fish-weir

### 1.5 Weir Flow

Flow over the weirs is either "plunging" or "streaming", depending on the depth of flow for a given slope, $S_0$, and pool length. In the plunging mode water head, $h$, above each the weir produces a water jet that is dissipating energy by turbulent mixing and diffusion mechanisms (Chris Katopodis, 1992). The water level below each weir is generally lower than the weir crest and the weir resembles the classical free-flow condition. Limited experimental results indicate that the discharge rating curve is similar to the one for sharp-crested weirs (Chris Katopodis, 1992). In the

streaming mode, a surface jet with approximately uniform depth, *d*, flows over recirculating water in the pools. The turbulent shear stress between the surface jet and the recirculating mass in the pool dominates while side wall shear stress may be neglected. The dimensionless discharge for the plunging ($Q_+$) and streaming ($Q^*$) modes are given in Figure 1-8 where *b* is the width of the weir. Maximum velocity in the plunging mode occurs near the top of the weir and decreases to about half at the water surface (Chris Katopodis, 1992).

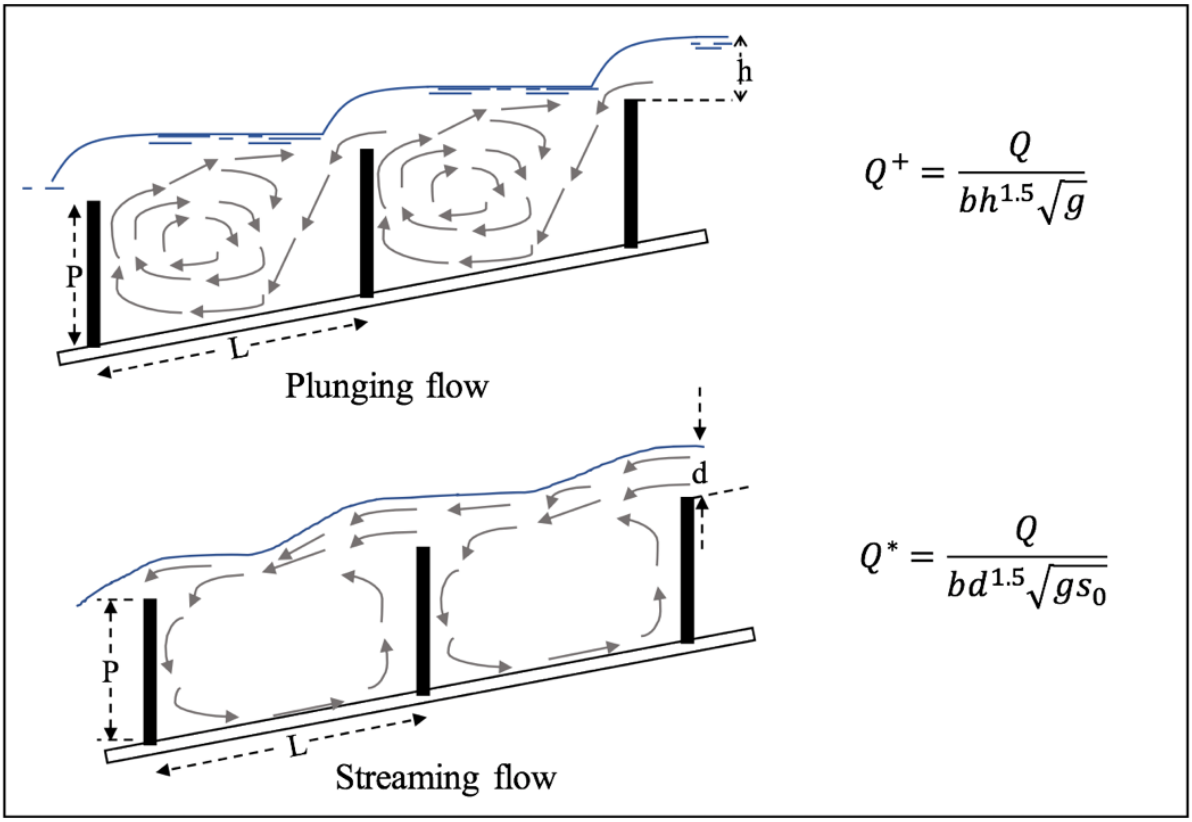


**Figure 1-8:** Weir fishways dimensionless discharge equations

### 1.6 Scope of the Study

Hydraulic characteristics of a new designed sharp crested labyrinth weir was previously discussed by Hakim and Azimi (2017). In this regard, a square pool was added to the vertex of a triangular

labyrinth weir in two different directions to form two new designs. However, dynamic characteristics of these weirs and their effect on fish behavior in weir- pool type fishway needs to be extensively studied.

The first objective of this study is to investigate the dynamic characteristics of the mentioned new designed sharp crested labyrinth weir such as turbulent kinetic energy and power spectrum density for free flow and submerged flow conditions by measuring instantaneous flow velocities in three dimensions. The second objective is to investigate the hydraulic and dynamic behaviours and its relationship to the fish behavior in weir- pool type fishway using the mentioned new designed labyrinth weir. The third objective of the present work is to conduct detailed experimental studies that can be used as a benchmark for computational fluid dynamics. The validated numerical models can be employed for further improvement of the proposed design.

### 1.7 Organization of the Thesis

In this thesis, two sets of experiments were conducted in order to achieve the afore mentioned objectives. This thesis organized as follows:

Chapter one is an introduction to sharp crested weirs and fishways. In chapter two, a literature review on sharp crested weirs and different types of fishway is thoroughly discussed. Subsequently, chapter 3 presents the dynamic behaviour of two new design triangular labyrinth weirs. In chapter four, hydraulic and dynamic behaviour of new designed weir-pool type of fishway is presented. Finally, in chapter five general conclusion based on previous chapters are summarized.

# Chapter 2

## 2.1 Literature Review

The major investigations directly pertaining to labyrinth weirs which have been carried out prior to the current study will be reviewed in this chapter. Weirs are widely used for discharge measurement, dissipate the excess energy of water, flow diversion, and headwater level control (Ackers et al., 1978). In general, weirs are classified into sharp-crested weirs and weirs of finite crest length (Ackers et al., 1978). Sharp-crested weirs are made of thin steel plates for irrigational canals or concrete walls for rivers. The discharge capacity of sharp-crested weirs is directly related to the weir length. In standard full-width sharp-crested weir, where the weir is installed perpendicular to the flow direction, the weir length is equal to the channel width $B$. A correlation between the water head upstream of the weir $h_0$ and discharge $Q_f$ can be formulated by using energy equation (Ackers et al., 1978). A discharge coefficient $C_d$ is introduced in the energy equation to incorporate the effects of streamline curvature, non-hydrostatic pressure distribution, and non-uniform velocity distribution in head-discharge relationship. The capacity of a weir to carry more flow with a same water head can be increased by increasing the approach velocity and increasing the weir length $L$. The weir length can be increased by installing a sharp-crested weir with an angle. This type of weirs is called oblique sharp-crested weir (Borghei et al. 2003, 2006; Kabiri-Samani et al., 2010) and also shown in Figure 1-3b.

The weir's discharge capacity can be further increased by folding a sharp-crested weir in a plan view. This type of weirs is called labyrinth weirs and they are particularly suited for use where the river width is restricted (Falvey, 2003). Labyrinth weirs can be folded in a plan view to form a single cycle of triangular, rectangular, and trapezoidal shapes. A single-cycle labyrinth weir can

be constructed in repetitive manner to cover the entire width of the river. The width of a one-cycle labyrinth weir $b$ can be calculated by dividing the river width $B$ by the number of cycles $n$ ($b=B/n$). Effects of the controlling parameters such as crest length, plan shape, crest shape, and number of cycles on the performance of labyrinth weirs have been studied in the past. Most of experimental and numerical investigations have been focused on rectangular, triangular, and trapezoidal labyrinth weirs due to their geometrical simplicity and ease of construction (Hay and Taylor, 1970; Sitompul, 1993; Falvey, 2003; Erpicum et al., 2011; Crookston et al. 2012; Dabling and Crookston, 2012). The effects of approach velocity, cycle number, and crest shape were investigated by Hay and Taylor (1970). The labyrinth weirs were made of a sharp-tip crest and the headwater to the weir height ratio was limited to $h/P<0.6$. It was found that the number of cycles could significantly increase the discharge for a constant head and the design curves were developed to predict the discharge. Effect of approach velocity can be incorporated with the water head to form a total head $H$, ($H=h+v^2/2g$) where $v$ is the average flow velocity and $g$ is the acceleration due to gravity. Lux (1989) introduced an empirical formulation based on the total upstream head $H$ and used a shape constant $k$ of 0.18 and 0.1 for triangular and trapezoidal labyrinth weirs, respectively.

Effects of approach velocity and crest length can be expressed by $H/P$ and sidewall angle $\alpha$ ($\sin\alpha=w/L$). Tullis et al. (1995) examined the effects of $\alpha$ and $H/P$ for $6\leq\alpha\leq35$ and $0.15\leq H_o/P\leq0.90$. investigated the performance of a wide range of triangular labyrinth weirs with a sidewall angle $\alpha$ ranging from 6 to 35 degrees. It was found that the discharge coefficient in triangular labyrinth weirs increased with increase $H/P$ and it reached a peak value for $0.15\leq H/P\leq0.35$. Effects of crest shape on the capacity of labyrinth weirs were reported to be less significant in comparison with the crest length and approach velocity. Kumar et al. (2011) conducted extensive investigation on triangular weirs in the free flow condition and demonstrated that triangular weirs are more efficient

than common sharp-crested weirs. They also found that the performance of triangular labyrinth weirs become more sensitive as the vertex angle and discharge decrease. Crookston and Tullis (2013a) reported that the capacity of triangular labyrinth weirs can be increased by 11% for low approach velocities ($H/P$=0.1) if a half-round crest is used instead of a quarter-round crest.

Dimensional analysis is a tool to combine the important parameters such as crest length, cycle number, approach velocity, etc. for the development of practical formulations to predict discharge over triangular labyrinth weirs. Such design formulations can predict flow discharge by 5.1±0.1% error (Azimi, 2013). Recently, (Azimi and Hakim, 2018) developed head-discharge formulation to predict the discharge over rectangular labyrinth weirs with a wide aspect ratio ranging from 0.25 to 3. It was found that the rectangular labyrinth weirs are very efficient for $h/P \leq 0.4$. Nappe breakers were designed to reduce flow oscillation and noise in labyrinth weirs. Dabling et al. (2013) conducted laboratory investigation on seven-cycle triangular staged labyrinth weirs with different crest elevations. They found that the discharge of the lower stage (i.e., the section with lower weir height) is location-depended and flow separation occurs when the approaching flow reaches to where crest elevation is changed. Bilhan et al., 2016 conducted laboratory experiments to analyze the efficiency of nappe breakers for trapezoidal and circular labyrinth weirs. They reported that the installation of nappe breaker for trapezoidal and circular labyrinth weirs reduced the weir performance by 4% and 2%, respectively.

The upstream water level in weirs begin to rise once the tailwater $t$ rises. The onset of headwater motion is called modular limit and the weir is called submerged or drowned once the tailwater passes the modular limit (Ackers et al., 1978). For common full-width sharp-crested weirs, submergence occurs even before the tailwater reaches the crest elevation (Wu and Rajaratnam, 1996; Azimi et al., 2016). For weirs of finite crest length and embankment weirs, the upstream

water level remains unchanged until the tailwater rises above the critical depth (Azimi et al., 2014; Hakim and Azimi, 2017). Laboratory experiments on triangular labyrinth weirs indicated a smaller discharge in submerged flow than that of free flow condition for the same water head $h$ (Tullis et al., 2007; Bijankhan and Kouchakzadeh, 2016). Flow discharge in submerged flow condition can be correlated with the submergence $t/h$. Tullis et al. (2007) studied the flow over submerged half-round crest triangular labyrinth weirs with different geometries and suggested a relationship between discharge parameters and submergence. For labyrinth weir with sharp apex angles and $h/P<0.6$, it was observed that the cycle number has significant influence on the weir's performance. Recent laboratory experiments show that labyrinth weirs are less sensitive to submergence than common linear sharp-crested weirs (Bijankhan and Kouchakzadeh, 2016; Hakim and Azimi, 2017).

For labyrinth weirs with small sidewall angles, nappe interaction reduces the effective length of the weir. Therefore, the performance of triangular labyrinth weirs decreases as the water head increases. Laboratory experiments on $n$-cycle triangular labyrinth weirs indicated that the effective weir length decreases with increasing flow rate and number of cycles (Crookston and Tullis, 2012b). One possible method of increasing the weir length without reducing the effective weir length is to install a pool either in the downstream or in the upstream of a triangular labyrinth weir. Recent laboratory experiments on a labyrinth weir with a downstream pool (Hakim and Azimi, 2018) and with an upstream pool (Azimi, 2018) indicated that both designs have higher performance in free flow condition. Considering the excess cost of construction for the new design, it was found that the triangular labyrinth weir with a downstream pool is also economical for $h/P\leq0.3$ (Hakim and Azimi, 2018). The new design also showed a slightly better performance in comparison with sharp-crested linear weir by passing more flow than sharp-crested weir with the

same $t/h$. For a single-cycle triangular labyrinth weir with an upstream pool the calculated discharge coefficient was up to 30% higher than the same weir with a downstream pool however, the weir model is only economical for $h/P<0.17$.

Different flow regimes were identified during the study of triangular labyrinth weirs with upstream or downstream pool as the flow discharge over the weir increased. The defined regimes were investigated by examining the variations of some hydraulic parameters with discharge such as discharge coefficient, modular limit, wave patterns, and discharge reduction factor.

The present research work is motivated to understand in detail the complex and three-dimensional flow pattern upstream of the newly design weir models. The main objective of the present study is to understand the three-dimensional flow behavior by investigating the three-dimensional mean and turbulence structure of triangular labyrinth weirs with a downstream or an upstream pool.

Recent experimental studies discussed about the formation of surface jets and surface jumps in single-cycle triangular labyrinth weirs with an upstream and a downstream pool (Hakim and Azimi, 2018). These weirs are expected to be suitable choices as pool-weir fishways and energy dissipators. Therefore, detailed velocity and turbulence measurements are required to characterized the performance of the weir models for employing as fishways and energy dissipators. Acoustic Doppler Velocimeter (ADV) probe has been successfully used to provide detailed three-dimensional velocity and turbulence measurements for fishways and energy dissipators (Haro and Kynard, 1997; Odeh et al., 2002; Silva et al., 2011, 2012). The second objective of the present work is to show the flow pattern in the upstream of the weirs to correlate the results with possible fish migration path. The third objective of the present work is to present detailed experimental data that can be used as a benchmark for computational fluid dynamics

(CFD). Validated numerical models can be employed for further improvement of the proposed design and for different hydraulic conditions.

The needs for fresh water are increasing due to irrigation, generating electricity and industrial, domestic and recreational purposes. Consequently, a need exists to create some infrastructures to achieve this important goal (Nilsson et al., 2005; Juan Francisco Fuentes-Pérez et al., 2016). These structures are usually close the path of some aquatic life such as fish. (Porcherand Travade, 2002; Branco et al., 2013; Juan Francisco Fuentes-Pérez et al.,2016). Fishways as hydraulic structures are widely used for allowing fish to pass over transversal obstructions since they have to migrate from downstream to upstream for different reasons such as spawning. Also, fish passages are required mostly for ecological and economical considerations (Rajaratnam et al. 1986). Fishways' efficiency can be defined as the proportional of the fish from a given population which are able to triumph the transversal obstructions as well as their hydrodynamic variables such as discharge, velocity, depth, turbulence fields, etc. Also, these hydrodynamic variables depend on environmental parameters such as flow fluctuations in different water levels in the both upstream and downstream of the structure. (Bermúdez et al., 2010; Fuentes-Pérez et al., 2014; Sanz-Ronda et al., 2015a; Juan Francisco Fuentes-Pérez et al., 2016). In general, fishways are classified into pool and weir, Denil, culvert, and vertical slot fishways (Bell 1973; Clay 1961; Decker 1967; Katopodis and Rajaratnam, 1983). A rocky ramp fishway is one of the nature-like fishways, consist of a long sloping channel and boulders on a slope (Katopodis et al., 2001). Muraoka et al. (2017) studied the boulder arrangement and height of boulder on rocky ramp fishway base on the swimming behavior of fish. They investigated the swimming performance of char (Salvelinus Richardson) and freshwater sculpin (Cottus Pollux) in the vicinity of boulders on experimental channel by ultra-high-speed cameras. The results demonstrated that sculpin, which count as a

bottom fish, need a density, and different linear arrangements of boulders to allow migration. As expanding the vertical low-velocity area, which is created behind high boulders does not always result in a good outcome for sculpin. Whereas, this solution is not appropriate for char, as a result, a diverse arrangement of boulders is needed on individual rocky ramp fishways to allow the movement and migration of multiple species.

Denil fishways have become common in recent years in Canada and in the United States for upstream fish passage. The regularly used Denil fishway recognized as the simple Denil is simply a rectangular channel, which in the so-called standard design, has a total width of 0.56 m and clear central width of 0.36 m (Figure 1-5). It has a set of baffles located at an interval of equal to 0.25 m, which are inclined at an angle of 45° against the flow, with the normal height to the crest equal to 0.13 m. The depth of flow in the Denil fishways could be different depending on specific flow situations. The length of a Denil fishway will depend on the swimming capacity of the fish that would boost this fishway. The common slope for Denil fishways are as high as 33% and the common slope is around 20% (Katopodis et al., 1997). Rajaratnam and Katopodis (1984) conducted study on standard version of the simple Denil fishway and measured time average longitudinal velocity profiles in the vertical center plane of the region fishway in the fully developed flow. They revealed that the shape of the velocity profiles depended on the $d/b$ ratio, where $d$ is the stream thickness and $b$ is the width of the pool. Furthermore, for $d/b$ less than about unity, the velocity profile had a low velocity region in the lower part of the flow and a high velocity surface stream. As well as, for flows with a greater amount of $d/b$ larger than around 3 the constant low velocity region vanishes and the velocity rises continuously from the bottom to the surface. They also suggested relation between dimensionless discharge $Q'$ and $d/b$ for $d/b$ lower than 3:

$$Q' = Q/(gS_0b^5)^{0.5} \quad (2\text{-}1)$$

$$Q' = 0.94(d/b)^2 \quad (2\text{-}2)$$

Where $Q'$ is the dimensionless discharge for Denil fishways, $g$ is the acceleration due to gravity, $Q$ is the discharge of the flow and $S_0$ is slop of the fishway. Katopodis et al. (1997) suggested formula for higher $d/b$ up to 5.5:

$$Q' = 1.15(d/b)^{1.8} \quad (2\text{-}3)$$

Culverts, which have varying characteristics in terms of water depth, velocity, and roughening elements are commonly employed to redirect rivers and streams under roads, railways, and other embankments (WDFW, 2003). Fish movements may be obstructed or stopped by culverts if the hydraulic conditions exceed fish swimming capacities or due to behavioural rejections (Haro et al., 2004; Gibson et al., 2005; Castro Santos and Haro, 2006). Hydraulic diversity may benefit fish that lessen energetic waste by utilizing low flowing zones in the lee side of natural structures (Everest and Chapman, 1972; Morantz et al., 1987). On the other hand, fish may be able to take out energy from the associated vortices to amplify swimming performance (Coutant 1998; Hinch and Rand 2000; Liao et al., 2003a). Flows that have cyclic components, such as steady Karman vortex streets behind a specific obstacle geometry, may be useful for fish, but flows presented by chaotic fluctuations in velocity may cause the energetic costs (Enders et al., 2003, 2005) and therefore push back fish (Cotel et al., 2006; Smith et al., 2006). Furthermore, the effect of turbulence on swimming capacity is strongly influenced by intensity, periodicity, orientation, and scale of vortices (Tritico and Cotel, 2010; Lacey et al., 2012). Some researchers have recommended the application of baffles (Rajaratnam et al., 1990), riprap (McKinnon and Hnytka, 1985) or the placement of natural bedload layer (e.g. cobbles and small boulders) within culverts (Behlke et al., 1991; Clay, 1995). These improve hydraulic incongruity and develop areas of lower velocity as fish may rest.

Enders et al. (2017) carried out control experiment on volitional performance of migratory of Alewife and Brook trout in turbulent flows produced by horizontally and vertically oriented baffles in rectangular box culverts. The high magnitude of the Reynolds shear stress $\overline{\rho u'w'}$ specified a dominance of laterally oriented roller vortices shedding from the baffles and advecting to the surface. On the other hand, the high magnitude of $\overline{\rho u'v'}$ specified a dominance of vertical vorticities spinning in counter clock wise direction. The result shows that Alewife and Brook trout staged outstandingly more attempts into the vertical baffled channel compared to the horizontal baffled channel. Whereas, Alewife traversed greater distances swimming in the channel with the horizontal baffles at the lower flow discharge. Brook trout also swam further under low flowrate but traversed similar distances in both channels. Baki et al. (2016) studied flow structures around a boulder in a boulder array under a wake interference flow condition. They indicated that the vertical profiles of normalized streamwise mean velocity and streamwise turbulent intensity were roughly similar around the boulder, however, either of them had different shapes in the upstream, downstream and left and right sides of the boulder.

Fish passes with vertical slots are one of the types of fishways that have been commonly employed to allow upstream migration for diadromous (i.e. whose migration occurs between freshwater and marine environment) and potamodromous species (i.e. whose migration occurs entirely in fresh water). Rajaratnam et al. (1986, 1992) recommended three particular design of vertical slot fishway based on overall hydraulic performance and simplicity in construction, all three designs being presented by constant $B/b$ and $L/b$ ratios (respectively 8 and 10) where $L$ is the length of the pool, $B$ is the width of the pool and $b$ is the width of the slot. Lenne in Larinier (1992) proposed a simplified design with lower $B/b$ and $L/b$ values (respectively 6.63 and 8.1). The main design specifications for a vertical slot fishway are the maximum head difference between pools, or drop

($\Delta H$), which define the maximum velocity in the pools and the maximum volumetric dissipated power or energy dissipation factor which is shown with $P_v$ (w/m$^3$). The dissipater power is a common indicator of the turbulence and agitation level in the pools of fishways (Bates, 2000). The energy dissipation is expressed as: $P_v = \rho g Q \Delta H / Vol$ where $\rho$ is the density of water (e.g., 1000 kg/m$^3$), $g$ is the acceleration due to gravity (e.g., 9.8 m/s$^2$), $Q$ is the flowrate in the system (m$^3$/s) and $Vol$ is the volume of the water in the pool (m$^3$).

The selection of the drop between pools relates to the swimming capacities of the fish. It can vary from less than 0.10 m for fishways specifically designed for small species to more than 0.30 m for trout or large diadromous species such as salmon or sea trout (Wang, 2010). The range of energy dissipation for specific species is defined through laboratory experiments. The value of $P_v$ =200 to 250 w/m$^3$ is commonly considered as the upper limit for salmonids (Bates, 2000; Larinier et al., 2002). Lower levels are suggested (100–150 w/m$^3$) for shad and rheophilic riverine species (Larinier et al., 2002). Even lower values (around 40–50 w/m$^3$) have been taken to enable upstream passage pass of all fish with length > 90 mm and roughly half of the fish between 20 to 70 mm on the Murray Darling basin in Australia (Barrett and Cooper, 2006; Stuart et al., 2008). Liu et al. (2006) presented the results of an experimental study using ADV probe on the mean and turbulence structures of flow in a vertical slot fishway with slope of 5.06% and 10.52%. They found two flow regions for each flow pattern known as a jet flow region and a recirculating flow region. Also, they realized the mean kinetic energy reduces dramatically in the jet region and the energy dissipation rate is under 200 w/m$^3$ in the most area in the pool. As well as, it has been found that its maximum velocity decays faster than a plane turbulent jet in a large motionless area. The jet showed vary turbulence structure for the two flow patterns and for each pattern, the turbulence characteristics

emerged different between the left and right halves of the jet. The normalized energy dissipation rate indicated some similarity and had a highest value on the center of the jet.

Pool weir fishways are the most common type of the fishways in Canada (Hatry et al., 2013). They are appropriate for species having strong swimming ability (Yagci, 2010). Also, dimensions and details of the design in fishways can have significant influence on flow patterns, circulation, and velocities distribution, but have limited effect on depth-discharge relationships (Katopodis, 2005). Pool and weir fishways are structured of couple of consecutive weirs series which result pools between them. The water flows from the upstream to the downstream region over the weir's series. Two purposes are followed in the design of pool-weir fishways, 1) to ensure sufficient dissipation of the energy of the water with no transfer of energy from one pool to another and 2) to offer resting areas for fish (Larinier and Marmulla, 2004). The essential limitation of the pool-weir fishway is the narrow range of operating flow (Bates, 2000). Kim (2001) conducted experimental study on three different designs of pool-weir fishways (e.g., trapezoidal weir without notch, straight and zigzag type of rectangular weir with notch) and indicated that optimal design for upstream migration of fish is the straight type of rectangular weir with both notch and orifice. Fish can pass over the weirs by swimming using the burst speed or jumping over them (Rajaratnam et al. 1988). The most basic ecological attention for fishway design is water velocity. The velocity over the weir or through an orifice should not be larger than the maximum burst speed of the intended fish species to let them pass upstream, on the other hand, the velocity in the pool should be less than the cruising speed to let the fish rest (Clay, 1995; Larinier, 2002a). The burst and the cruising velocities of different fish species and body types have been comparatively well studied by Beach, 1984; Jones, Kiceniuk, & Bamford, 1974 and summarized by Katopodis and Gervais (2012). To understand the fish movement, maneuver, and accelerate within their fluid medium,

hydrodynamic data should be obtained from laboratory experiments. Also, it can provide knowledge that how fish maintain their speeds and tolerance (Katopodis, 2005). Since fish have ability of oscillating their body motion in presence of vortex field, they outperform similar to steady motion propulsion (Triantafyllou et al., 2000). Fish are able to change their motion in turbulent flow from regular swimming mode to relax body bending so they do not use their main muscles for riding eddies and consequently save more energy. They use their body similar to wing-like hydrofoils so tack against the current like a sailboat tacks upwind (Liao et al., 2003).

Flow over the weirs itself is classified into plunging and streaming modes (Clay 1961). It is called plunging when the water level in the pool immediately after the weir is lower than weir's crest and consider as streaming when the water level in that area is above the weir's crest and streaming surface skimming the water surface in the pool (Rajaratnam et al. 1988). By increasing the flowrate, the flow regime in pool-weir fishway changes from plunging flow to streaming flow. Rajaratnam et al. (1988) suggested a standard to predict the transition from plunging to streaming flow. Later on, Ead et al. (2004) found different sub-regimes in the transitional regime. They expanded their work to identify five flow sub-regimes within the transitional flow regime, as well as a supercritical jet flow. There are different kind of pool and weir fishways that are in streaming mode which enhance the upstream movement of different fish species, and are appropriate for rivers having fish with wide morpho-ecological traits (Silva et al.,2009; Branco et al., 2013; Sanz-Ronda et al., 2015b; Juan Francisco Fuentes-Pérez et al., 2016). The effect of pool's length, slope of the channel and flow discharge have been studied by Rajaratnam et al. (1988). It was found that the dimensionless flow discharge $Q_+$ for plunging regime and $Q^*$ for streaming regime are 0.61 and $1.5(L/d)^{1/2}$, respectively, where $L$ is the length of the pool and $d$ is the thickness of the surface

stream. Also, they found the criterion for predicting the transition from plunging to streaming regime ($Q_t$) and reported to be equal to 0.25.

$$Q^* = Q/(b_w\, d^{3/2}\sqrt{g}S_0) = \sqrt{(2/C_f)} \quad (2\text{-}4)$$

$$Q = 2/3 b_w\, C_d\sqrt{2g}\, h^{3/2} \quad (2\text{-}5)$$

$$Q_+ = Q/(b_w\sqrt{g}\, h^{3/2}) = 2/3\sqrt{2}C_d \quad (2\text{-}6)$$

$$Q_t = Q/(b_w S_0 L^{1.5}\sqrt{g}) \quad (2\text{-}7)$$

where $Q$ is the discharge, $g$ is the acceleration due to gravity, $b_w$ is width of the fishway, $S_0$ is the slope of the fishway, $h$ is the water depth in the pool, and $C_d$ is the coefficient of discharge. Fuentes-Pérez et al., (2016), conducted an experimental study on the submerged notch and orifice fishways. They proposed a new formula which not only adapt to fishways but also considered non-uniform scenario so consequently the formula differed with the classical one. They detected a new sensible distribution pattern for coefficient of discharge in plunging mode. Also, they suggested and observed higher coefficient of discharge than the traditional one. Some of the fish have less swimming capacity or do not have good leaping abilities than others. Therefore, an orifice offers a passage to certain fish species in which swimming or leaping against overflow weirs may not be possible (Yagci, 2010). Guiny et al. (2005) carried out experimental study on variety of vertical slots, orifices, weirs, and combinations of all three components in a fishway. They found that significant percentage of fish swam through submerged orifices and vertical slots rather than through overflow weirs for any given flowrate, velocity, and head losses. They also revealed that equal velocity orifices may be more proper than vertical slots since the decay rate of the velocity within the jet is higher for slots than orifices. Yagci (2010) tested a physical model of pool-weir fishways with orifice and notch. He revealed that both orifice and notch can only be useful for a limited range of discharge values. Kupferschmidt and Zhu (2016) conducted laboratory

experiments using acoustic Doppler velocimeter on V shape pool weir fishways with different discharges and bed slopes. It was found that the V shape pool weir reduced the mean streamwise velocity in the pools by about 20% but the maximum velocity increased by a factor of two. They also developed two staged-discharge relationships and modified the discharge coefficients to account for both flow over the weir and orifice flow through the base of the weir.

Baki et al. (2017) conducted numerical modeling on the relationship between rock-weir hydraulics and fish passage for different channel and structure configurations. They found out that rock-weir fishway created water depth and flow velocities fitting to fish passage under different channel characteristics and structure geometries. Suitable slow velocity areas for fish resting in rock-weir fishways (velocity less than 0.4 $U_{max}$) was produced for bed slope less than 5.5%, pool spacing $L$ less than 2.5$B$ and weir height larger than 0.125 m. The average volumetric energy dissipation rate is responsive to both channel slopes and flow rates, however, is was less affected by the boulder-weir geometry. They also reported that the boulder weir fishway ensured flow fields low enough to be suitable for 200 mm long salmonid or cyprinids for bed slope lower than 7% and specific pool spacing 0.5$B$ to 3$B$ for the former and 0.5$B$ to 2.5$B$ for the latter fish spices.

# Chapter 3

# Dynamic Assessment of Triangular Labyrinth Weir

## 3.1. Experimental Setup

Laboratory experiments were conducted in a rectangular horizontal glass-wall flume located in the Water Research Laboratory at Lakehead University. The flume was 12 m long, 0.61 m wide and 0.5 m deep and it was connected to a hydraulic circuit allowing for discharge recirculation. The flume was equipped with an inline magnetic flowmeter with an accuracy of ± 0.01 L/s (FMG-3102, Omega, Quebec, Canada). During experiments, flow rate was kept constant at $Q_f$=28.52 L/s for both free and submerged flow conditions. In submerged flow condition, the submergence $t/h$ was kept constant with a value of $t/h$=0.74 for both weir models. As described, two weir models with an upstream and a downstream square pool were fabricated for this study. The weir models had a sidewall angle of $\alpha$=45º, a pool length of $L_p$= 0.16 m and a weir height of $P$= 0.25 m. The weir models were installed 7 m from the upstream tank wall to ensure uniform flow upstream of the weir models.

An Acoustic Doppler Velocimeter (ADV) probe (Vectrino, Nortek, Norway) was employed for instantaneous three-dimensional measurements. The ADV probe was mounted to a three-dimensional linear stage with an accuracy of ±0.5 mm. A sampling rate of 200 Hz was selected for flow measurements. The sampling volume was a cylinder with a height of 7 mm measuring 50 mm bellow the probe location. Cumulative averaging method was used to determine the sampling duration. Preliminary measurements with a duration of ten minutes were recorded to determine the sampling duration. Figure 3-2 shows the cumulative average of all instantaneous velocities with time. It was found that a time duration of 120 seconds provides a steady average for this study. Other techniques such the circular block bootstrap technique (Buffin-Bélanger and Roy, 2005;

Quaresma et al., 2017) also show that a sampling time of 120 seconds represents a steady state flow condition for this study. Three dimensional posthaste velocities ($u$, $v$, $w$) were measured in both free and submerged flows for two weir models with an upstream pool and a downstream pool (see Figure 3-3 and 3-4).

To capture a high-resolution velocity field, instantaneous velocity measurements were carried out at 793 points in the upstream of each weir models. Data points were recorded for a half of the velocity field assuming flow symmetry in the upstream. The origin of the coordinate system is located in the middle of the flume and 0.59 m upstream of the weir tip. The flume bed is the origin in $z$ direction. Measurement points were 60 mm and 90 mm apart in the longitudinal direction $x$, 30 mm and 60 mm apart in the transverse direction $y$, and 10 mm and 30 mm apart in the vertical direction $z$ (see Figure 3-1). Smaller measurement distances were selected in locations with a potential higher velocity gradient such as near wall and close to the weir walls.

During data sampling with ADV, statistical parameters such as the signal-to-noise ratio (SNR), data correlation, and signal amplitude were observed to secure the quality of measurements. To prevent phase wrapping, and signal aliasing during measurement, velocity range was frequently updated in the software's configuration during data sampling. The flume water was seeded with 20 μm polyamide particles to improve signal-to-noise (SNR) ratio of greater than 15 (Vectrino, Nortek, Norway). The SNR value during the entire measurement was above 15 with a correlation of at least 70%. Only 3.7% of measurements had a correlation in the range of 63%-69%. Post processing techniques and dispiking algorithms (Blanckaert & Lemmin, 2006; Goring & Nikora, 2002; Khorsandi, Mydlarski, & Gaskin, 2012) were employed to remove random spikes, Doppler noises and more accurate turbulence measurements (Quaresma et al., 2017). Phase-space threshold was used for despiking (Goring & Nikora, 2002) and Doppler noise reduction (Hurther and

Lemmin, 2001; Quaresma et al. 2017). Linear interpolation was applied between measurement points to improve the visual quality of contour and vector plots.

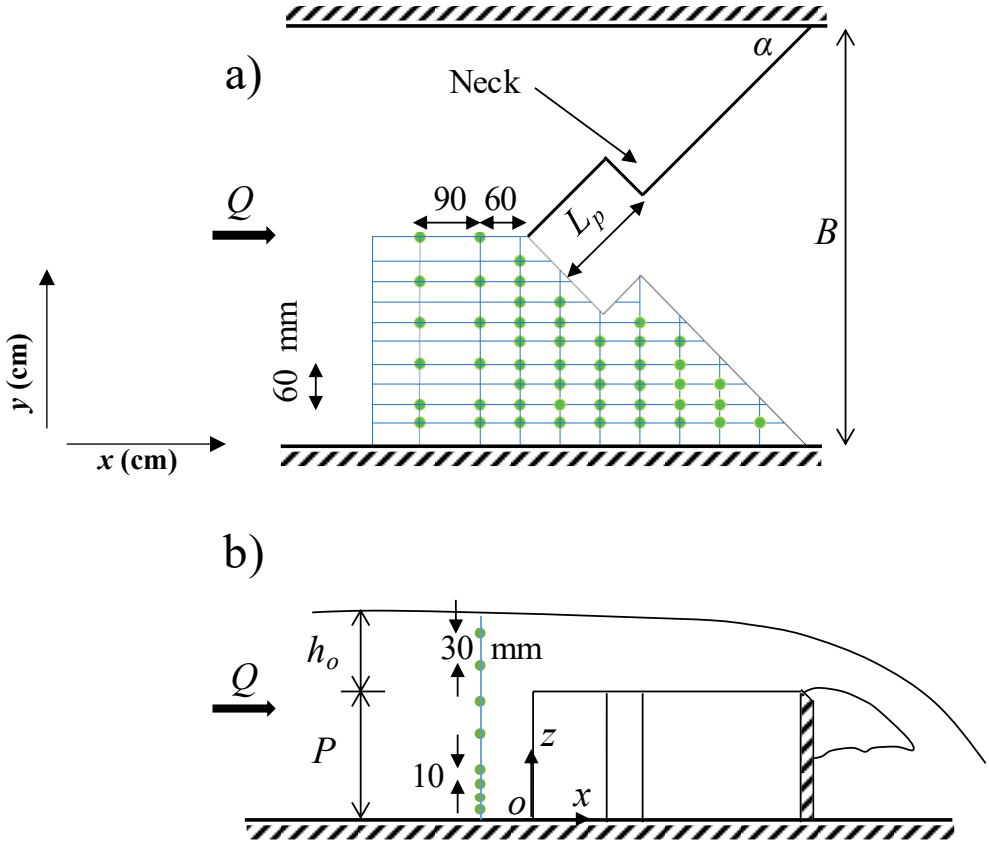


**Figure 3-1:** Top and side view schematics and ADV measurement points for triangular labyrinth weirs with a downstream pool; (a) top view; (b) side view.

### 3.2 Velocity of Weirs with Downstream Pool

In this section, 3D velocity distribution in the channel through the upstream of the triangular labyrinth sharp-crested weir with downstream pool has been discussed. For two different flow conditions, free and submerged flow, variation of the dimensionless longitudinal velocity ($u/u_{ave}$) was plotted as a contour plot in *XY* plane in different dimensionless elevations $z/(h_o+P)$ (Figure 3-5), where, $u_{ave}$ is mean velocity of the upstream flow.

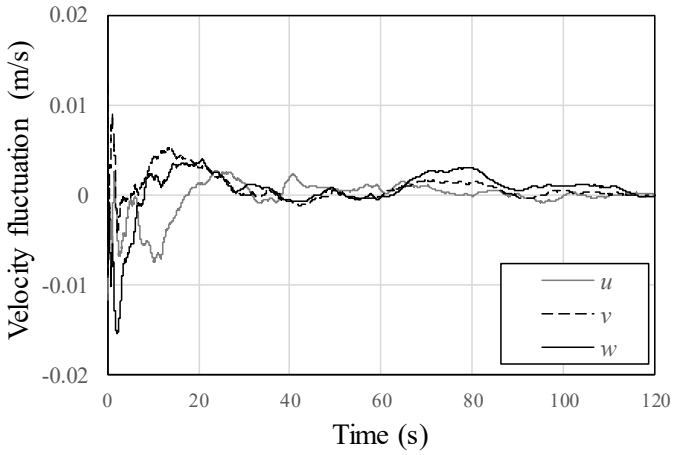


**Figure 3-2: Time** variations of the time-averaged axial, transverse, and vertical velocities.

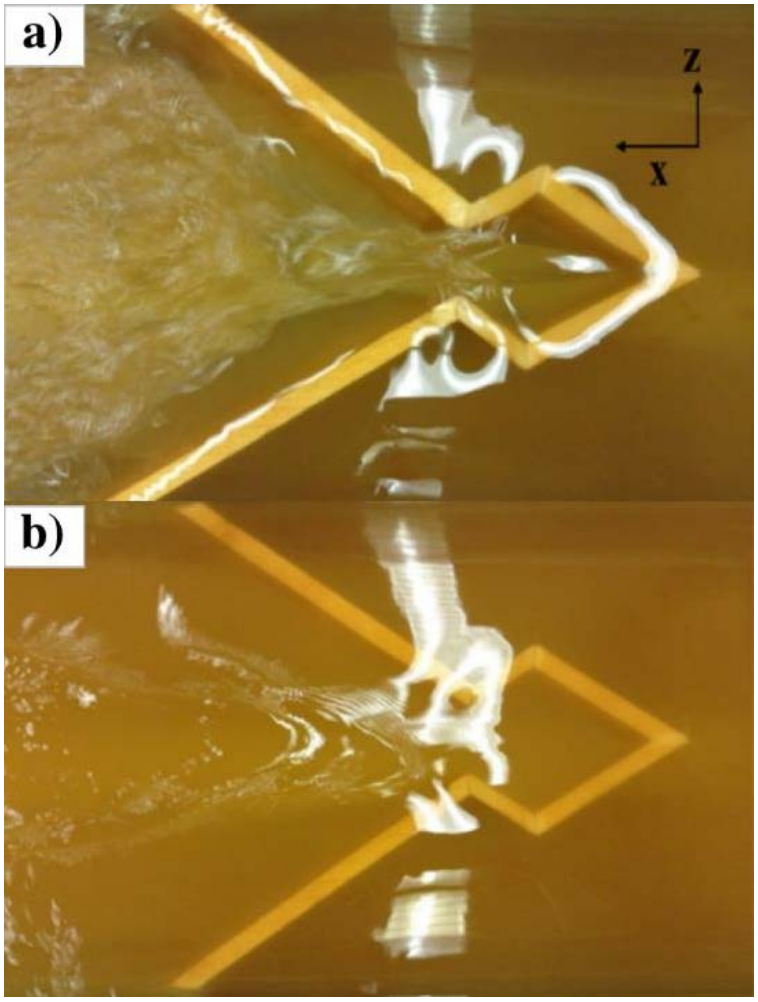


**Figure 3-3:** Top view of flow over a labyrinth weir with downstream pool in (a) free flow condition; (b) submerged flow condition.

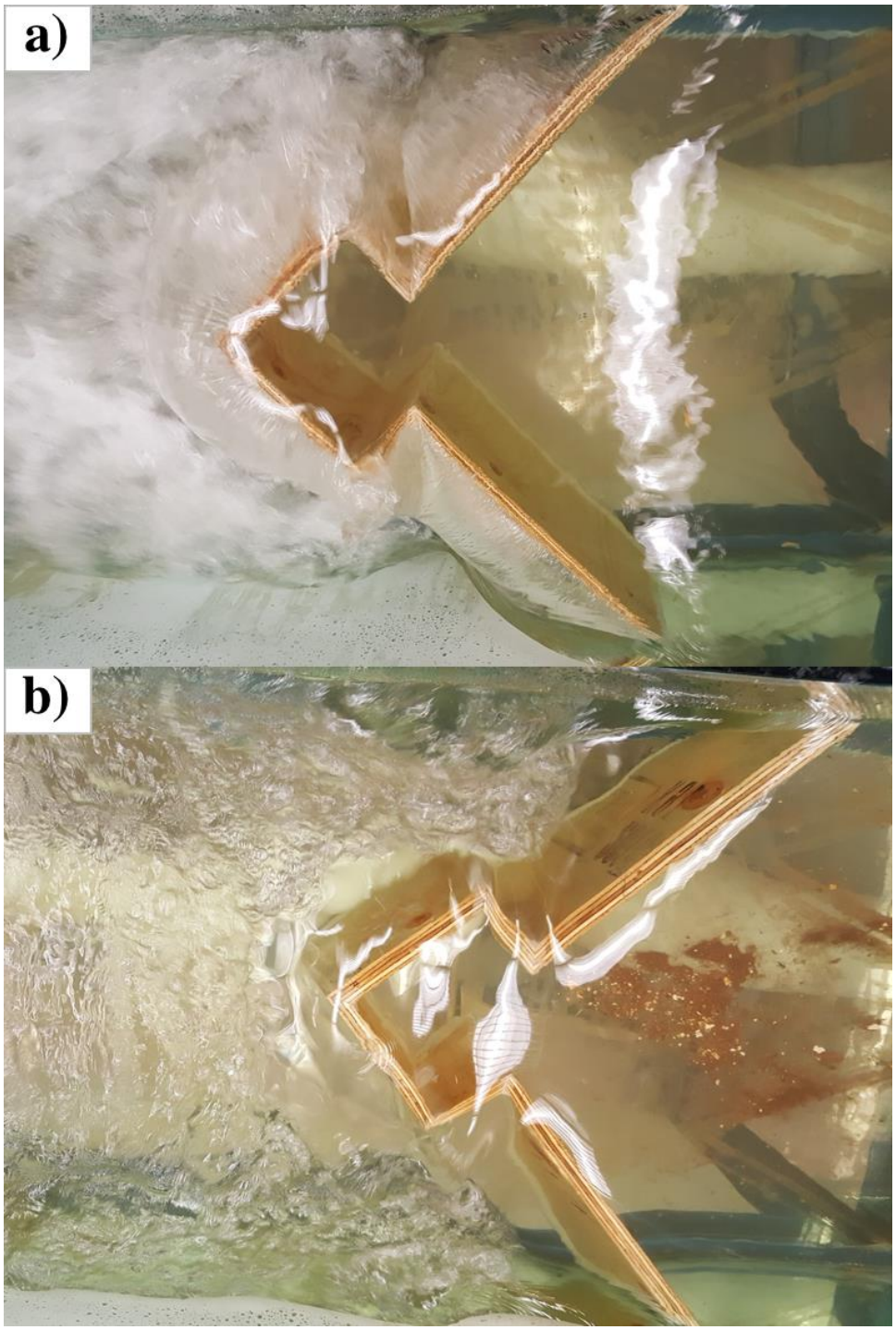


**Figure 3-4:** Top view of flow over a labyrinth weir with upstream pool in (a) free flow condition; (b) submerged flow condition.

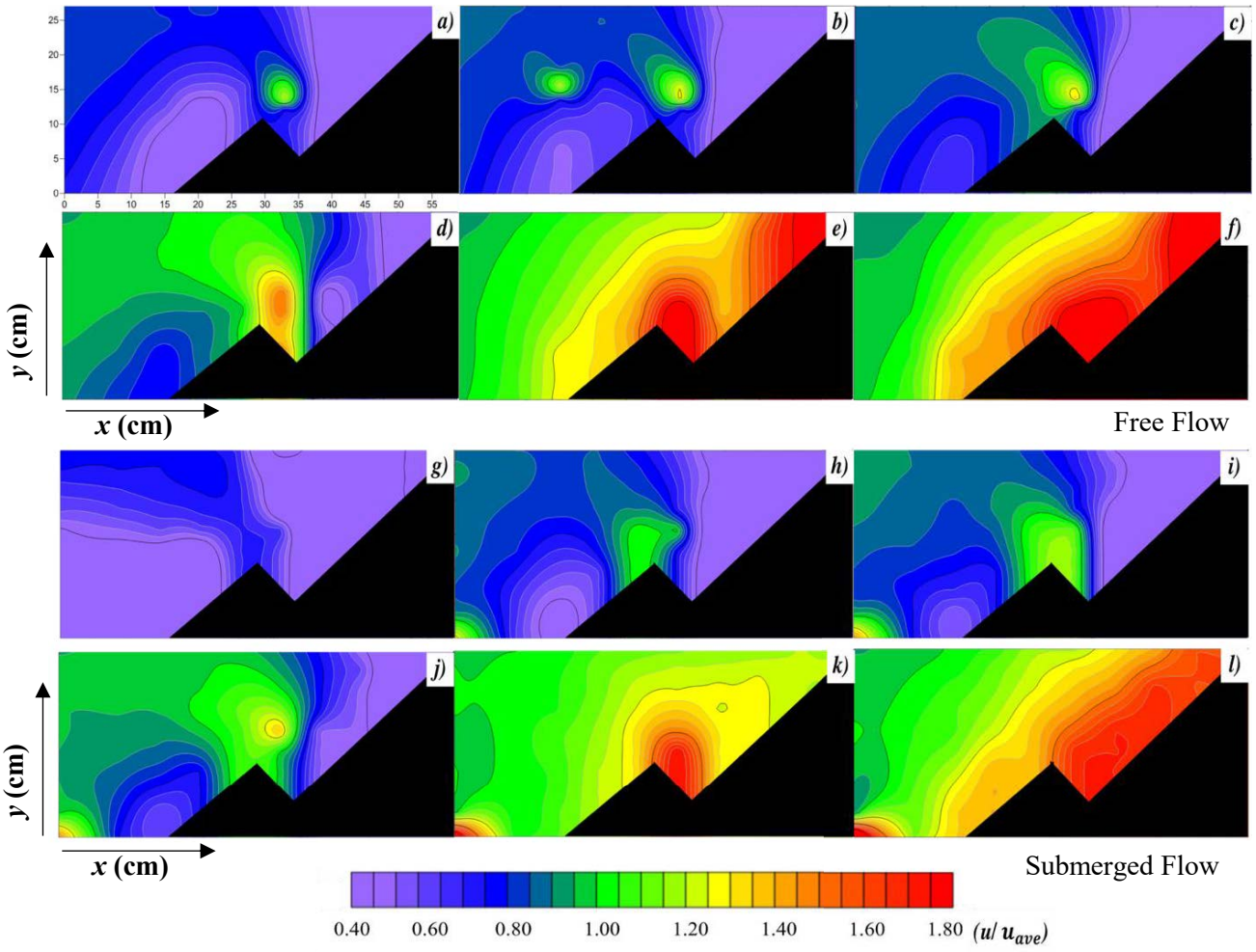


**Figure 3-5:** Contour plots of dimensionless axial velocity ($u/u_{ave}$) for labyrinth weir with a downstream pool in free flow condition and submerged flow conditions; a) $z/(h_o+P)$=0.04; b) $z/(h_o+P)$=0.07; c) $z/(h_o+P)$=0.013; d) $z/(h_o+P)$=0.35; e) $z/(h_o+P)$=0.7; f) $z/(h_o+P)$=0.85; g) $z/(h_o+P)$=0.04, $t/h$=0.74; h) $z/(h_o+P)$=0.07, $t/h$=0.74; i) $z/(h_o+P)$=0.013, $t/h$=0.74; j) $z/(h_o+P)$=0.35, $t/h$=0.74; k) $z/(h_o+P)$=0.7, $t/h$=0.74; l) $z/(h_o+P)$=0.85, $t/h$=0.74.

As it is shown in Figure 3-5 that in the free flow condition near the pool of the labyrinth weir ($x$=10), the longitudinal velocity in all planes smoothly increased from the apex of the weir to the neck of the weir and the maximum velocity occurred in the vicinity of the vertex angle between the main sidewall and the pool's sidewall (neck of the weir, 30>$x$>35). Afterwards, for the planes lower than 0.7($h_o$+$P$) the velocity started decreasing at the neck of the weir until reached to the corner of the weir and the sidewall of the flume. While, for the planes higher than or equal to 0.7($h_o$+$P$) it had the same trend before reaching to the middle of the main side wall of the weir. In

the submerged flow condition, longitudinal velocity increased from the apex of the weir to the adjacency of the vertex angle between the pool's sidewalls ($25>x>32$) where the maximum velocity happened. For the planes near to the free surface ($z > 0.7(h_o+P)$), the maximum velocity occurred near to the smaller pool's sidewall. Then, the velocity in all planes had descending trend from the point with maximum velocity to the place where the flume and the weir met each other. In terms of transversal direction in the both free and submerged flow conditions, $u/u_{ave}$ declined in the lower planes ($z < (h_o+P)$) from the flume's sidewall to the weir edge except for the area with maximum velocities. Whereas, in the elevations more than or equal to $0.7(h_o+P)$, the trend altered for the whole area. In addition, it can be demonstrated that the longitudinal velocity increased when the vertical distance from the channel floor in the both flow conditions was increased.

Figure 3-6 presents the variation of the dimensionless lateral velocity ($v/u_{ave}$) as a contour plot in *XY* plane along the upstream of the weir. It follows from Figure 3-6 that near the larger sidewall of the pool in the both flow conditions direction of the lateral velocity was toward the weir for all the planes with depth smaller than $0.7(h_o+P)$. Whereas, in the higher planes the direction was away from weir in the same area. After that, when the flow arrived in the vicinity of the neck of the weir, lateral velocity tended to move away from weir (toward the flume's sidewall). Also, it is observed from Figure. 3-6 that by closing to the free surface the lateral velocity magnitude increased as well. On the other hand, flow in the free flow condition in the higher elevations had larger lateral velocity's magnitude compared to the submerged condition in the corresponding dimensionless elevations ($z/(h_o+P)$).

In Figure 3-7, variation of the dimensionless vertical velocity, $w/u_{ave}$ was plotted in *XY* plane. Flow in the depth lower than $0.35(h_o+P)$ had zero magnitude in vertical direction either in free and submerged flow conditions. For larger ratio of $Z/H$, the magnitude of vertical velocity increased

before reaching to the $z/(h_o+P)$=0.7 where the maximum $w/u_{ave}$ took place, next by increasing the elevation, the value of the vertical velocity started declining.

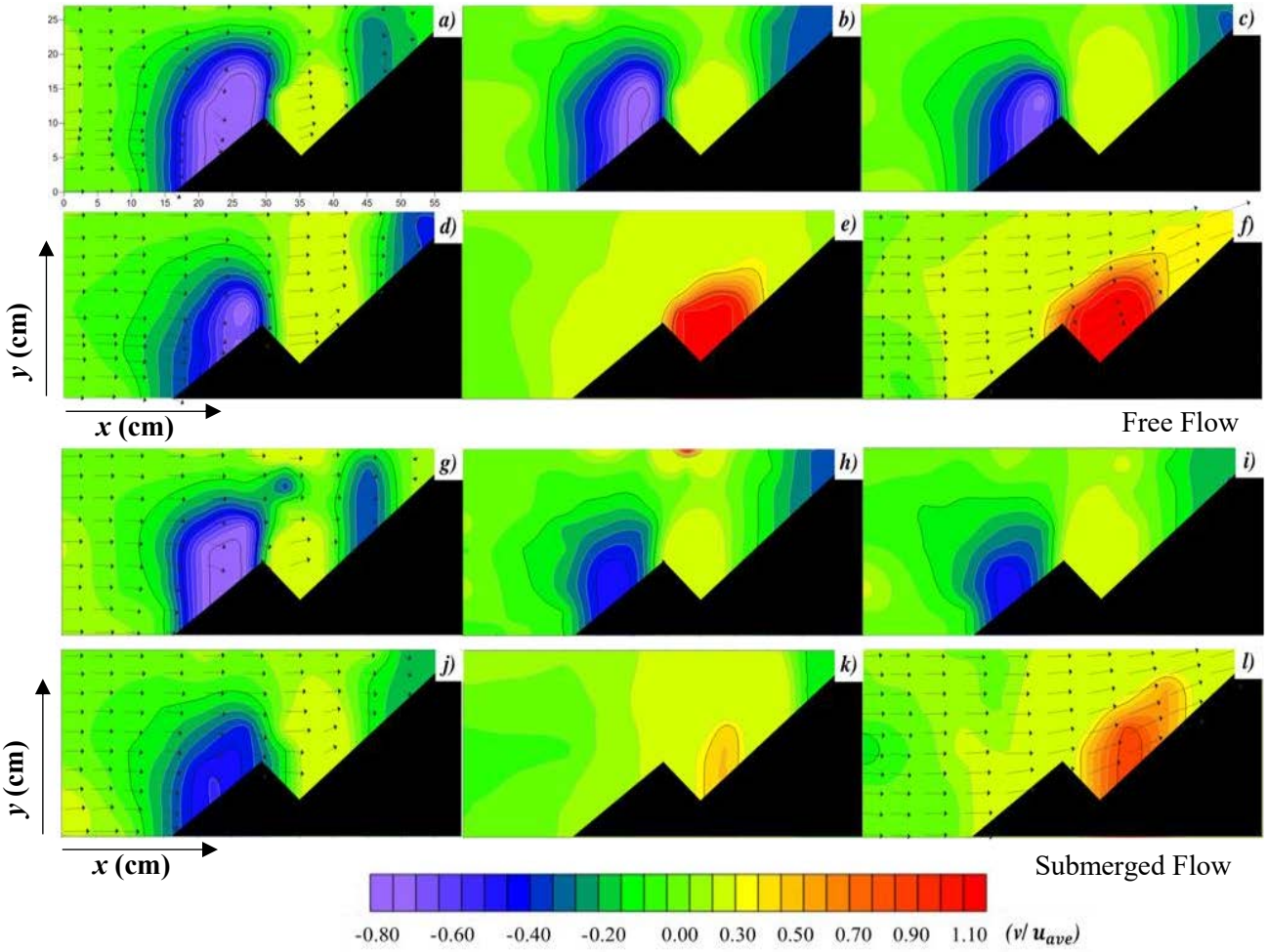


**Figure 3-6:** Contour plots of dimensionless transversal velocity ($v/u_{ave}$) for labyrinth weir with a downstream pool in free flow condition and submerged flow conditions; a) $z/(h_o+P)$=0.04; b) $z/(h_o+P)$=0.07; c) $z/(h_o+P)$=0.013; d) $z/(h_o+P)$=0.35; e) $z/(h_o+P)$=0.7; f) $z/(h_o+P)$=0.85; g) $z/(h_o+P)$=0.04, $t/h$=0.74; h) $z/(h_o+P)$=0.07, $t/h$=0.74; i) $z/(h_o+P)$=0.013, $t/h$=0.74; j) $z/(h_o+P)$=0.35, $t/h$=0.74; k) $z/(h_o+P)$=0.7, $t/h$=0.74; l) $z/(h_o+P)$=0.85, $t/h$=0.74.

In total, the most discharge happens in the area limited between main sidewall of the weir and the flume's sidewall and it can be illustrated that the magnitude of the mean velocity grew with increasing the vertical distance from the channel floor to a distance near the free surface.

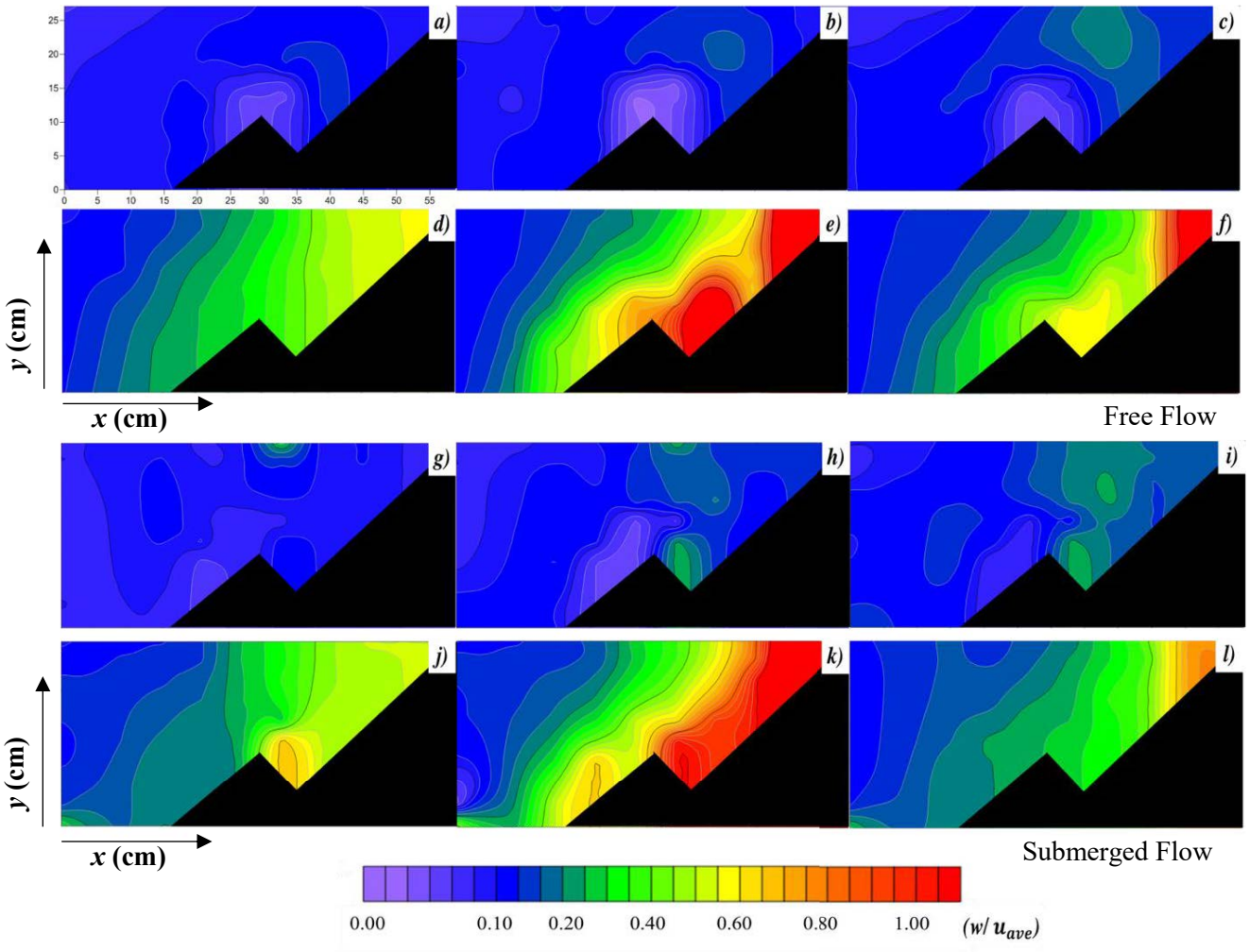


**Figure 3-7:** Contour plots of dimensionless vertical velocity ($u/u_{ave}$) for labyrinth weir with a downstream pool in free flow condition and submerged flow conditions; a) $z/(h_o+P)$=0.04; b) $z/(h_o+P)$=0.07; c) $z/(h_o+P)$=0.013; d) $z/(h_o+P)$=0.35; e) $z/(h_o+P)$=0.7; f) $z/(h_o+P)$=0.85; g) $z/(h_o+P)$=0.04, $t/h$=0.74; h) $z/(h_o+P)$=0.07, $t/h$=0.74; i) $z/(h_o+P)$=0.013, $t/h$=0.74; j) $z/(h_o+P)$=0.35, $t/h$=0.74; k) $z/(h_o+P)$=0.7, $t/h$=0.74; l) $z/(h_o+P)$=0.85, $t/h$=0.74.

### 3.3 Turbulent Kinetic Energy of weirs with Downstream Pool

In this section, the distribution of the turbulent kinetic energy (TKE) in the upstream of the triangular labyrinth sharp crested weir with downstream pool has been discussed. From Figure 3-8, it can be demonstrated that in the both free and submerged flow conditions TKE plunged to a minimum amount at the near free surface ($z/(h_o+P)$=0.85). In addition, the limited area between

the main sidewall and the smaller pool's sidewall was the critical area for TKE. For free flow condition,

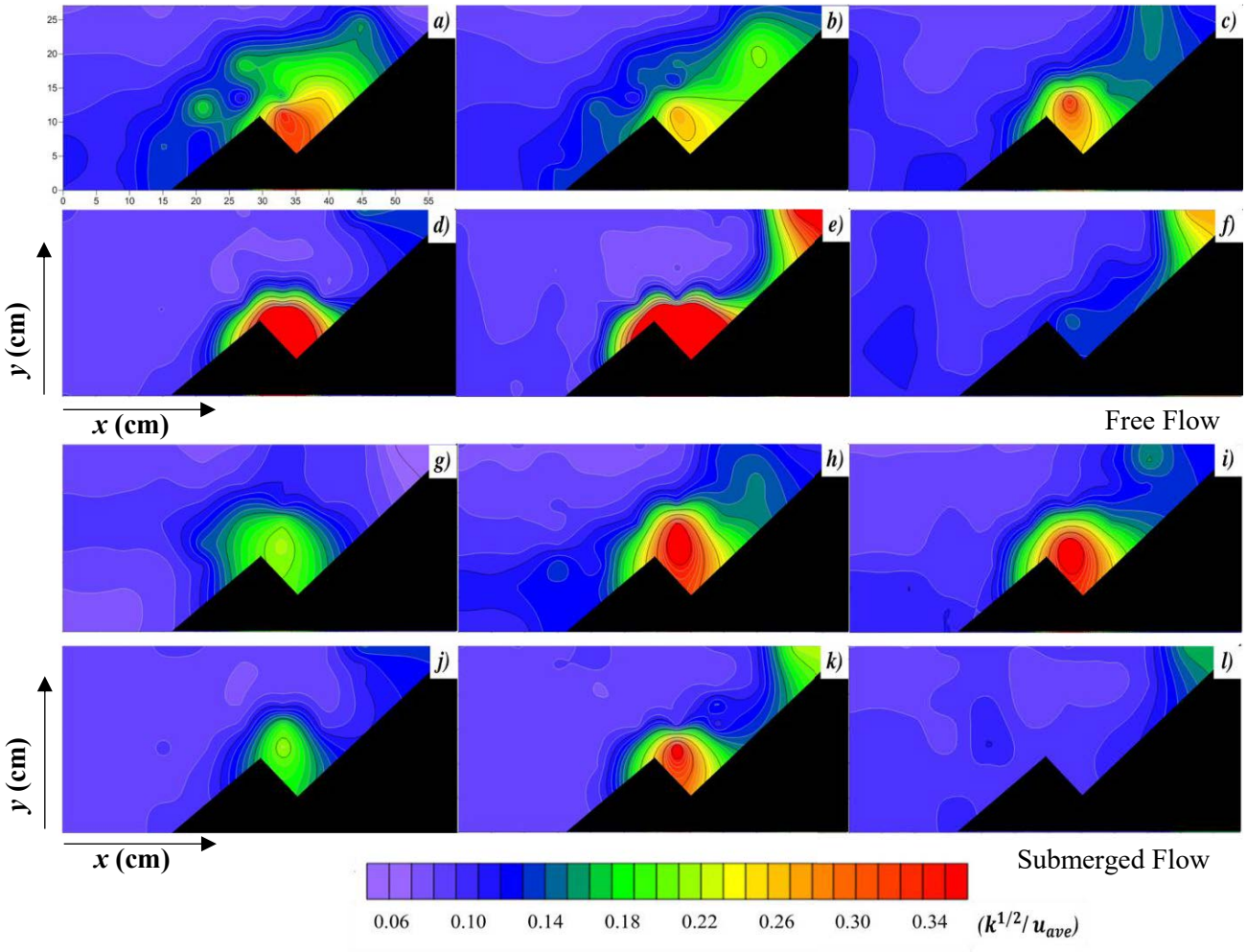


**Figure 3-8:** Contour plots of dimensionless turbulent kinetic energy ($k^{1/2}/u_{ave}$) for labyrinth weir with a downstream pool in free flow condition and submerged flow conditions; a) $z/(h_o+P)$=0.04; b) $z/(h_o+P)$=0.07; c) $z/(h_o+P)$=0.013; d) $z/(h_o+P)$=0.35; e) $z/(h_o+P)$=0.7; f) $z/(h_o+P)$=0.85; g) $z/(h_o+P)$=0.04, $t/h$=0.74; h) $z/(h_o+P)$=0.07, $t/h$=0.74; i) $z/(h_o+P)$=0.013, $t/h$=0.74; j) $z/(h_o+P)$=0.35, $t/h$=0.74; k) $z/(h_o+P)$=0.7, $t/h$=0.74; l) $z/(h_o+P)$=0.85, $t/h$=0.74.

TKE had additive trend by increasing the depth of the water $z/(h_o+P)$ before reaching to the $z/(h_o+P)$=0.7. It is noticeable that in the plane near to the channel's floor TKE had significant amount compared to the level above that plane. On the other hand, in the submerged flow condition, planes in the vertical distance saw a fluctuation in the TKE rate. In other words, it got

larger in critical area from flume's bed to the plane $z/(h_o+P)$=0.15 which is followed by descending until reached to the elevation $z/(h_o+P)$=0.35 before increasing again from that elevation to the depth $z/(h_o+P)$=0.7.

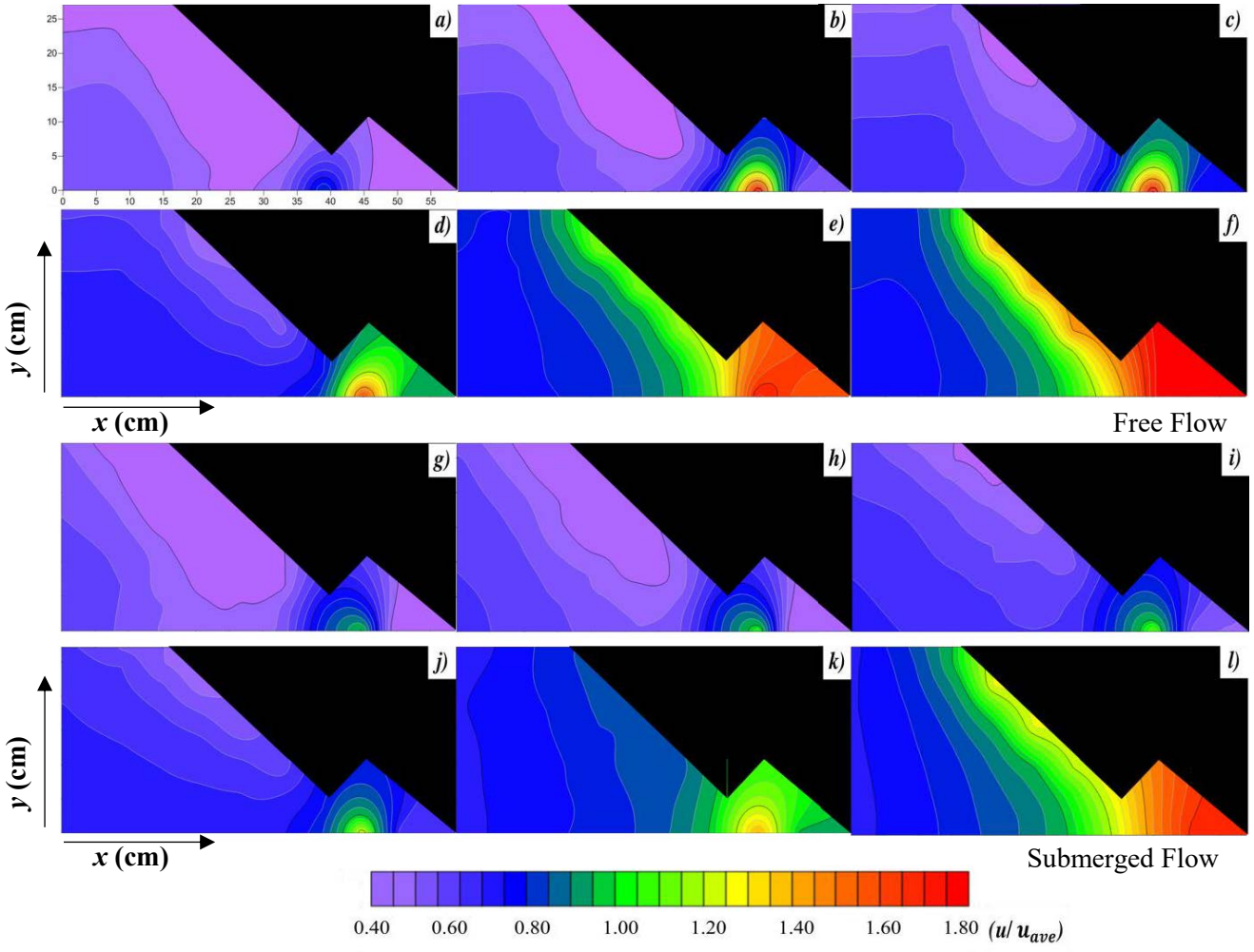


**Figure 3-9:** Contour plots of dimensionless axial velocity ($u/u_{ave}$) for labyrinth weir with an upstream pool in free flow condition and submerged flow conditions; a) $z/(h_o+P)$=0.04; b) $z/(h_o+P)$=0.07; c) $z/(h_o+P)$=0.013; d) $z/(h_o+P)$=0.35; e) $z/(h_o+P)$=0.7; f) $z/(h_o+P)$=0.85; g) $z/(h_o+P)$=0.04, $t/h$=0.74; h) $z/(h_o+P)$=0.07, $t/h$=0.74; i) $z/(h_o+P)$=0.013, $t/h$=0.74; j) $z/(h_o+P)$=0.35, $t/h$=0.74; k) $z/(h_o+P)$=0.7, $t/h$=0.74; l) $z/(h_o+P)$=0.85, $t/h$=0.74.

### 3.4 Velocity of Weirs with Upstream Pool

For two different free and submerged flow conditions, the variation of the dimensionless longitudinal velocity ($u/u_{ave}$) was plotted as a contour plot in $XY$ plane in different dimensionless elevations $z/(h_o+P)$ (Figure 3-9) for the triangular labyrinth sharp crested weir with upstream pool. It is observed from Figure 3-9 that the dimensionless longitudinal velocity ($u/u_{ave}$) reached to the maximum of its amount at the inside of the pool in all the planes for either free or submerged conditions. However, by increasing the depth $z/(h_o+P)$, the maximum velocity grew in that specific area. There was a gradual decrease in the longitudinal velocity in $0<X<30$ and a gradual rise in $30<x<45$ for both free and submerged flow conditions except for the planes near to the free surface ($z/(h_o+P)>0.7$). For ($z/(h_o+P)>0.7$). in the free and submerged flow condition, the velocity slightly increased in $15<X<60$ and $5<x<60$, respectively. It was observed that for all the planes lower than 85% of total depth ($z/(h_o+P)<0.85$), all the maximum longitudinal velocity occurred at $x=45$. In total, maximum ($u/u_{ave}$) in each planes for the free flow condition was higher than the maximum vertical velocity in the corresponding planes for the submerged flow condition.

Figure 3-10 presents the variation of the dimensionless lateral velocity ($v/u_{ave}$) contour plot in $XY$ plane along the upstream of the weir. It is observed from Figure 3-10 that the lateral direction of the flow near the edge of the main sidewall of the weir changed at $z/(h_o+P)=0.7$ from the leftward to the rightward for the both free and submerged flow conditions. For all conditions, close the weir's edge lateral velocity magnitude increased, however, for the planes lower than $0.7H$ by rising the depth $z/(h_o+P)$ magnitude of the lateral velocities declined compare with the corresponding points at the different planes. Generally, the transversal velocities magnitude for the free flow condition in the area near the weir's edge are higher than the transversal velocities magnitude for

the submerged flow condition in the same areas. As a result, it can be demonstrated that the most discharge happened from the apex of the weir.

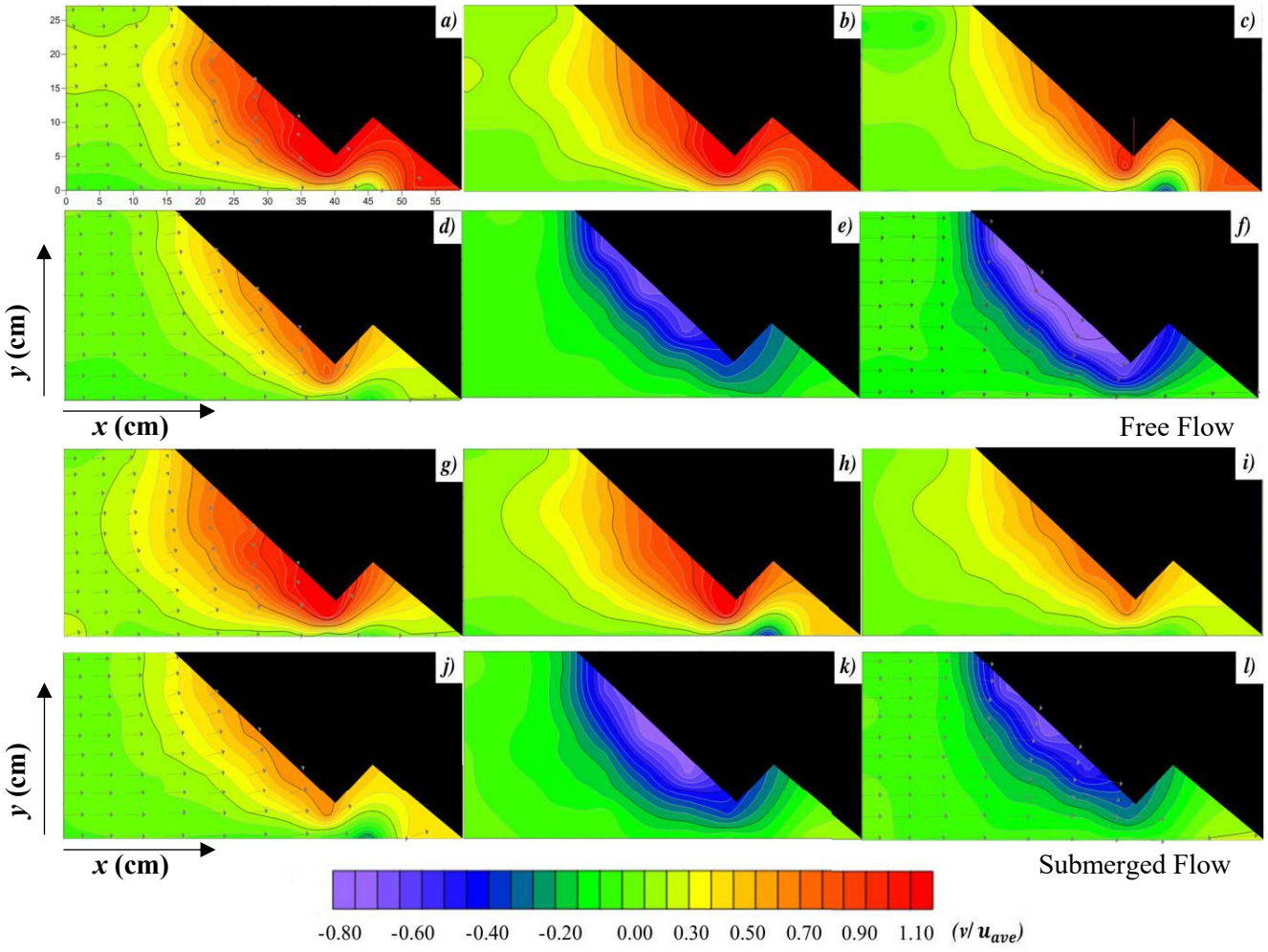


**Figure 3-10:** Contour plots of dimensionless lateral velocity ($v/u_{ave}$) for labyrinth weir with an upstream pool in free flow condition and submerged flow conditions; a) $z/(h_o+P)$=0.04; b) $z/(h_o+P)$=0.07; c) $z/(h_o+P)$=0.013; d) $z/(h_o+P)$=0.35; e) $z/(h_o+P)$=0.7; f) $z/(h_o+P)$=0.85; g) $z/(h_o+P)$=0.04, $t/h$=0.74; h) $z/(h_o+P)$=0.07, $t/h$=0.74; i) $z/(h_o+P)$=0.013, $t/h$=0.74; j) $z/(h_o+P)$=0.35, $t/h$=0.74; k) $z/(h_o+P)$=0.7, $t/h$=0.74; l) $z/(h_o+P)$=0.85, $t/h$=0.74.

In Figure 3-11, variation of the dimensionless vertical velocity, ($w/u_{ave}$) was plotted in *XY* plane. It is observed that the vertical velocity adjacent to the main sidewall was downward in the planes with elevations lower than or equal to 0.04 ($h_o+P$) in the both free and submerged flow conditions.

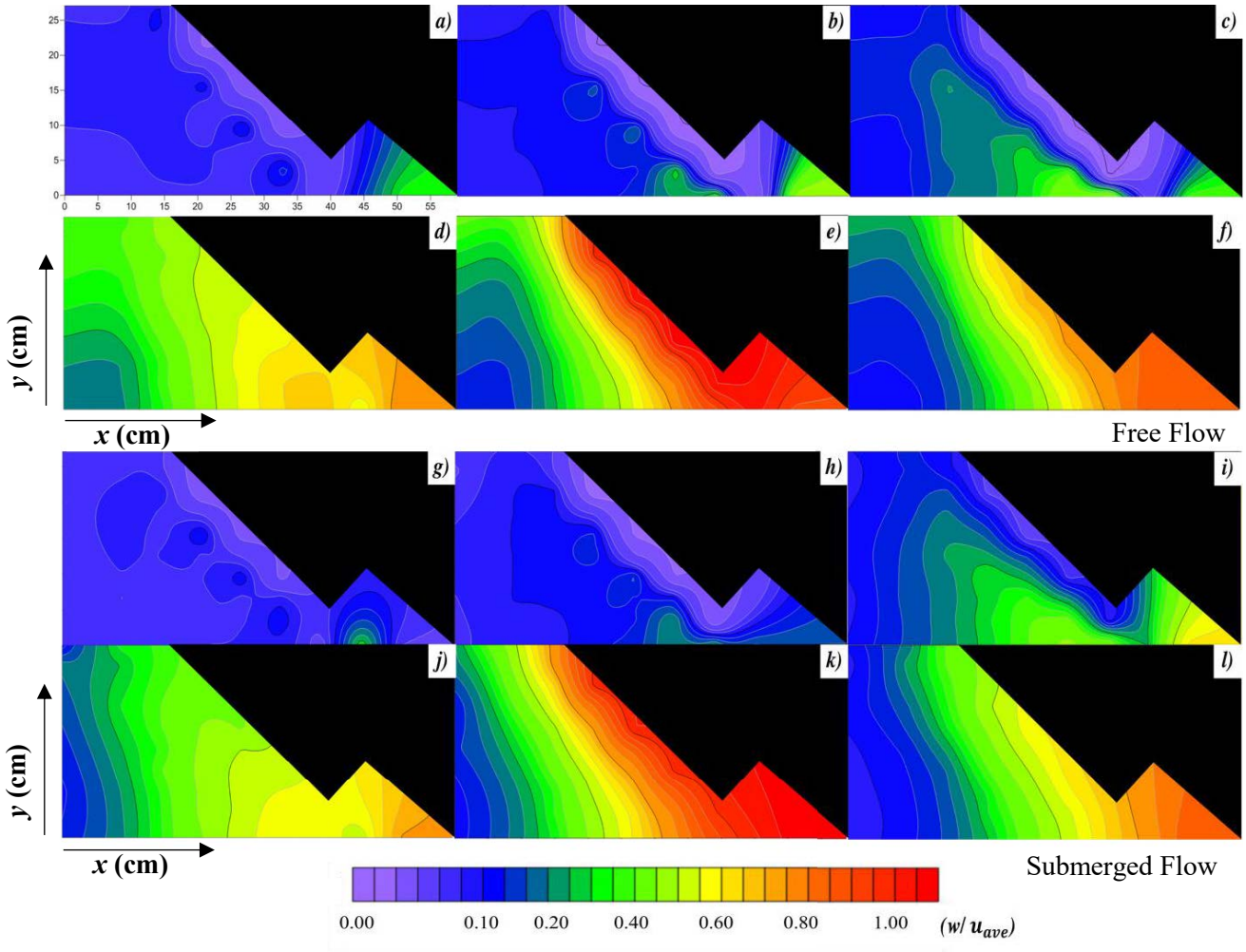


**Figure 3-11:** Contour plots of dimensionless lateral velocity ($v/u_{ave}$) for labyrinth weir with an upstream pool in free flow condition and submerged flow conditions; a) $z/(h_o+P)$=0.04; b) $z/(h_o+P)$=0.07; c) $z/(h_o+P)$=0.013; d) $z/(h_o+P)$=0.35; e) $z/(h_o+P)$=0.7; f) $z/(h_o+P)$=0.85; g) $z/(h_o+P)$=0.04, $t/h$=0.74; h) $z/(h_o+P)$=0.07, $t/h$=0.74; i) $z/(h_o+P)$=0.013, $t/h$=0.74; j) $z/(h_o+P)$=0.35, $t/h$=0.74; k) $z/(h_o+P)$=0.7, $t/h$=0.74; l) $z/(h_o+P)$=0.85, $t/h$=0.74.

In the vertex of the pool for the free and submerged flow, the vertical velocity was upward in all elevations. It was observed that $w/u_{ave}$ increased and reached to the peak in the both conditions by increasing the water depth from $z$=0.04 ($h_o+P$) to $z$=0.7 $z/(h_o+P)$ before declining again for the planes near to the free surface ($z$>0.7 $z/(h_o+P)$). As it can be seen in the Figure 3-11 by looking individually on planes for the water depth higher than or equal to 0.35$H$ and closing to the weir's edge for the both conditions, the vertical velocity had gradual increased.

### 3.5 Turbulent Kinetic Energy of Weirs with Upstream Pool

Figure 3-12 presents the variation of the turbulent kinetic energy (TKE) as a contour plot in *XY* plane along the upstream of the weir.

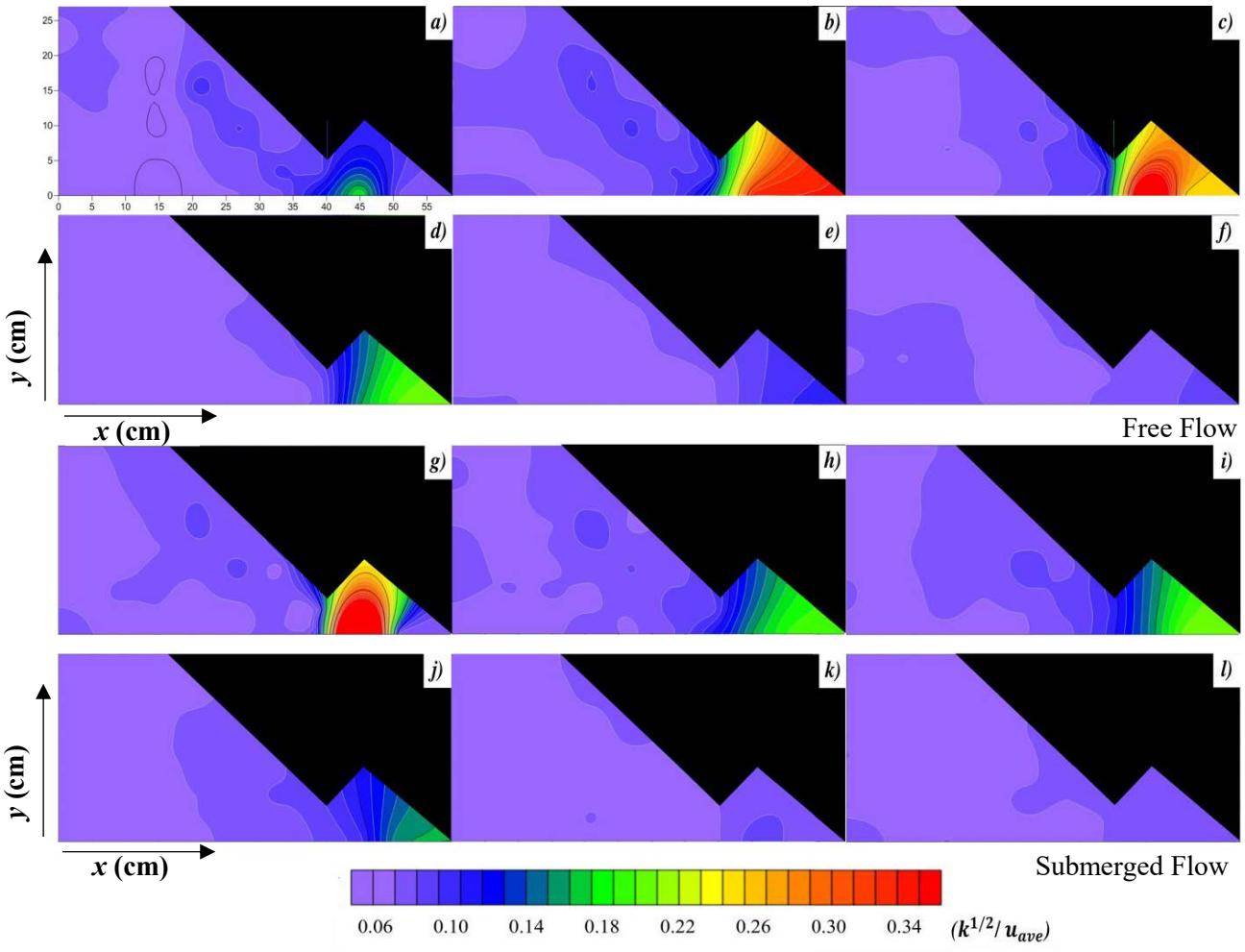


**Figure 3-12:** Contour plots of dimensionless turbulent kinetic energy ($k^{1/2}/u_{ave}$) for labyrinth weir with an upstream pool in free flow condition and submerged flow conditions; a) $z/(h_o+P)$=0.04; b) $z/(h_o+P)$=0.07; c) $z/(h_o+P)$=0.013; d) $z/(h_o+P)$=0.35; e) $z/(h_o+P)$=0.7; f) $z/(h_o+P)$=0.85; g) $z/(h_o+P)$=0.04, $t/h$=0.74; h) $z/(h_o+P)$=0.07, $t/h$=0.74; i) $z/(h_o+P)$=0.013, $t/h$=0.74; j) $z/(h_o+P)$=0.35, $t/h$=0.74; k) $z/(h_o+P)$=0.7, $t/h$=0.74; l) $z/(h_o+P)$=0.85, $t/h$=0.74.

It is observed from Figure 3-12 that in the pool of the weir, TKE in the free flow condition increased between adjacent bottom of the flume and $z$=0.04 ($h_o+P$). Subsequently, it decreased for the reminder of the elevations. However, for the submerged condition in the weir's pool the water

depth lower than 0.35($h_o$+$P$) saw an increase in the TKE rate by increasing the water depth, which followed by leveling off at the same rate for the rest of the water depth.

### 3.6 Point Analysis of Weirs with Downstream Pool

To further analyze the dissipation of energy in labyrinth weirs with a downstream pool, a power spectrum of all velocity components in longitudinal, transverse, and vertical directions was obtained from instantaneous velocity measurements in the location of maximum turbulent kinetic energy (i.e, $x/(h_o+P)$=0.50, $y/(h_o+P)$=0.24, and $z/(h_o+P)$=0.35). The sampling location for spectral analysis is shown in Figure 13b. Spectral analysis has been used in the literature to understand the magnitude and frequencies of turbulent eddies. This technique helps to better predict the influences of turbulence in hydraulic structures (Guan et al., 2018; Mignot and Cienfuegos, 2010).

Figure 3-13 shows the power spectra of all velocity components in free and submerged flow conditions. A line with a slope of –5/3, indicating the energy dissipation rate in Kolmogolov's inertial subrange, is added in Figure 3-13 for comparison. The power spectra of all velocity components in free flow conditions are shown in Figure 3-13a. A dominant frequency $f$ of 0.2 Hz was obtained for the longitudinal and vertical velocity signals. In free flow conditions, the energy dissipation through large eddies occurred with a slower rate than the Kolmogorov's inertial subrange. A slope of –1 was found to be a suitable representation of the energy cascade. Similar energy dissipation of larger eddies in wall-bounded turbulence was found in the literature (Nikora, 1999; Czernuszenko et al., 2007). Energy dissipation rates of the vertical velocity reach the Kolmogorov's inertial subrange for $f$>10 Hz. Figure 3-13b shows the power spectral density variations of all velocity components in submerged flow conditions (i.e., $t/h$=0.74). Due to submergence, the energy associated with the dominant frequency for longitudinal velocity (i.e.,

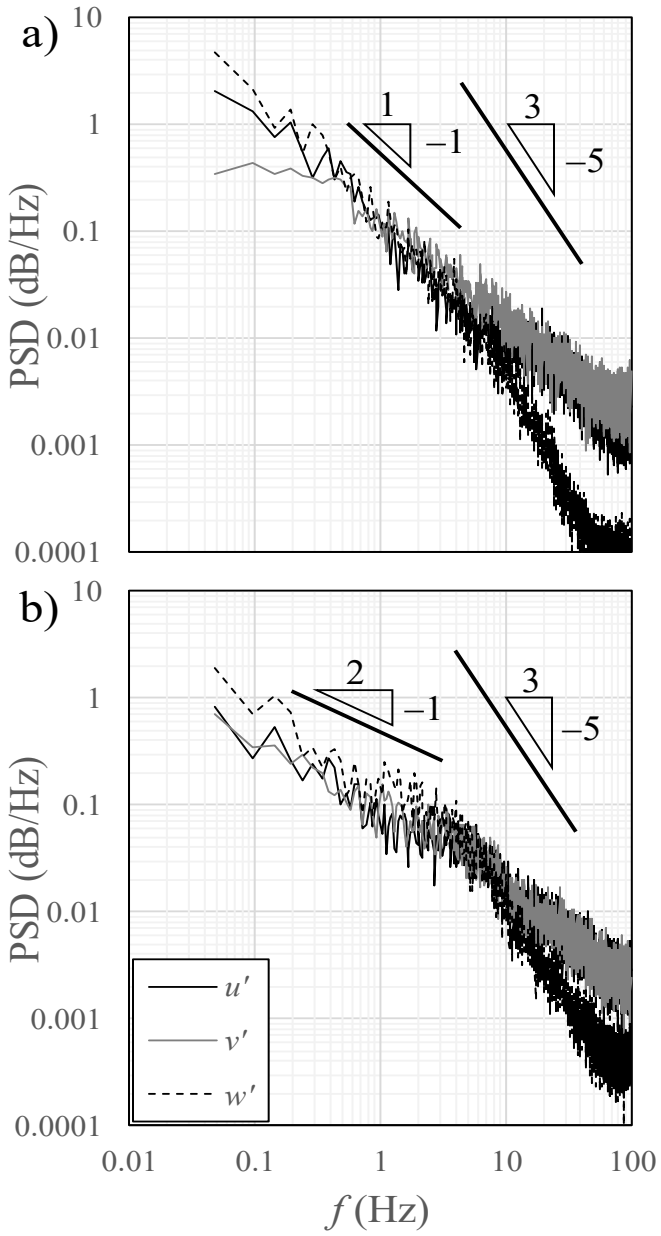


**Figure 3-13:** Power spectral density variations of axial, transverse, and vertical velocities for triangular labyrinth weirs with a downstream pool in the locations of the highest TKE; a) free flow; and b) submerged flow, $t/h$=0.74.

solid line) decreased from 1.0 dB/Hz to 0.3 dB/Hz, whereas the energies associated with the transverse and vertical velocity components remained unchanged. In submerged flow conditions, the energy cascade of large and low-frequency eddies is less than the Kolmogorov's inertial

subrange. As can be seen in Figure 3-13b, the kinetic energy of eddies with a frequency of less than 1 Hz decreased with a slope of –0.50.

Momentum transfer due to turbulent fluctuations can be quantified by investigating the direction and the magnitude of Reynolds shear stresses. Turbulent shear stresses can be decomposed into four quadrant events (Wallace, 2016). The positive velocity fluctuations in a vertical plane is classified as the first quadrant event $Q_1$ (+$u$', +$w$') and $Q_2$ contains the product of -$u$' and +$w$'. The third quadrant event $Q_3$ contains (-$u$', –$w$') and $Q_4$ contains (+$u$', –$w$'). The events in $Q_2$ and $Q_4$ contribute positively to the downward momentum flux and are called bursting/ejections and sweeps, respectively (Kline et al., 1967; Wallace, 2016). The sweep event $Q_4$ is characterized by the downward flow of high-speed fluid towards the boundary. The $Q_4$ event results in the motion of flow with low-concentration sediment toward the bed. In contrast, the bursting event $Q_2$ is defined as the upward flow of low-speed fluid containing high concentration of sediments. The $Q_2$ event contributes to sediment dispersion in vertical direction and away from the bed. The events $Q_1$ and $Q_3$ are called outward and inward interactions respectively. Both quadrants two and four contain velocity fluctuations with opposite signs indicating the contribution of Reynolds shear stress in turbulent mixing, whereas $Q_1$ and $Q_3$ have similar signs indicating the elongation and stretch of turbulent eddies. The contribution to Reynolds shear stress from these events provides a key insight about the sediment transport process and mixing (Papanicolaou et al., 2002; Hamidouche et al., 2018). The ratio of the turbulent momentum transfer due to turbulence ($Q_1$+$Q_3$) and the momentum transfer due to mean velocity gradient ($Q_2$+$Q_4$) is called the exuberance ratio (ER). This ratio is defined and adopted to quantitatively study the quadrant events and the coherent structures in turbulent flows (Shaw et al., 1983; Viestenz and Cal, 2016). Studying the magnitude and location of minimum exuberance ratios can provide more information on sediment transport

and erosion in the vicinity of hydraulic structures (Cellino and Lemmin, 2004; Nezu and Azuma, 2004; Bey et al., 2007).

Figure 3-14 shows the contour plot of the exuberance ratio for both free and submerged flow conditions in three different depths of $z/(h_o+P)$=0.04, 0.35, and 0.85. As can be seen, the exuberance ratio was less than unity in all water levels. This indicates that the bursting and sweep events generated by mean velocity gradients are dominant. In free flow conditions, the exuberance ratio slightly varied in the bed. A balance between the gradient-type Reynolds stresses ($Q_2+Q_4$) and non-gradient-type stresses ($Q_1+Q_3$) was observed around the weir's neck with ER=1. A minimum exuberance ratio of 1/6 was observed in both free and submerged flow conditions. The regions of low ER in free and submerged flow conditions are found in sections (a-a) and (b-b), respectively. The presence of local minimum exuberance ratio in the mid-water depth indicates a strong turbulent mixing and high potential of sediment re-suspension (see section (a-a) in Figure 3-14b). The locations of minimum exuberance ratios change as the weir submerges. The change in the location of minimum ER can be seen in section (b-b) in Figures 3-14d and 3-14e. The high turbulent mixing region in free flow conditions (section a-a) shifted towards the oblique walls (section b-b) and towards the bed.

Effects of submergence on the flow mixing and sediment transport of the proposed weir model are investigated by analyzing the distribution of exuberance ratios in vertical planes (a-a) and (b-b) as shown in Figure 3-14a. Section (a-a) is located in the pool vertex (i.e., $x$=0m), and section (b-b) is located in the neck ($x$=19 cm), where the turbulent kinetic energies are minimum and maximum respectively. As can be seen from Figure 3-15a, the minimum exuberance ratio corresponding to the highest mixing potential in section (a-a) was located 10 cm above the bed. As the flow approached the neck region (i.e., section (b-b)), the minimum ER region split into two regions with

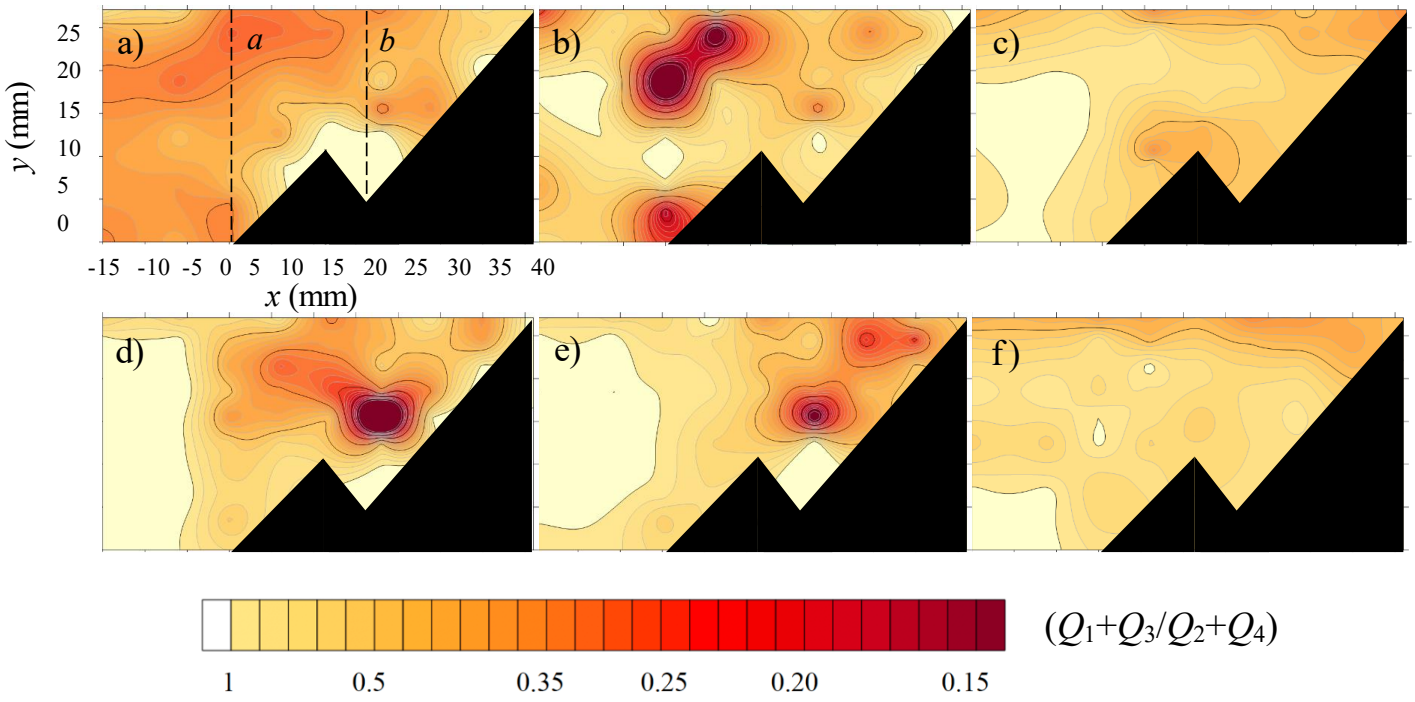


**Figure 3-14**: Contour plots of the exuberance E ratio $(Q_1+Q_3)/(Q_3+Q_1)$ for triangular labyrinth weir with a downstream pool in free flow condition and submerged flow conditions and different depths; a) $z/(h_o+P)$=0.04, free flow; b) $z/(h_o+P)$=0.35, free flow; c) $z/(h_o+P)$=0.85, free flow; d) $z/(h_o+P)$=0.04, t/h=0.74; e) $z/(h_o+P)$=0.35, $t/h$=0.74; f) $z/(h_o+P)$=0.85, $t/h$=0.74.

relatively less intensity. The magnitude of the gradient-type quadrants (i.e., $Q_2$ and $Q_4$) increases close to the neck wall due to the existence of mean shear stresses. As shown in Figure 3-15b, the average exuberance ratio in section (b-b) was smaller than the average ER in section (a-a). This indicates a higher mixing strength in section (b-b) due to strong wall shear stresses. The high mixing zone in section (b-b) covered almost 2/3 of the total water depth. The effect of submergence on the distribution of exuberance ratio in vertical sections of (a-a) and (b-b) are shown in Figures 3-15c and 3-15d, where the local minimum exuberance ratio shifted from section (a-a) in free flow to section (b-b) in submerged flow. The strong mixing region in section (b-b) covered one-half of the water depth, from the bed to $z/(h_o+P)\approx0.50$.

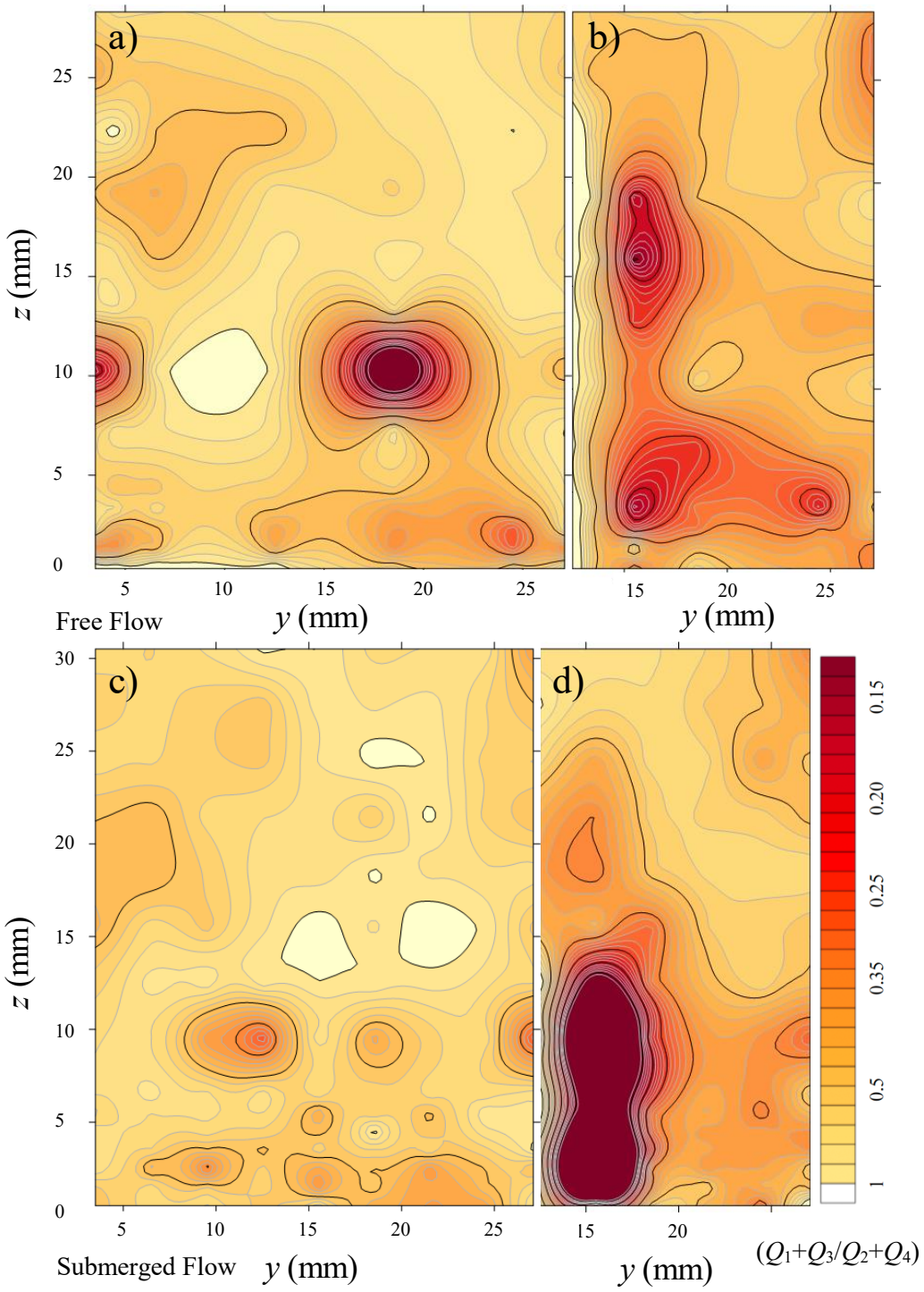


**Figure 3-15:** Vertical plane distribution of exuberance for labyrinth weir with a downstream pool in free and submerged flow conditions; a) $x$=0, free flow, b) $x$=160 mm, free flow, c) $x$=0, submerged flow, d) $x$=160 mm, submerged flow.

Figure 3-16 shows the quadrant maps of the fluctuating component of velocity *u*' and *w*' in the vertical plane (x-z) at the locations of the minimum exuberance ratio (i.e., sections (a-a) and (b-b)) in free and submerged flow conditions and for three different levels of $z/(h_o+P)$=0.04, 0.35, and 0.85. Velocity fluctuations were normalized by the cross-sectional averaged velocity *U* and data were contoured in terms of probability densities of 98%, 95%, and 90%. The darkest zones in each plot indicate the ranges of velocity fluctuations with a probability of occurrence of 90%. In addition, the sizes and shapes on the joint probability distribution functions (JPDFs) in different water levels and flow conditions demonstrate different turbulence properties. A circular shape in JPDFs indicates an isotropic turbulence structure which normally occurs in free flow condition and away from the bed, and can be seen in the middle and right columns in Figures 3-16a and 3-16b. The velocity fluctuations close to the bed (i.e., $z/(h_o+P)$=0.04) showed a similar turbulent intensity for both free and submerged flow conditions and appear as an elliptical shape. It was found that the magnitude of the longitudinal velocity fluctuations are almost twice the magnitude of the vertical velocity fluctuations.

A significant change in the structure of turbulence occurred in the neck region (section b-b) at $z/(h_o+P)$=0.35 when the flow regime changed from free to submerged. A careful examination of data in free and submerged flow conditions and at $z/(h_o+P)$=0.35 reveals that the magnitude of both velocity fluctuations increased in submerged flow conditions, however, Figure 3-8d and 3-8j show the turbulent kinetic energies slightly decreased from free to submerged flow conditions. This reveals the significance of the transverse velocity fluctuations *v*' in the neck region and in free flow condition. Close to the water surface (i.e., $z/(h_o+P)$=0.85), velocity fluctuations in both free and submerged flow conditions remained unchanged. The middle plots in Figures 3-16b and 3-16d show the change in the turbulent structure. In this specific location, velocity fluctuations

were isotropic with a symmetrical distribution in free flow condition (i.e., circular JPDFs) whereas in submerged flow condition, the normalized JPDFs adopted an elliptical shape with a major axis skew into the $Q_2$ and $Q_4$ quadrants.

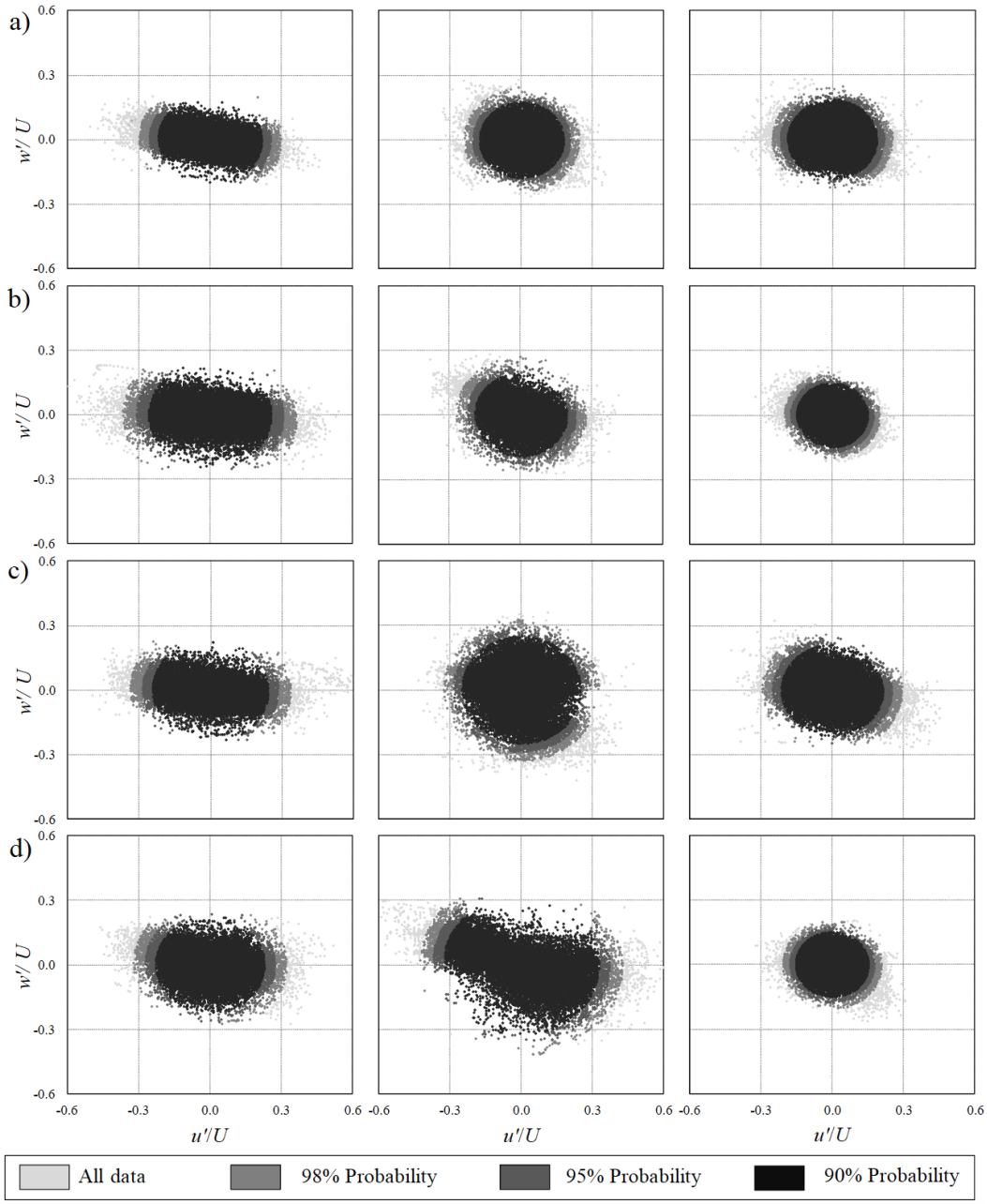


**Figure 3-16:** Joint probability distribution functions (JPDFs) of normalized velocity fluctuations $u'/U$ and $w'/U$ at the locations of the minimum exuberance ratio in sections (a-a) and (b-b) and in free and submerged flow conditions. Left column ($z/(h_0+P)$=0.04), middle column ($z/(h_0+P)$=0.35), and right column ($z/(h_0+P)$=0.85); a) section (a-a), free flow; b) section (b-b), free flow; c) section (a-a), submerged flow; d) section (b-b), submerged flow.

# Chapter 4

## Hydraulic and Dynamic Behaviour of Weir-Pool Fishway with Triangular Labyrinth Weirs with Downstream and Upstream Pools.

### 4.1. Experimental Setup

Experiments were conducted in weir-pool fishways with two kinds of labyrinth sharp-crested weir upstream and downstream pool as well as with three different distances 1.5, 1.0 and 0.75 meter and different flow discharges. The weir models were fabricated in a flume at the water research laboratory at the Lakehead University. The length, height, and width of the flume were 12 m, 0.5 m and 0.61 m, respectively. The longitudinal slope was adjusted at 3% built by wooden sheets. The wooden ramp consisted of an arrangement of wooden sharp-crested weirs. These weirs have been fabricated in two downstream pool and upstream pool shapes with $L_p$= 0.22 m also the height of each weir was 0.13 m and was attached to 0.02 m of base (i.e., the base was used in order to glue and detach weirs easily). The weirs placed along the whole flume extension. A total of 4 weirs were arranged and glued by silicon glue with 1.5 m, 1 m and 0.75 m distances apart. For hydraulic analysis, seven different discharges (0.007 $m^3/s$, 0.0098 $m^3/s$, 0.0194 $m^3/s$, 0.0198 $m^3/s$, 0.025 $m^3/s$, 0.028 $m^3/s$, 0.032 $m^3/s$) and for dynamic analysis three different flowrates (0.0194 $m^3/s$, 0.025$m^3/s$, 0.032 $m^3/s$) have been served. The discharges were measured using an inline magnetic flowmeter with an accuracy of ± 0.01 L/s (FMG-3102, Omega, Quebec, Canada). Water depths were measured with a point gauge with accuracy of 0.01mm. Velocity was measured with an Acoustic Doppler Velocimeter (ADV) probe (Vectrino, Nortek, Norway). A three-dimensional linear stage with an accuracy of ±0.5 mm was employed to replace the ADV through measurement points. Measurements were taken in the measurement zone as shown in Figurer 4-1.

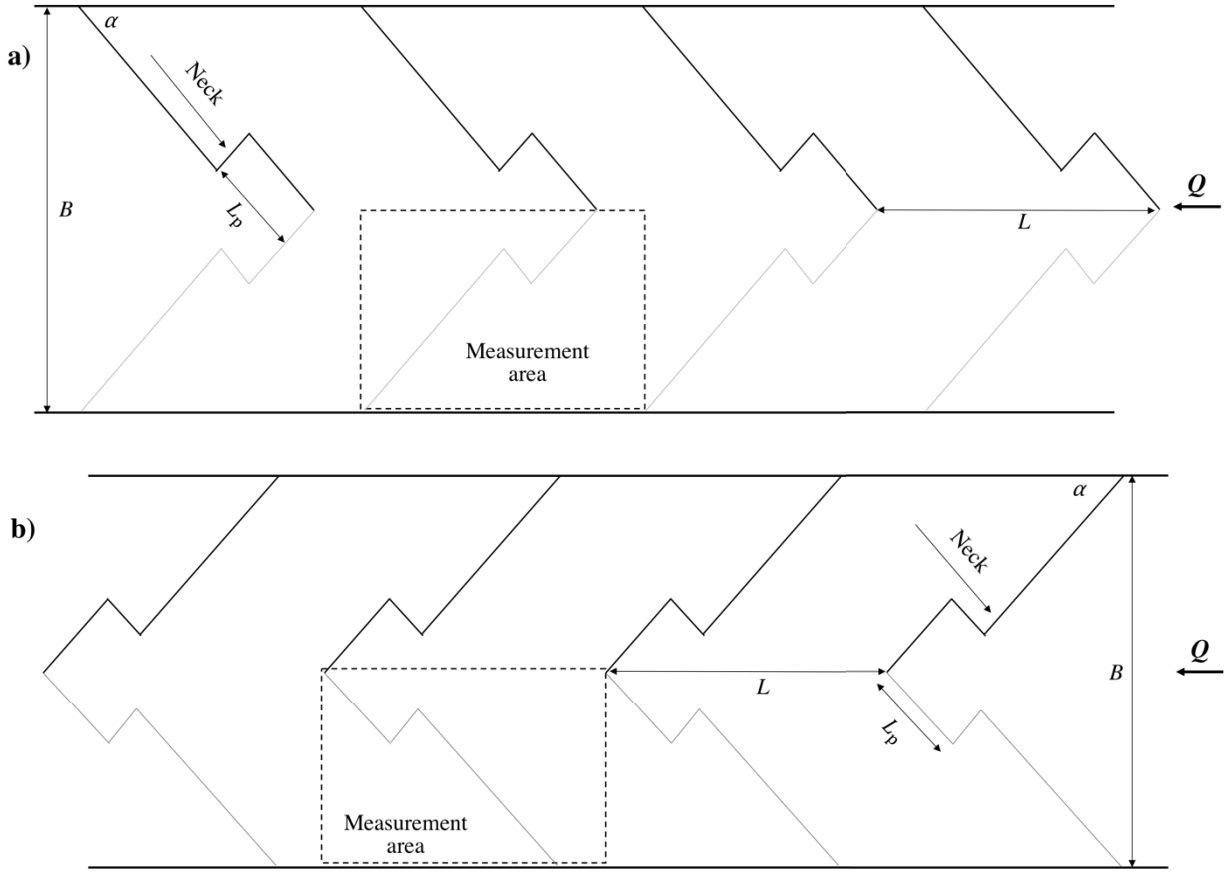


**Figure 4-1:** Top view schematics for fishway with triangular labyrinth weirs with a downstream pool and an upstream pool; a) downstream pool; b) upstream pool.

Instantaneous velocity measurements were carried out in 341 and 318 points for downstream pool and upstream pool, respectively, in three different flowrates (1977 measurements in total). Measurement points were 60 mm apart in the longitudinal direction $x$ and 30 mm apart in the transverse direction $y$ (see Figure 4-2). The probe was located 5cm+0.25$H$ above the bottom of the flume, where $H$ is level of the water. Two types of data were taken with the ADV probe; short velocity time series (2 min duration) for spatial analysis and long velocity time series (30 min duration) for point analysis. Sampling frequency was set to 200 Hz and the sampling volume was a cylinder with a height of 7 mm was located at 0.25$H$ above the flume's bottom.

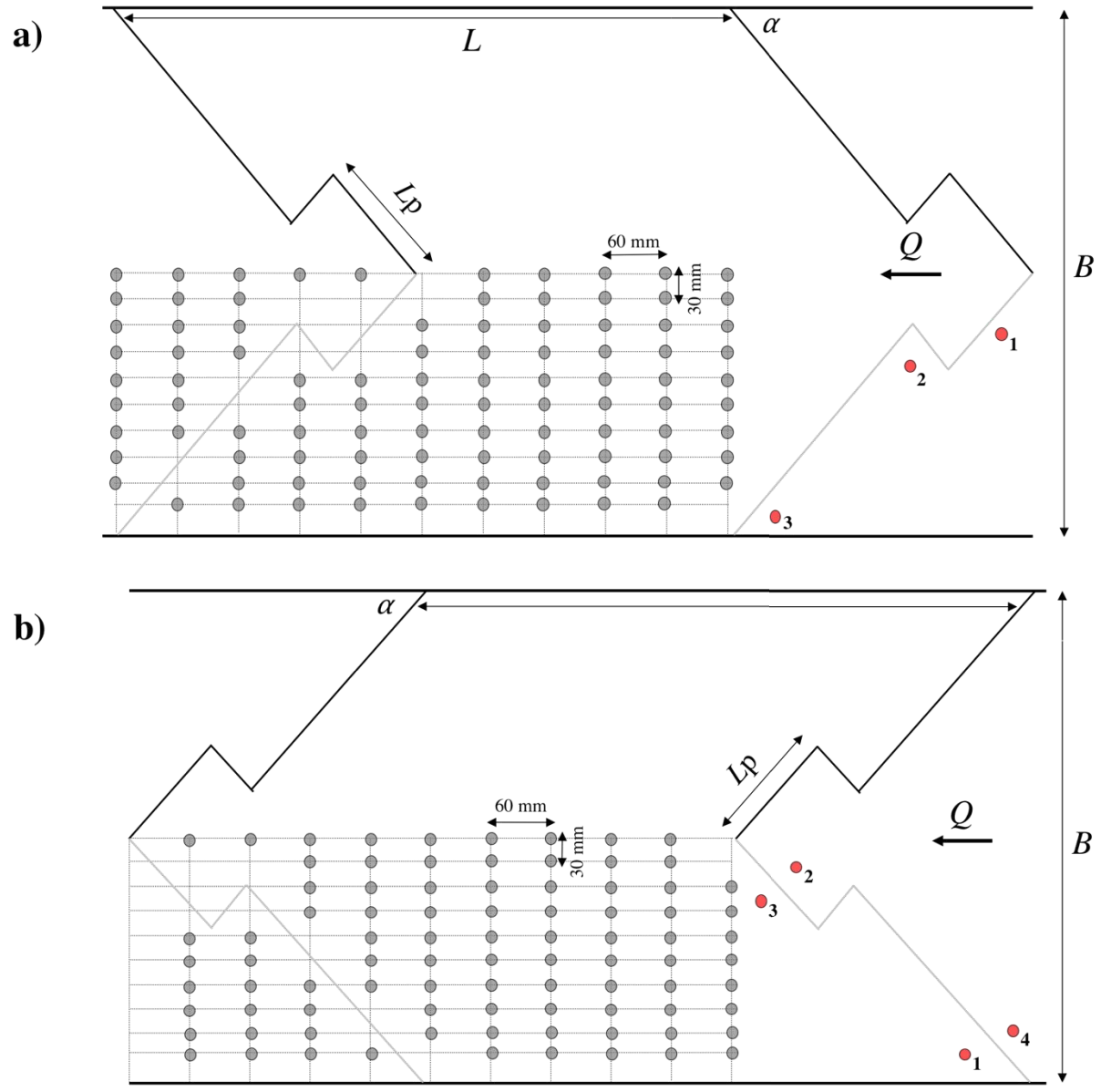


**Figure 4-2:** Top view schematics and ADV measurement points for triangular labyrinth weirs with a downstream pool and a upstream pool; a) downstream pool; b) upstream pool.

During data sampling with ADV, statistical parameters such as the signal-to-noise ratio (SNR), data correlation, and signal amplitude were observed to secure the quality of measurements. Velocity time series were noisy because the flow was highly turbulent and contained significant air bubbles (average correlation and signal-to-noise ratio was about 65 and 20, respectively).

Hence, the data were filtered by the Phase-Space Thresholding (PST) method proposed by Goring and Nikora (2002) using WinADV as recommended by Wahl (2003). Approximately 10.4% of instantaneous velocity data were removed by this filter. Linear interpolation was applied between measurement points to improve the visual quality of contour plots.

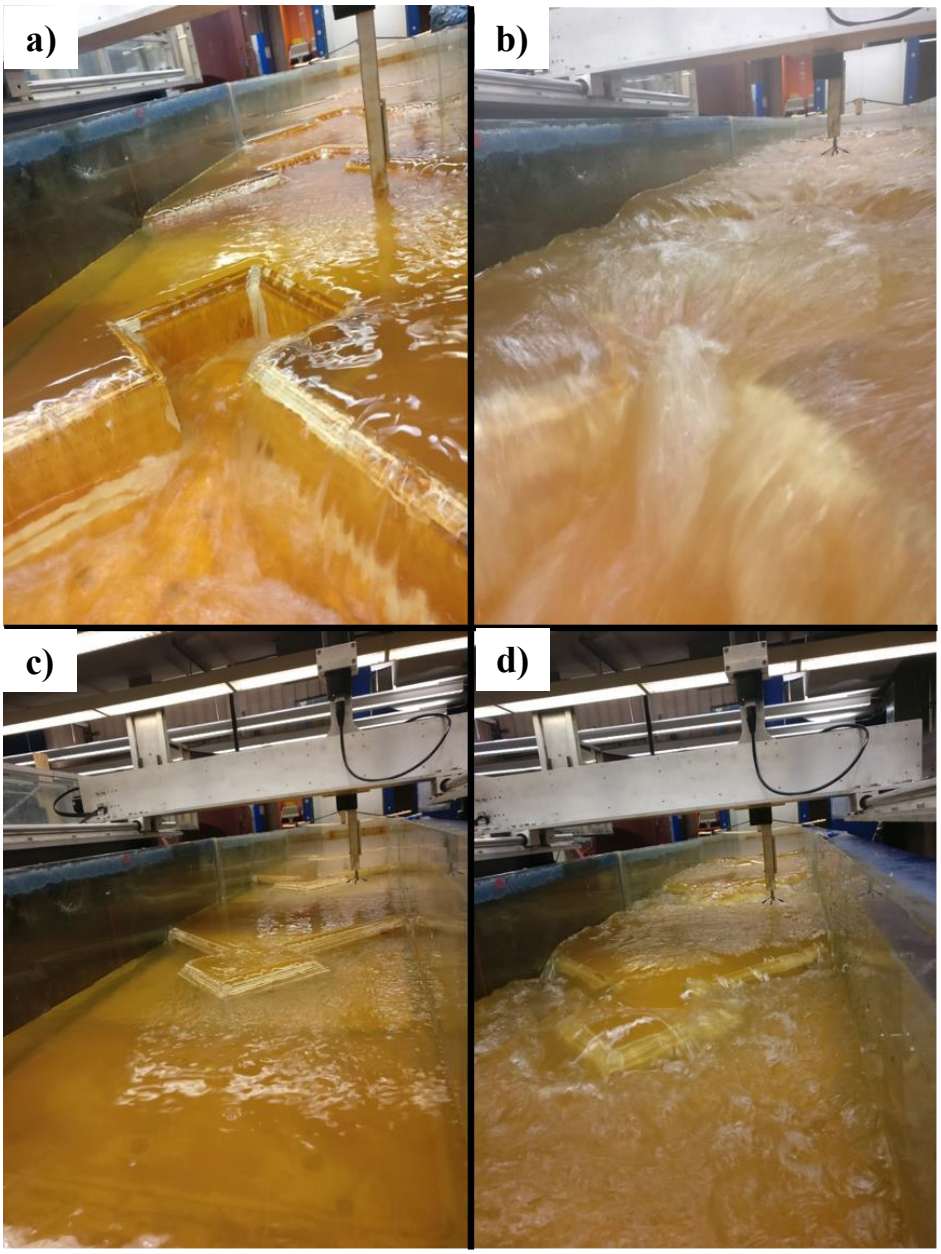


**Figure 4-3:** View of experimental setup; a) fishway with downstream pool weir $Q$=24.8 *L/s*, 0.75 *m* distance; b) fishway with downstream pool weir $Q$=42.4 *L/s*, 0.75 *m* distance; c) fishway with upstream pool weir $Q$=24.8 *L/s*, 1 *m* distance; d) fishway with upstream pool weir $Q$=31.1 *L/s*, 1 *m* distance.

For point analysis, three and four points have been chosen at the downstream pool and the upstream pool, respectively, for 1 m and 0.75 m distances (see Figure 4-2). To compute the spectral and autocorrelation functions, these data were filtered with a modified PST technique (mPST) proposed by Parsheh et al. (2010).

## 4.2 Hydraulic Analysis

### 4.2.1 Flow regimes

Clay (1961) was one of the initial researchers who characterized the plunging, transitional, and streaming or shooting flow regimes in pool and weir fishways. Rajaratnam et. al. (1988) confirmed the observation of Clay and expanded quantitative descriptions for these regimes. These regimes are indeed the major flow regimes found in traditional pool and weir fishways. However, Ead et. al (2004) found in their study that when the bed slope, weir spacing, and height are varied over a larger range, several sub-regimes were found to exist in addition to a supercritical jet flow. In plunging flow, plunging jet dives into the pool creating two rotating cells or eddies. The first eddy with a clockwise rotation, is positioned under the plunging jet from the weir and is also confined by the bed and the weir. The second eddy is located near the surface and forms immediately downstream of the line where the plunging jet enters the pool. This counterclockwise rotating surface eddy is somewhat similar to the surface roller of a hydraulic jump. When the flow regime tends to alter form plunging to transitional flow, even though, this flow patterns bear some similarity to the plunging regimes, there are substantial differences in the flow structure and the water surface profiles. The surface roller is comparatively shorter and shallower. The bounded roller, positioned under the nap, expands downstream to the middle of the pool. Plunging-transitional regime takes place at, or shortly after weir submergence sets in.

In transitional flow regime, the significant flow features of this regime are the larger clockwise rotating cell, the elevated plunging jet, the absence of the surface eddy, and the wavy water surface. In transitional-streaming flow regime, it shares some resemblance to the flow pattern of a fully developed streaming flow. In a general sense, transitional-streaming state has the clockwise circulating cell and the overriding surface flow resemble the streaming flow but, the effects of the transitional regime do still exist. Supercritical jet flow regime is simply a plunging jet that impinges into the bed to form a supercritical jet and is followed by a hydraulic jump (Ead et. al, 2004).

Two dimensionless parameters $Q_t^*$ and $L/d$, where $Q_t^*$ is dimensionless discharge at transition, $L$ is pool spacing and $d$ is height of weir, were developed to predict the flow regimes. Figure 4-4a shows distinct domains for each flow regime. Firstly, the observed hydraulics from each experiment confirmed that plunging flows can occurred for values of $L/d$ greater than unity if the corresponding range of $Q_t^*$ is smaller than 0.5. The majority of experiments in this study were identified as plunging flow. Secondly, transitional flows can occur for shorter pool spacing (i.e., for $L/B$ equal to 1.2, where $B$ is width of the flume) if the corresponding range of $Q_t^*$ is greater than 0.4. Thirdly, supercritical jet flows can take place for values of $L/B$ equal to 1.6 if the $Q_t^*$ is smaller than 0.4. These observations compared well with Ead et. al (2004) while there are some differences with the study of Baki et. al (2017). The probable differences in $Q_t^*$ between this study and Baki et. al (2017) is the geometry of the fishway and the composition of boulders instead of solid wall.

An additional dimensionless parameter, relative submergence ($H/d$), was defined by Baki et. al (2017) to identify the transition regime between plunging and transitional flow regimes, where $H$ is the pool averaged water depth and d is the diameter of rocks. They specified the threshold as $H/d$ equals to 1.6 which for values greater than 1.6 the transitional flow regime will occur. Figure

4-4b indicates that the threshold defined by Baki et. al (2017) cannot be compared well with this study since the geometry of the weirs are different.

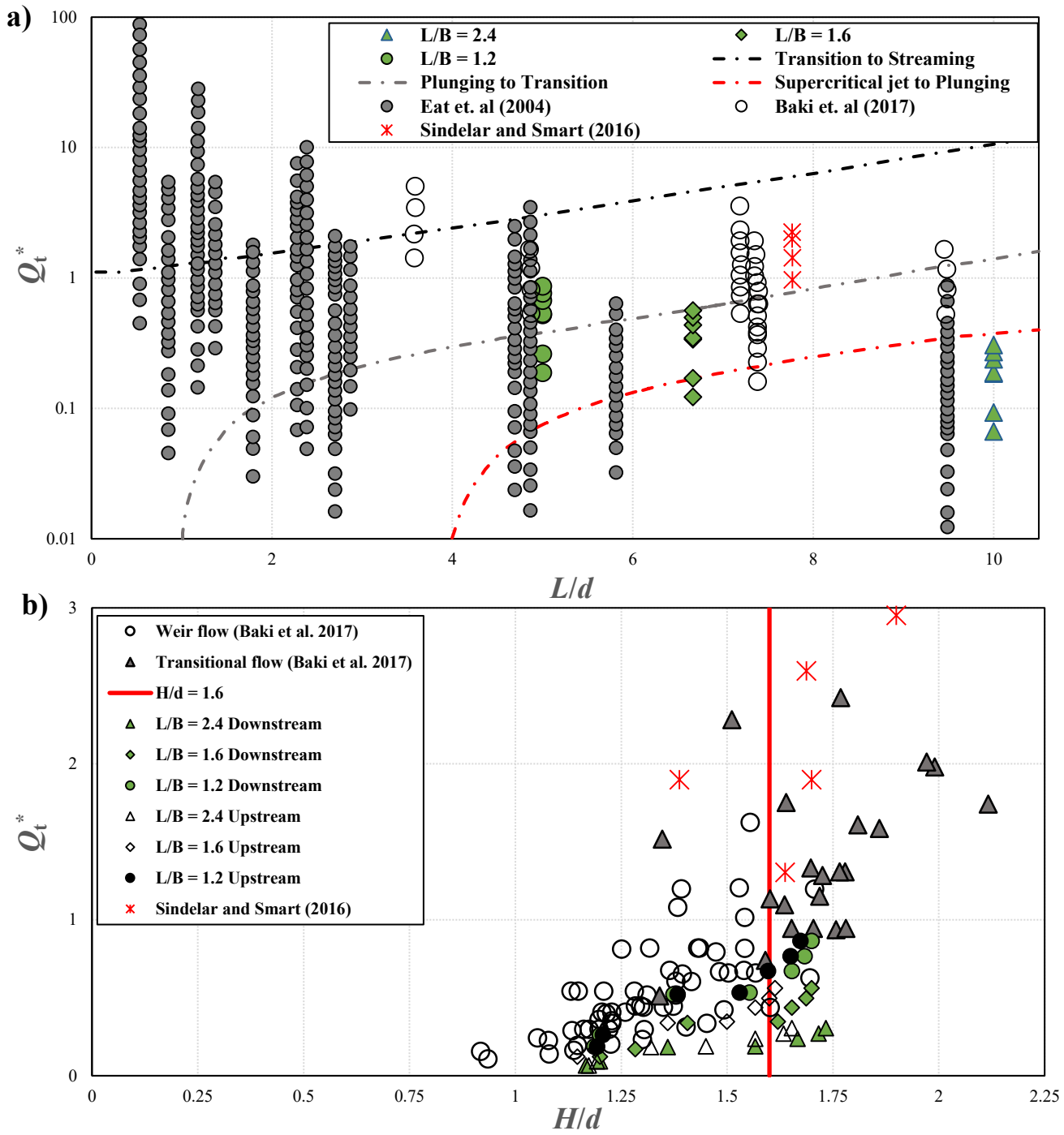


**Figure 4-4:** (a) Consolidated plot of the four different flow regimes based on $Q_t^*$ and $L/d$ for all weir-pool fishway design and (b) weir and transitional regimes based on $Q_t^*$ and $H/d$.

Figure 4-5 shows the variation of $Q_+$ versus $h/d$ for the present experiments and those of Ead et. al (2004) where $h$, is height of water over the weir. It can be observed that the experimental data for this study fits well with Eat et. al (2004). The Rehbock's equation was used by Ead et. al (2004) to estimate $C_d$ as

$$Q_+ = 0.57+0.075\ h/d \tag{4-1}$$

which the data in this study fits well with this equation except for low flow rate ($Q$=0.007 $m^3/s$). Also, Figure 4-5 indicates that $Q_+$ is a function of $h/d$.

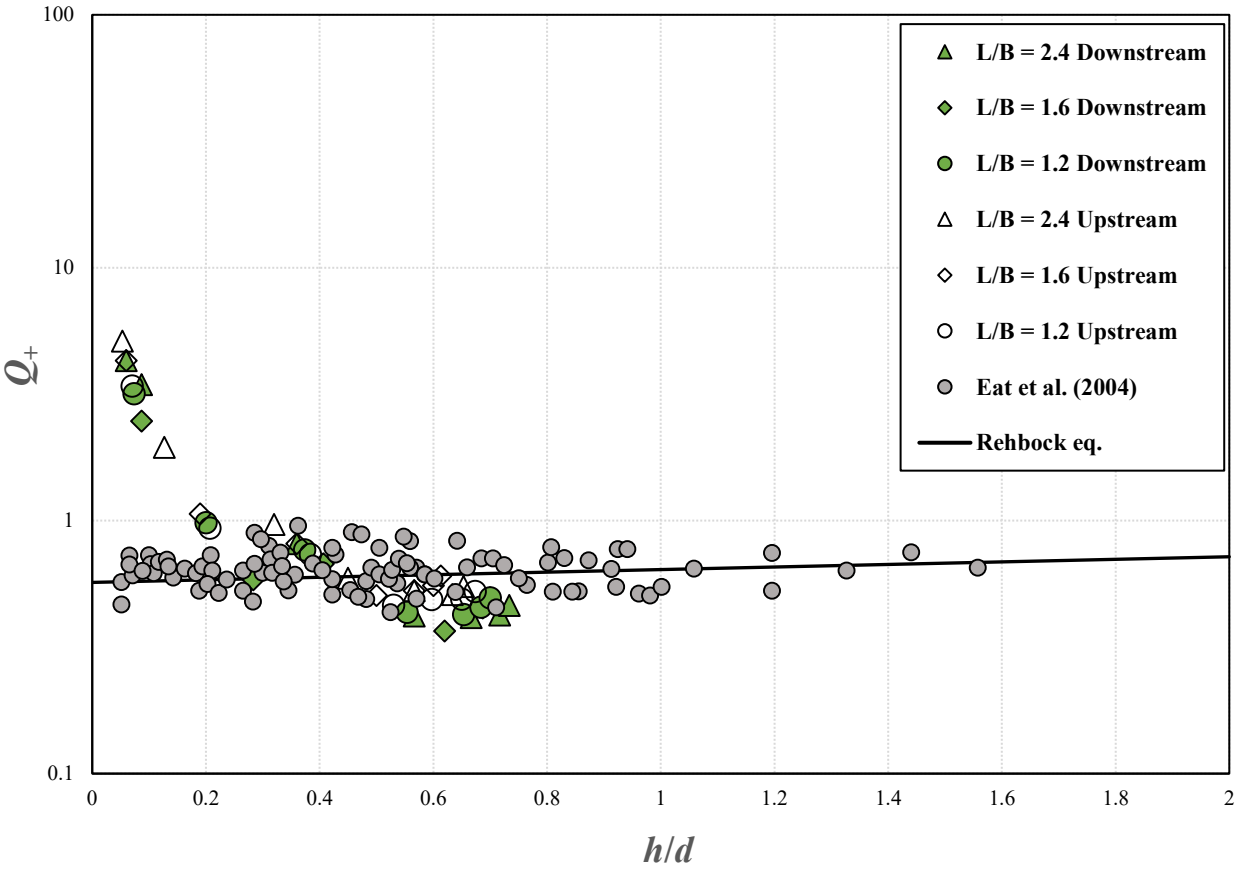


**Figure 4-5:** Plunging flow variation of $Q_+$ with $h/d$.

### 4.2.2 Stage-discharge relationship

A stage-discharge analysis was performed using the standard weir equation,

$$Q = 2/3 b_w \, C_d \sqrt{2g} \, h^{3/2} \quad (4\text{-}2)$$

The head over the weir, $h$, was calculated by subtracting the height of the weir from the mean water elevation in the pool and was used to determine the discharge coefficient $C_d$. For open channel flow, the velocity is a function of the square root of the channel slope, so $C_d$ was plotted against the head over the weir divided by the square root of the bed slope (Figure 4-6). It can be observed that when $C_d$ was plotted against head over the weir divided by the square root of the channel slope, the discharge coefficients yield a curve which can be represented by,

$$C_d = 0.285(h/\sqrt{s})^{-0.9} \quad (4\text{-}3)$$

It indicates that discharge coefficients in this study are lower than the results of Kupferschmidt et. al (2017) because not only, did the discharge in their experiments took place over the weir, but also, it occurred through the gaps between the boulders.

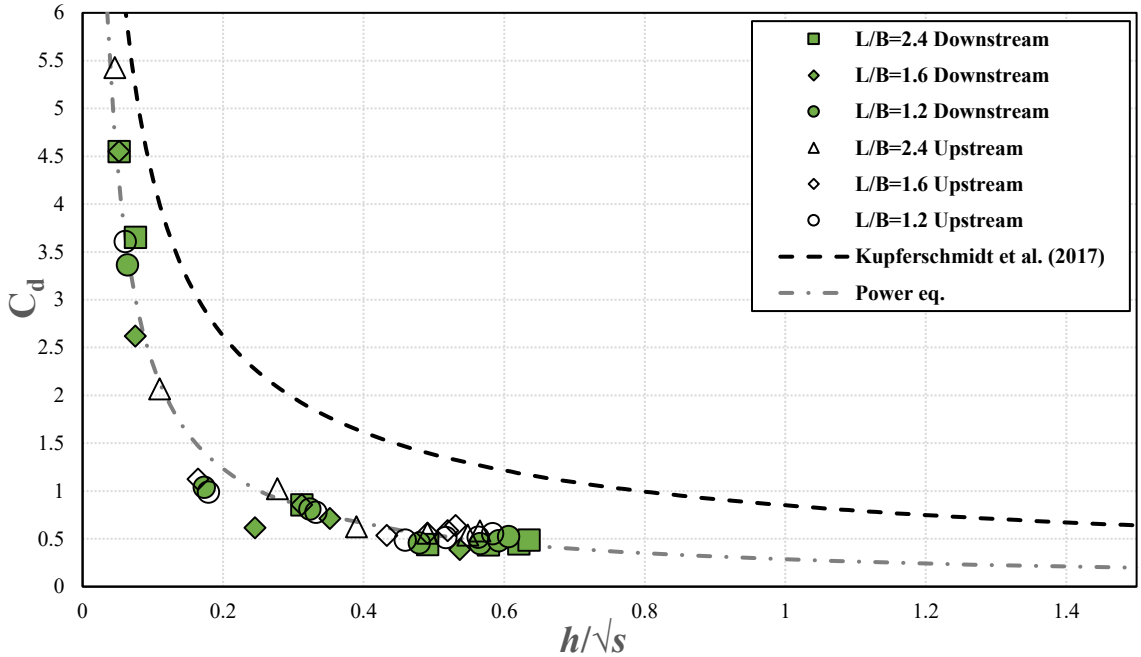


**Figure 4-6:** The discharge coefficient shown as a function of the head normalized by the square root of the bed slope. Applying relationship $C_d = 0.285(h/\sqrt{s})^{-0.9}$ produced a R-squared value of 0.9495.

### 4.2.3 Energy dissipation

Pool type fishways are developed to cause energy dissipation to contribute higher water depth and lower current velocity in the downstream pool section while persisting acceptably low levels of turbulence (Towler et al., 2015). The average volumetric energy dissipation rate ($k$) in a pool is calculated using following basic formula,

$$k = \rho g Q S_0 / BH \quad (4\text{-}4)$$

where $\rho$ is the density of water and $H$ is the average depth of a pool. The relationship between $k$ and $q$ (flow rate per unit channel width or specific discharge) was plotted for the inquiry relating to channel and structure configuration in Figure 4-7a. Energy dissipation, $k$, generally increases with specific discharge, $q$; for example, $k$ increases from 21 to 64 W/m$^3$ as specific discharge increases from 0.011 to 0.053 m$^2$/s. This is consistent with the finding of Yagsi (2010), Baki et. al (2017b) and Kupferschmidt et. al (2017) who found energy dissipation, $k$, increased with increasing discharge at the constant bed slope for a pool-weir and rock-weir fishway (Figure 4-7b). However, due to dissimilarity in geometry of the fishway between this study and Baki et. al (2017b), it was found that the energy dissipation corresponding with the same specific discharge and bed slope ($S_0$=3%) is lower than the data of Baki et. al (2017b). This indicates that the weir layouts have significant influence on the energy dissipation, $k$. The exponent in a power relationship between volumetric energy dissipation and specific discharge is 0.7 for all series which is 6% greater than the exponent finding by Baki er. al (2017b) for the same flow regime. This dissimilarity occurs since a plunging flow regime is present, which is dominated by eddies located under the plunging jet from the weir and close to the surface which are varied in length depending on the physical dimensions of the pool and the discharge (Ead et. al 2004).

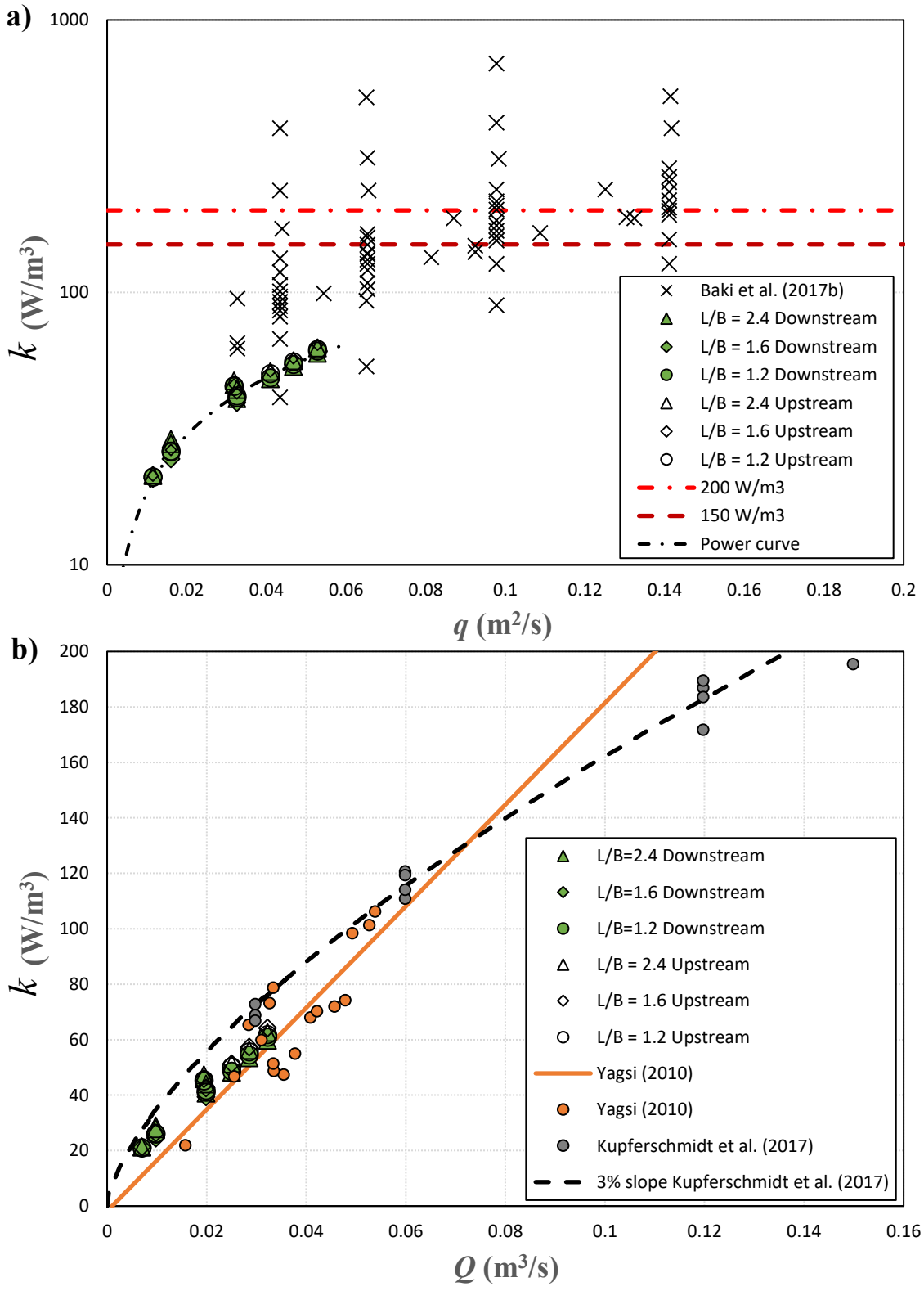


**Figure 4-7:** (a) Relationship between average volumetric energy dissipation rate $k$ and flow rate per unit channel width (specific discharge) for all series; (b) Relationship between average volumetric energy dissipation rate $k$ and flow rate.

According to Teijeiro et al. (2006) and Larinier (2008), the average volumetric energy dissipation rate should not exceed 200 w/m$^3$ for large salmon and sea trout and 150 w/m$^3$ for smaller shad and riverine species. For all series, the average volumetric energy dissipation rates were below both criteria of 150 and 200 w/m$^3$.

### 4.2.4 Slow velocity zone

The zones of slow velocity are crucial for fish resting (Baki et al. 2017b). The availability of these zones for different flow rates, weir layouts, and pool spacing was examined by measuring velocities in 3 different dimensions and calculating distribution of that in a horizontal plane at $z$= 0.25$H$, assuming that the target fish species typically like to swim in a horizontal plane at $z$= 0.25$H$. Results are presented for 0.0194, 0.025 and 0.032 m$^3$/s. These distributions provide an estimate of the average percentage of the pool area (i.e., slow velocity zones) present in the horizontal plane, where fish will rest for short periods without expending excessive energy (Wang et al. 2010). For the engineered pool-weir fishway, Bell (1986) recommended that velocity must be kept under 0.3 m/s in 30%–50% of the volume of the pool. Assuming that the velocity must be kept under 0.4$U_{max}$ (Baki et al. 2016), the experimental results of pool-weir fishway in this study confirmed that the average percentage of areas where the velocity is lower than 0.4$U_{max}$ ranged from 16% to 71% for the upstream pool layout where the pool spacing ranged from 1.2$B$ to 2.4$B$ and $Q$ = 0.019 to 0.032 m$^3$/s. The average percentage of areas where the velocity is lower than 0.4$U_{max}$ ranged from 10% to 57% for the downstream pool layout where the pool spacing range from 1.2$B$ to 2.4$B$ and $Q$ = 0.019 to 0.032 m$^2$/s. It was found that an increase in pool spacing from 1.2$B$ to 2.4$B$ increased the resting area for all series except for the downstream pool layout with $Q$ = 0.019 and 0.025 m$^3$/s and the upstream pool layout with $Q$ = 0.019 m$^3$/s. For the former ($Q$ = 0.025 m$^3$/s) increasing the pool spacing from 1.2$B$ to 1.6$B$ resulted in resting area increasing from 26.5% to 46.9%, the

increased from 1.6*B* to 2.4*B* resulted in a declined to 38.62%. For the latter design, increasing pool spacing from 1.2*B* to 1.6*B* resulted in resting area increasing from 46.27% to 57.43%; the increased from 1.6*B* to 2.4*B* resulted in a declined to 54.44% (see Table 1). For the rock-weir fishway (Baki et al. 2017b) found that increasing pool spacing from 0.5*B* to 2.5*B* increased areas where the velocity is lower than $0.4U_{max}$ from 29% to 48%, the increase from 2.5*B* to 3*B* resulted in a decline to 35%.

**Table 1:** Flow characteristics and weir geometrics of fishway with downstream and upstream pool design; * sign indicates ADV experiments.

| Experiment Number | Weir Model | *L*/*B* | $Q_f$ (l/s) | Depth of the center pool (*Y*) (cm) | *Y*/*B* | $Q_+$ | $Q_t^*$ | $C_d$ | *k* (W/m$^3$) | $U_{max}$ (cm/s) | Areas with velocity lower than 0.4 $U_{max}$ (%) |
|---|---|---|---|---|---|---|---|---|---|---|---|
| 1 | MP-D-0.15 | 1.2 | 7.00 | 0.16 | 0.26 | 3.18 | 0.19 | 3.37 | 20.97 | | |
| 2 | MP-D-0.15 | 1.2 | 9.76 | 0.18 | 0.30 | 0.98 | 0.26 | 1.04 | 26.15 | | |
| 3 | MP-D-0.15* | 1.2 | 19.43 | 0.21 | 0.34 | 0.77 | 0.52 | 0.81 | 45.49 | 63.67 | 25.30 |
| 4 | MP-D-0.15 | 1.2 | 19.85 | 0.23 | 0.38 | 0.43 | 0.53 | 0.46 | 41.09 | | |
| 5 | MP-D-0.15* | 1.2 | 25.00 | 0.25 | 0.41 | 0.43 | 0.67 | 0.45 | 48.62 | 80.98 | 26.50 |
| 6 | MP-D-0.15 | 1.2 | 28.52 | 0.25 | 0.41 | 0.46 | 0.77 | 0.48 | 54.47 | | |
| 7 | MP-D-0.15* | 1.2 | 32.20 | 0.26 | 0.42 | 0.50 | 0.87 | 0.53 | 60.90 | 83.62 | 53.00 |
| 8 | MP-D-0.15 | 1.6 | 7.00 | 0.16 | 0.27 | 2.47 | 0.12 | 2.62 | 20.71 | | |
| 9 | MP-D-0.15 | 1.6 | 9.76 | 0.19 | 0.32 | 0.58 | 0.17 | 0.62 | 24.45 | | |
| 10 | MP-D-0.15* | 1.6 | 19.43 | 0.21 | 0.35 | 0.68 | 0.34 | 0.72 | 44.41 | 62.25 | 61.06 |
| 11 | MP-D-0.15 | 1.6 | 19.85 | 0.24 | 0.40 | 0.37 | 0.35 | 0.39 | 39.40 | | |
| 12 | MP-D-0.15* | 1.6 | 25.00 | 0.25 | 0.41 | 0.43 | 0.44 | 0.45 | 48.62 | 79.25 | 46.90 |
| 13 | MP-D-0.15 | 1.6 | 28.52 | 0.25 | 0.41 | 0.45 | 0.50 | 0.48 | 54.37 | | |
| 14 | MP-D-0.15* | 1.6 | 32.20 | 0.26 | 0.42 | 0.50 | 0.56 | 0.53 | 60.90 | 81.03 | 38.05 |
| 15 | MP-D-0.15 | 2.4 | 7.00 | 0.16 | 0.26 | 4.29 | 0.07 | 4.55 | 21.23 | | |
| 16 | MP-D-0.15 | 2.4 | 9.76 | 0.16 | 0.27 | 3.45 | 0.09 | 3.66 | 28.88 | | |
| 17 | MP-D-0.15* | 2.4 | 19.43 | 0.20 | 0.33 | 0.81 | 0.18 | 0.86 | 45.93 | 58.72 | 71.03 |
| 18 | MP-D-0.15 | 2.4 | 19.85 | 0.24 | 0.39 | 0.42 | 0.19 | 0.44 | 40.74 | | |
| 19 | MP-D-0.15* | 2.4 | 25.00 | 0.25 | 0.41 | 0.41 | 0.24 | 0.44 | 48.23 | 69.51 | 38.62 |
| 20 | MP-D-0.15 | 2.4 | 28.52 | 0.26 | 0.42 | 0.42 | 0.27 | 0.45 | 53.42 | | |

| | | | | | | | | | | | |
|---|---|---|---|---|---|---|---|---|---|---|---|
| 21 | MP-D-0.15* | 2.4 | 32.20 | 0.26 | 0.43 | 0.46 | 0.31 | 0.49 | 59.73 | 71.21 | 16.55 |
| 22 | MP-U-0.15 | 1.2 | 7.00 | 0.16 | 0.26 | 3.41 | 0.19 | 3.61 | 21.04 | | |
| 23 | MP-U-0.15 | 1.2 | 9.76 | 0.18 | 0.30 | 0.94 | 0.26 | 0.99 | 26.01 | | |
| 24 | MP-U-0.15* | 1.2 | 19.43 | 0.21 | 0.34 | 0.74 | 0.52 | 0.78 | 45.16 | 72.38 | 46.27 |
| 25 | MP-U-0.15 | 1.2 | 19.85 | 0.23 | 0.38 | 0.46 | 0.53 | 0.49 | 41.72 | | |
| 26 | MP-U-0.15* | 1.2 | 25.00 | 0.24 | 0.39 | 0.49 | 0.67 | 0.52 | 50.35 | 88.83 | 39.39 |
| 27 | MP-U-0.15 | 1.2 | 28.52 | 0.25 | 0.41 | 0.49 | 0.77 | 0.52 | 55.57 | | |
| 28 | MP-U-0.15* | 1.2 | 32.20 | 0.25 | 0.41 | 0.53 | 0.87 | 0.56 | 61.87 | 95.38 | 30.30 |
| 29 | MP-U-0.15 | 1.6 | 7.00 | 0.16 | 0.01 | 4.29 | 0.12 | 4.55 | 21.23 | | |
| 30 | MP-U-0.15 | 1.6 | 9.76 | 0.18 | 0.01 | 1.06 | 0.17 | 1.13 | 26.37 | | |
| 31 | MP-U-0.15* | 1.6 | 19.43 | 0.20 | 0.01 | 0.81 | 0.34 | 0.86 | 45.93 | 70.96 | 57.43 |
| 32 | MP-U-0.15 | 1.6 | 19.85 | 0.23 | 0.01 | 0.51 | 0.35 | 0.54 | 42.55 | | |
| 33 | MP-U-0.15* | 1.6 | 25.00 | 0.24 | 0.17 | 0.53 | 0.44 | 0.56 | 51.31 | 74.91 | 37.84 |
| 34 | MP-U-0.15 | 1.6 | 28.52 | 0.24 | 0.04 | 0.55 | 0.50 | 0.59 | 57.31 | | |
| 35 | MP-U-0.15* | 1.6 | 32.20 | 0.24 | 0.02 | 0.60 | 0.56 | 0.64 | 64.18 | 77.78 | 30.63 |
| 36 | MP-U-0.15 | 2.4 | 7.00 | 0.16 | 0.26 | 5.12 | 0.07 | 5.43 | 21.37 | | |
| 37 | MP-U-0.15 | 2.4 | 9.76 | 0.17 | 0.28 | 1.95 | 0.09 | 2.07 | 27.85 | | |
| 38 | MP-U-0.15* | 2.4 | 19.43 | 0.20 | 0.32 | 0.97 | 0.18 | 1.03 | 47.33 | 55.45 | 54.44 |
| 39 | MP-U-0.15 | 2.4 | 19.85 | 0.22 | 0.36 | 0.59 | 0.19 | 0.63 | 44.02 | | |
| 40 | MP-U-0.15* | 2.4 | 25.00 | 0.24 | 0.39 | 0.53 | 0.24 | 0.56 | 51.31 | 61.16 | 22.22 |
| 41 | MP-U-0.15 | 2.4 | 28.52 | 0.25 | 0.40 | 0.51 | 0.27 | 0.54 | 56.14 | | |
| 42 | MP-U-0.15* | 2.4 | 32.20 | 0.25 | 0.41 | 0.55 | 0.31 | 0.58 | 62.62 | 62.16 | 10.00 |

## 4.3 Dynamic Analysis

### 4.3.1 Turbulent flow field for fishway with downstream pool weirs

The distribution of flow properties was plotted in contour plot to examine the physical characteristics of potential habitat used by fish. Considering that the overbar means the average in time of the variable below it, Figure 4-8 shows the spatial distribution of main velocity for fishway with downstream pool weir, $\sqrt{\bar{u}^2 + \bar{v}^2 + \bar{w}^2}$, where $u$, $v$ and $w$ are the longitudinal, lateral, and vertical instantaneous velocities, respectively. Main velocity contour plot has been used instead of

any other directions such as longitudinal velocity since fish are sensitive to the magnitude of the velocity more than its direction. The contour plot shows a high variability controlled by distance between weirs as less distance is more variability of velocity magnitude. In general, low velocity were found in the corner of the weir's pool and weir's side wall as well as inside the weir's pool for 0.75 m distance while the upstream velocity was high. On the other hand, for 1 m distance between weirs, the low velocity replaced to the upstream side of the weir and high velocity occurred in the corner of the weir and the flume. No significant variability in velocity magnitude in 1.5 m distance was found. The maximum dominant velocity for distance 0.75 m was 63.67 cm/s, 80.98 cm/s and 83.62 cm/s for low, medium, and high flow discharge, respectively, while low mean velocity for the same distance and for all the flow discharge was around 5 cm/s. The maximum mean velocity for 1 m distance was found to be 62.65 cm/s, 79.25 cm/s and 81.03 cm/s for low, medium, and high flow discharge, respectively Whereas, low dominant velocity magnitude for the same distance was 10 cm/s for medium, and high flowrates and 5 cm/s for low flowrate. For 1.5 m distance, the maximum mean velocity was around 70 cm/s for medium and high flow discharge and 60 cm/s for low flow discharge while minimum mean velocity was around 10 cm/s for medium and high flow discharge and 4 cm/s for low flow discharge. Some relative rapid currents with velocities ranging from 20 cm/s to 50 cm/s and slow flow regions with velocities less than 20 cm/s exist and may be found by fish passing thorough these fishway structures.

Figure 4-9 shows spatial distribution of plane Reynolds shear stress for fishway with a downstream pool weir, - $\overline{\rho u'v'}$ with $\rho$ being water density and $u'$, $v'$ being the longitudinal and lateral fluctuating velocities, respectively. Reynolds shear stress for distance 0.75 m and high discharge varied from -20 Pa to +20 Pa that is perfectly comparable with the study of Breton et al. (2013), which worked on the nature like fishway with rocky ramp, with exception of couple of points which are greater

than this amount. It was found that by increasing the distance between the weirs as well as decreasing the flowrate this range becomes smaller as in 1.5 m distance most of the points had the Reynolds shear stress value between -10 Pa to 10 Pa. The Fish prefers a path with low values of turbulent stress and it starts from corner of the weir and the flume, passing near the main side wall of the weir until crossing from neck of the weir for 0.75 m distance.

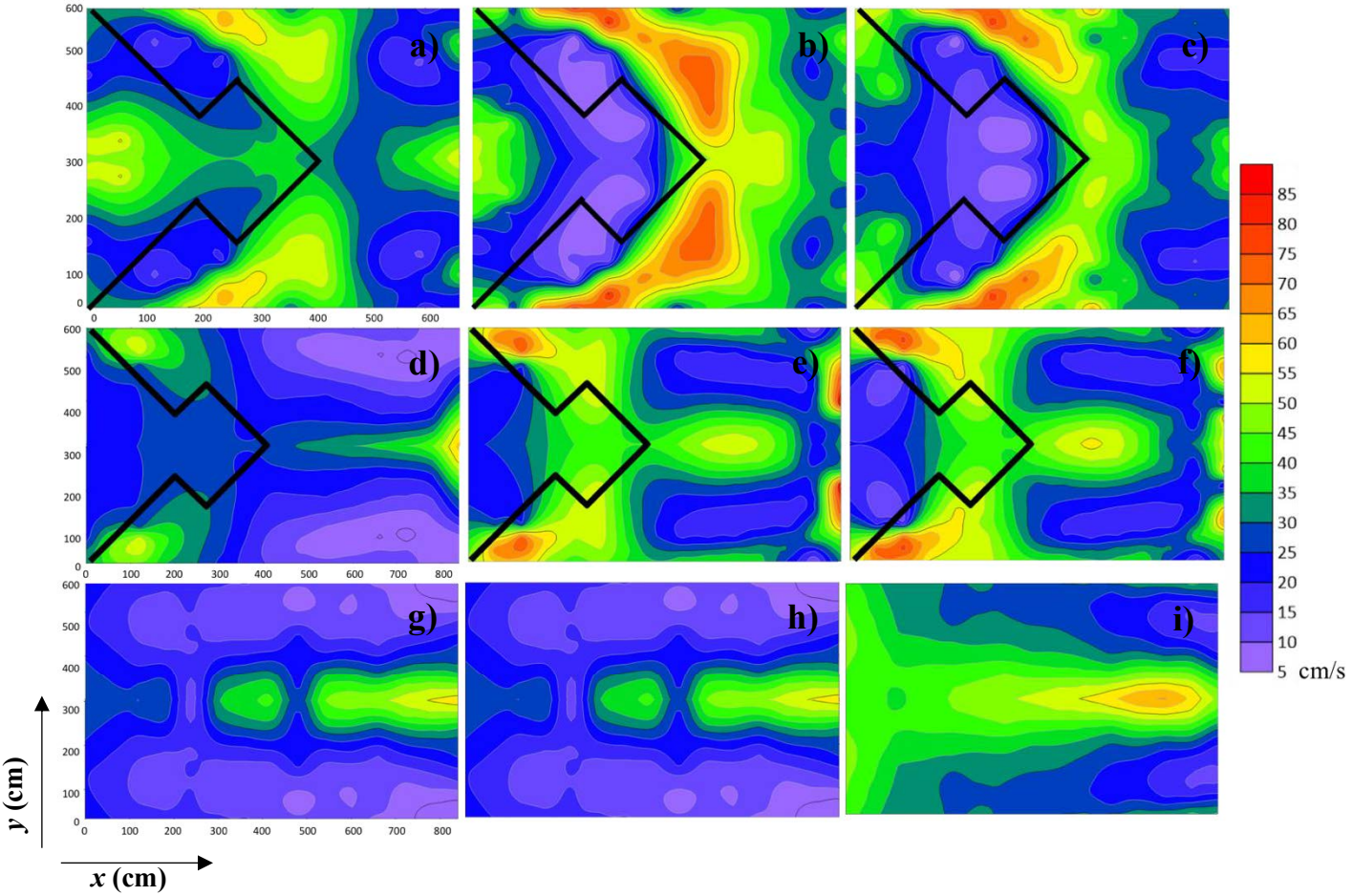


**Figure 4-8:** Counter plot of main velocity $\sqrt{U^2+V^2+W^2}$ for fishway with labyrinth weir with a downstream pool; a) $D$=0.75$m$, $Q$=19 $L/s$; b) $D$=0.75$m$, $Q$=25 $L/s$; c) $D$=0.75$m$, $Q$=32 $L/s$; d) $D$=1$m$, $Q$=19 $L/s$; e) $D$=1$m$, $Q$=25 $L/s$; f) $D$=1$m$, $Q$=32 $L/s$; g) $D$=1.5$m$, $Q$=19 $L/s$; h) $D$=1.5$m$, $Q$=25 $L/s$; i) $D$=1.5$m$, $Q$=32 $L/s$.

Figure 4-10 shows spatial distribution of turbulent kinetic energy for fishway with downstream pool weir, 0.5 * $\sqrt{u'^2 + v'^2 + w'^2}$ where $u'$, $v'$ and $w'$ being the longitudinal, lateral and vertical fluctuating velocities.

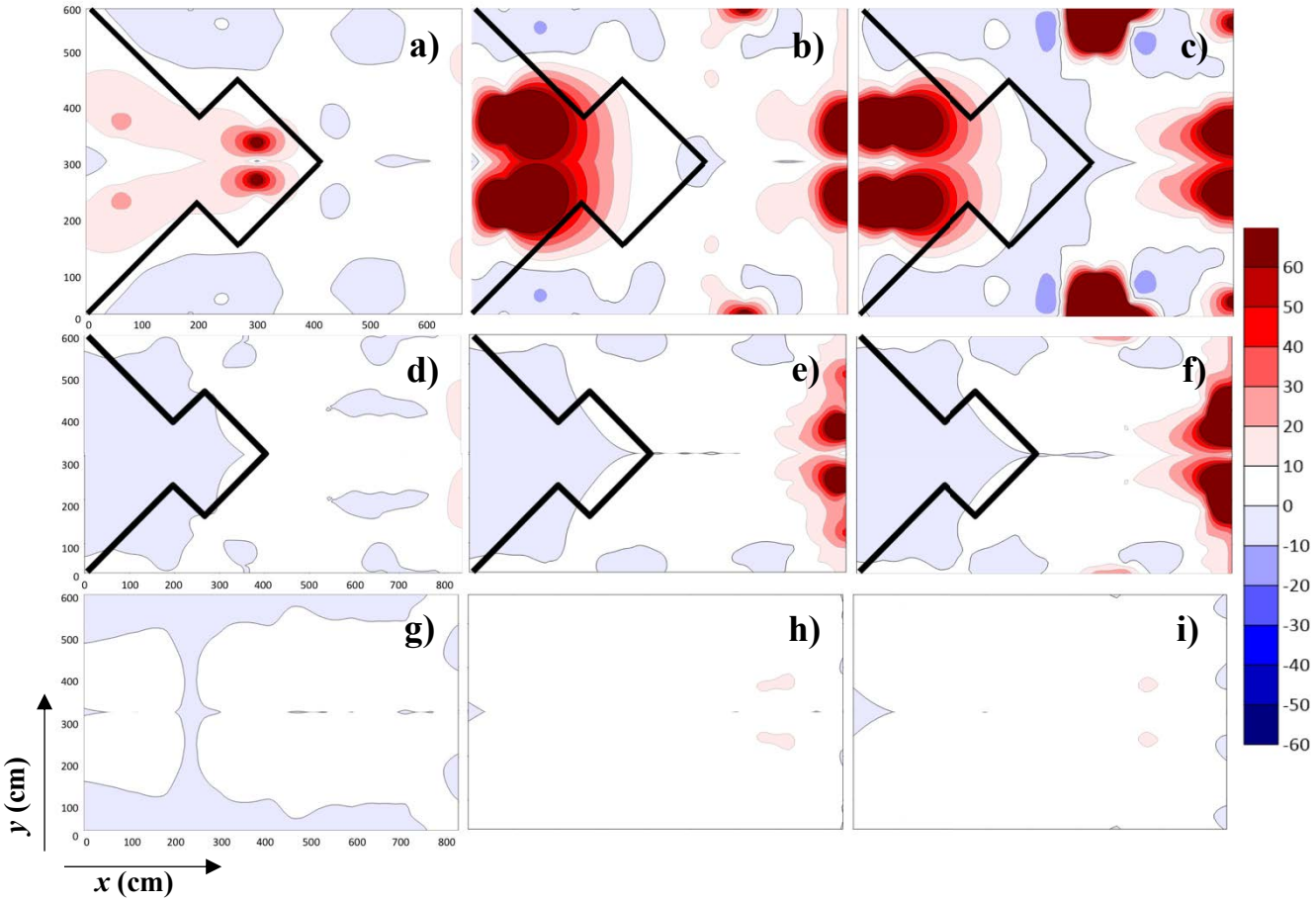


**Figure 4-9:** Counter plot of plane Reynolds shear stress *-pu'v'* for fishway with labyrinth weir with a downstream pool; a) *D*=0.75*m*, *Q*=19 *L*/*s*; b) *D*=0.75*m*, *Q*=25 *L*/*s*; c) *D*=0.75*m*, *Q*=32 *L*/*s*; d) *D*=1*m*, *Q*=19 *L*/*s*; e) *D*=1*m*, *Q*=25 *L*/*s*; f) *D*=1*m*, *Q*=32 *L*/*s*; g) *D*=1.5*m*, *Q*=19 *L*/*s*; h) *D*=1.5*m*, *Q*=25 *L*/*s*; i) *D*=1.5*m*, *Q*=32 *L*/*s*.

To compare the results with field data the contour plot of TKE magnitude has been plotted in dimensional format similar to the study of Lacey et al (2012). The TKE values ranged from 0.008 $m^2/s^2$ up to 0.35 $m^2/s^2$. Areas with low TKE (less than 0.125 $m^2/s^2$) are plotted in blue tones while the zones with high turbulent energy (more than 0.150 $m^2/s^2$) are plotted in red tones. Spatial differences are related to the position of the weirs and discharge magnitude, e.g., low TKE values

were found more in low discharge mode and fishways with larger gap between weirs. The variability of TKE in fishway with 0.75 m distance and high flowrate is appropriate for fish in terms of having a hydraulic environment where they can choose their way through the fishway. They may prefer different levels of turbulent intensities based on their swimming capability (Cotel et al. 2006). The TKE values compare well with values reported both in other standard fishways (Guiny et al. 2005; Liu et al. 2006; Silva et al. 2010; Breton et al. 2013) and in situ measurements of Lacey et al. (2012).

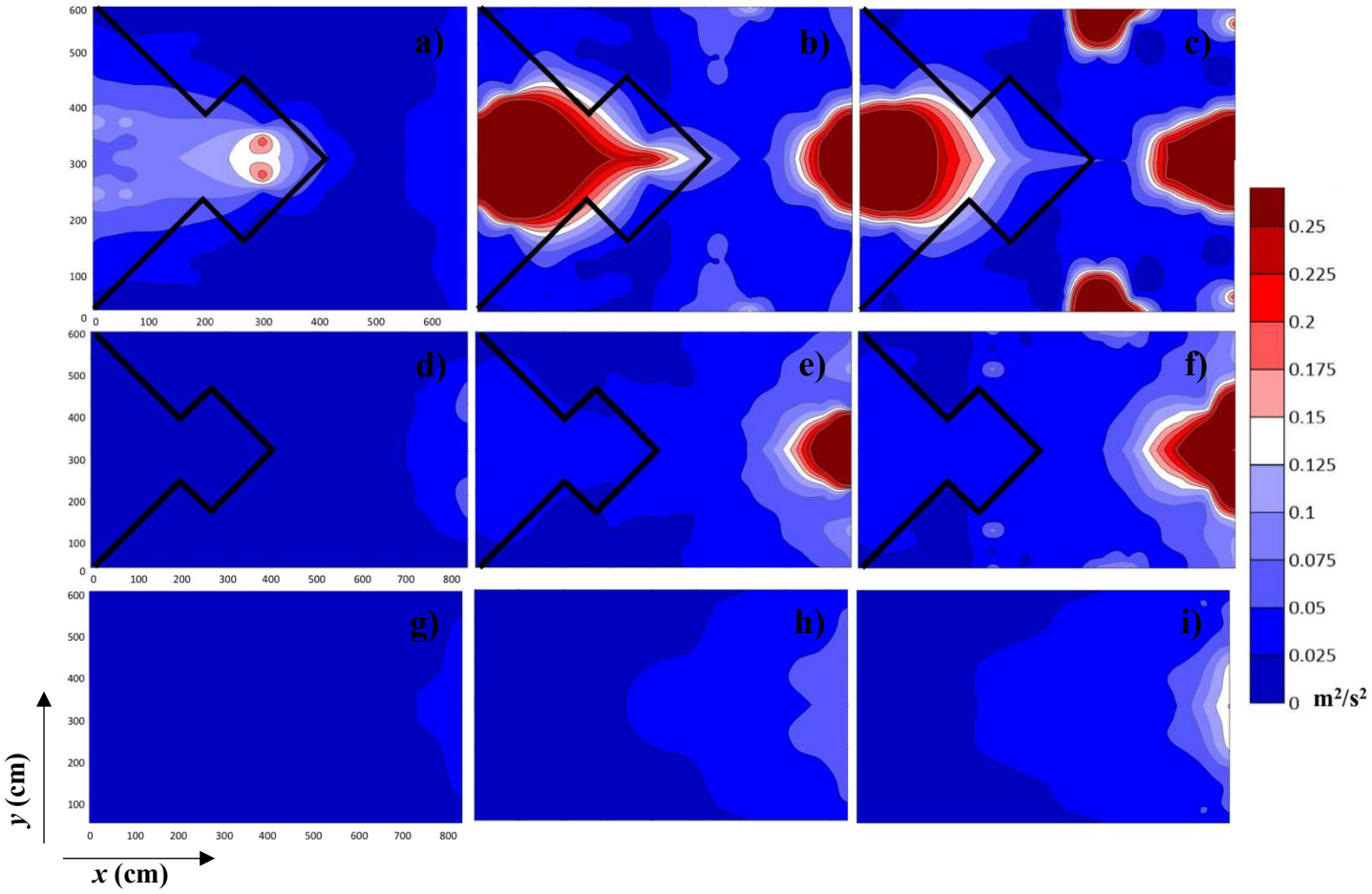


**Figure 4-10:** Counter plot of turbulent kinetic energy $0.5(u'^2+v'^2+w'^2)$ for fishway with labyrinth weir with a downstream pool; a) $D$=0.75$m$, $Q$=19 $L/s$; b) $D$=0.75$m$, $Q$=25 $L/s$; c) $D$=0.75$m$, $Q$=32 $L/s$; d) $D$=1$m$, $Q$=19 $L/s$; e) $D$=1$m$, $Q$=25 $L/s$; f) $D$=1$m$, $Q$=32 $L/s$; g) $D$=1.5$m$, $Q$=19 $L/s$; h) $D$=1.5$m$, $Q$=25 $L/s$; i) $D$=1.5$m$, $Q$=32 $L/s$.

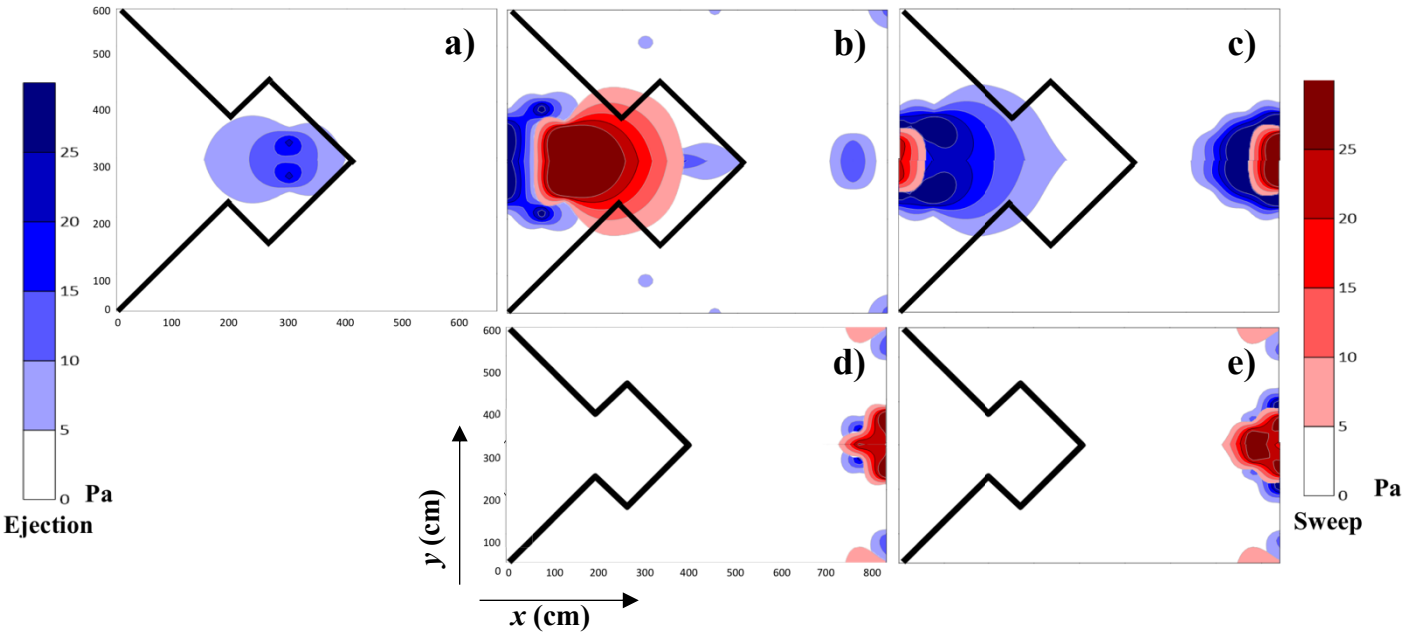


**Figure 4-11:** Predominance of sweep and ejection events presented as the vertical Reynolds shear stresses, *-pu'w'* , of series with predominance of quadrants *Q4* and *Q2* for fishway with labyrinth weir with a downstream pool; a) *D*=0.75*m*, *Q*=19 *L*/*s*; b) *D*=0.75*m*, *Q*=25 *L*/*s*; c) *D*=0.75*m*, *Q*=32 *L*/*s*; d) *D*=1*m*, *Q*=25 *L*/*s*; e) *D*=1*m*, *Q*=32 *L*/*s*.

Figure 4-11 shows spatial distribution of sweep and ejection events for fishway with downstream pool weir presented as the vertical Reynolds shear stress, $\overline{\rho u'w'}$, for those locations where sweep and ejection events are predominant. Only areas with shear stresses greater than 5 Pa has been coloured. By analysing asymmetries in velocity distribution sweep or ejection events have been identified. When velocity time series had a negative $\overline{u'}$ and a positive $\overline{w'}$ ($Q_2$) predominance of ejection events were identified. Sweep events were associated with velocity time series having a positive $\overline{u'}$ and negative $\overline{w'}$ ($Q_4$). It has been found that for fishway with 0.75 m distance between weirs, ejection events are more frequent than sweep events which is well compare with values reported in the study of Breton et al. (2013). For the fishway with 1 m spacing and for medium and high discharges near the downstream of the weir, sweep and ejection events were observed

which both ejection and sweep events had similar distribution. For the former, the most intense shear stress tends to occur near to the middle of the flume and for the latter occurs near to the boundary of the flume where ejection zones did not spread around the entire cross section. For the other setups there were no sweep and ejection events were found.

### 4-3-2 Turbulent flow field for fishway with upstream pool weirs

Figure 4-12 shows the spatial distribution of mean velocity for fishway with an upstream pool weir. It was found that similar to the fishway with a downstream pool weir, the variability of velocity magnitude for 0.75 m was more than those ones with larger distance. Low velocity was observed inside of the weir's pool and in the downstream section close to the weir's pool edge for fishways with 0.75 m and 1 m spacing. Whereas, higher velocities occurred in the upstream section close to the main side wall of the weir. For 1.5 m distance, high velocity values were found near the flume's boundary for all flow discharges, while, low velocity magnitudes were observed in the downstream section close to the weir for high and medium flow discharges and in the middle of the flume for lower flowrates. Maximum velocity for 0.75 m distance was 72.38 cm/s, 88.83 cm/s and 95.38 cm/s for low, medium, and high flow discharges, respectively, whereas, minimum velocity was measured as 5.5 cm/s for low and medium flowrates and 9.5 cm/s for high flowrate. For fishways with 1 m spacing, the maximum velocity was around 70 and 75 cm/s for low and medium flow discharges, respectively, and 78 cm/s for high flow discharge. The minimum velocity for low flowrate was 8 cm/s and 10 cm/s for medium and high flowrates. For fishways with 1.5 m spacing, the maximum velocity was 60 cm/s for high and medium flowrates and 55 cm/s for low flowrate. The minimum velocity was found to be around 5 cm/s for all flowrates.

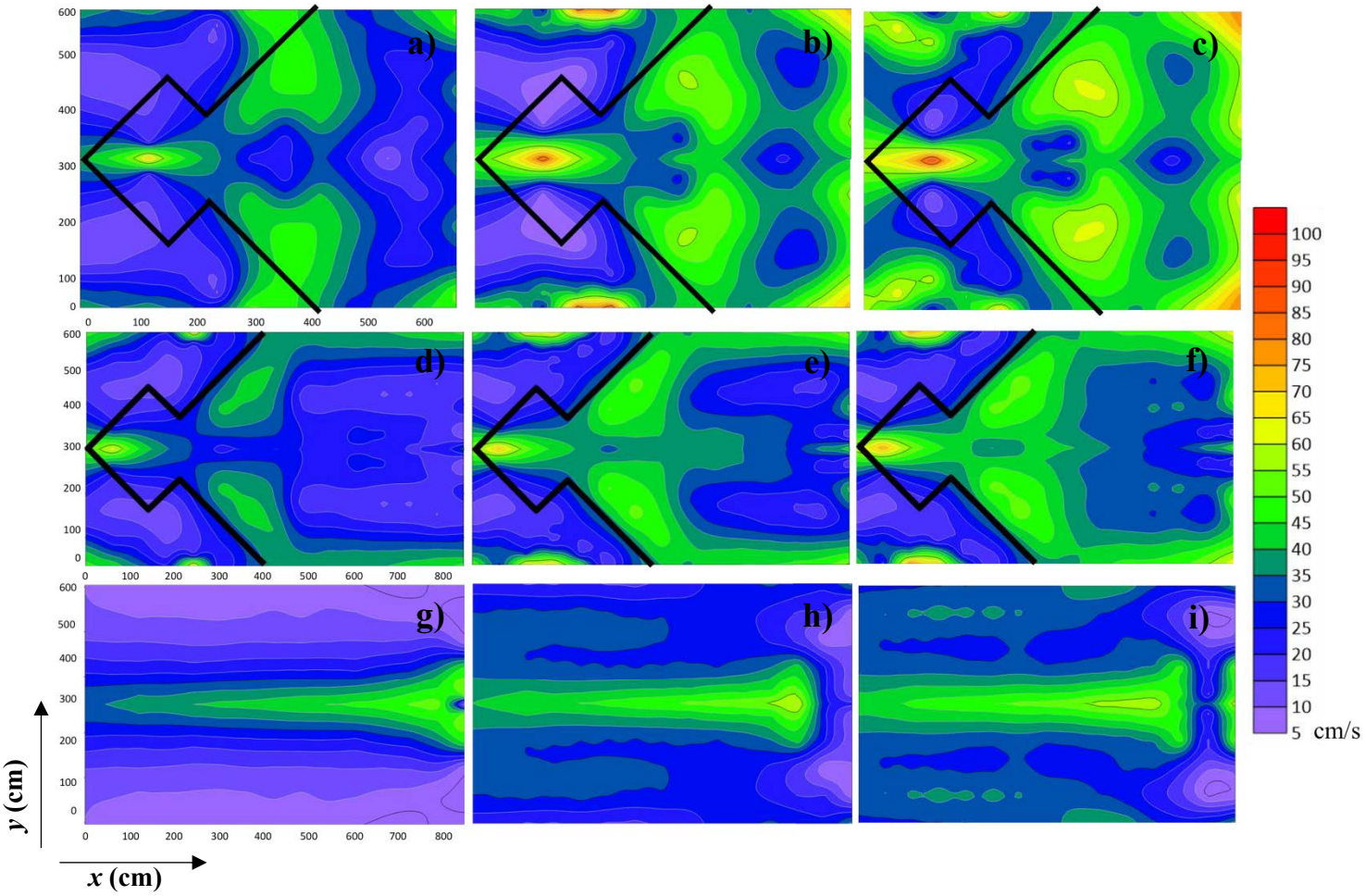


**Figure 4-12:** Counter plot of main velocity $\sqrt{U^2+V^2+W^2}$ for fishway with labyrinth weir with an upstream pool; a) $D$=0.75$m$, $Q$=19 $L/s$; b) $D$=0.75$m$, $Q$=25 $L/s$; c) $D$=0.75$m$, $Q$=32 $L/s$; d) $D$=1$m$, $Q$=19 $L/s$; e) $D$=1$m$, $Q$=25 $L/s$; f) $D$=1$m$, $Q$=32 $L/s$; g) $D$=1.5$m$, $Q$=19 $L/s$; h) $D$=1.5$m$, $Q$=25 $L/s$; i) $D$=1.5$m$, $Q$=32 $L/s$.

Figure 4-13 shows the counter plot of plane Reynolds shear stresses for fishway with an upstream pool weir. It was observed that most of the plane Reynolds shear stresses in all flow conditions was in the range of -10 Pa to 10 Pa which is totally different with fishway with a downstream pool weir. There were couple of points with higher magnitude of shear stresses in 0.75 m and 1 m distance whereas, higher magnitude of shear stresses was not observed in 1.5 m distance.

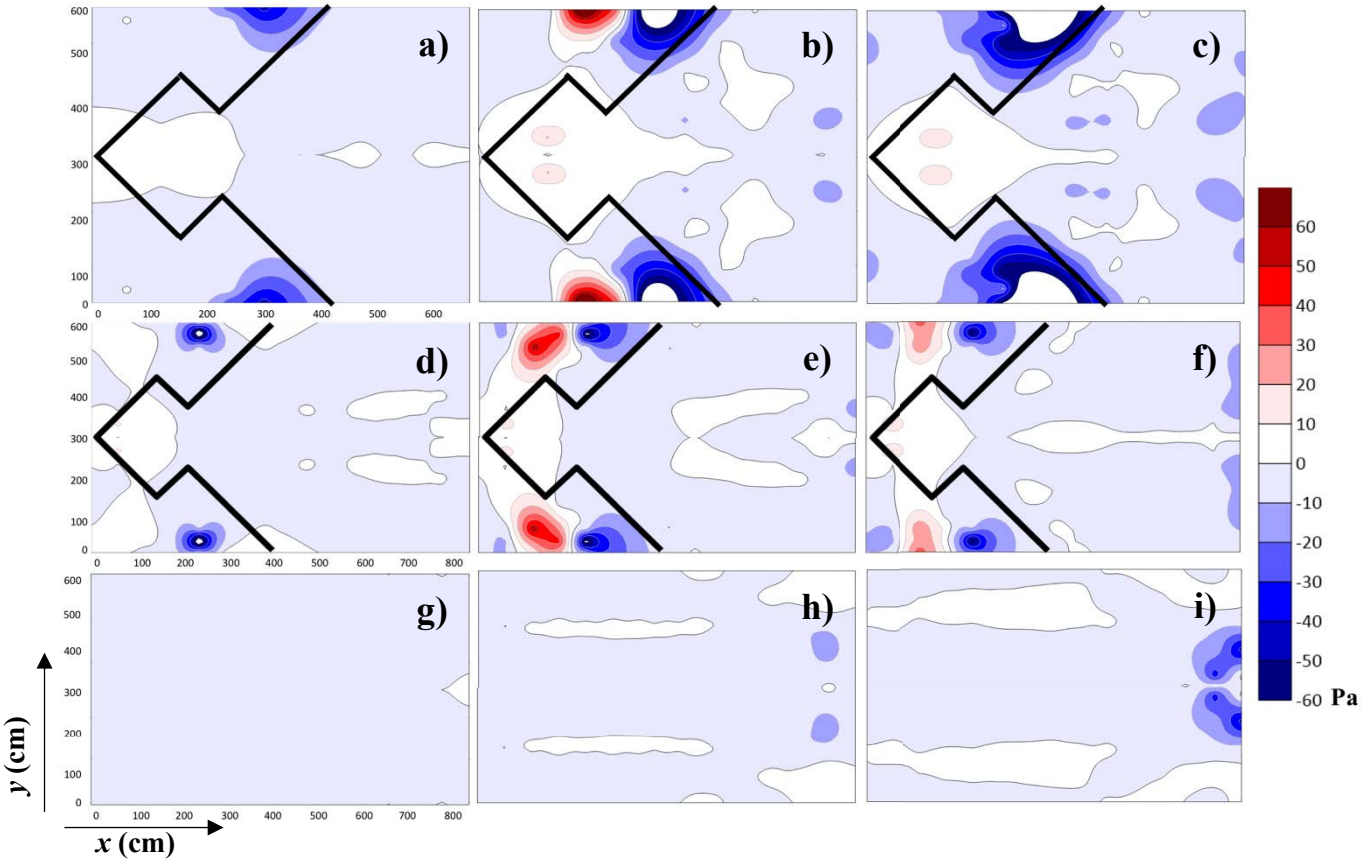


**Figure 4-13:** Counter plot of plane Reynolds shear stress *-pu'v'* for fishway with labyrinth weir with an upstream pool; a) *D*=0.75*m*, *Q*=19 *L*/*s*; b) *D*=0.75*m*, *Q*=25 *L*/*s*; c) *D*=0.75*m*, *Q*=32 *L*/*s*; d) *D*=1*m*, *Q*=19 *L*/*s*; e) *D*=1*m*, *Q*=25 *L*/*s*; f) *D*=1*m*, *Q*=32 *L*/*s*; g) *D*=1.5*m*, *Q*=19 *L*/*s*; h) *D*=1.5*m*, *Q*=25 *L*/*s*; i) *D*=1.5*m*, *Q*=32 *L*/*s*.

Figure 4-14 shows spatial distribution of turbulent kinetic energy for fishway with an upstream pool weir. It indicates that low TKE happened more when flowrate was low and the distance between weirs was high like fishway with a downstream weir pool. The variability of TKE was larger in 0.75 m distance when the flowrates were medium and high which compare well with the fishway with a downstream pool weir.

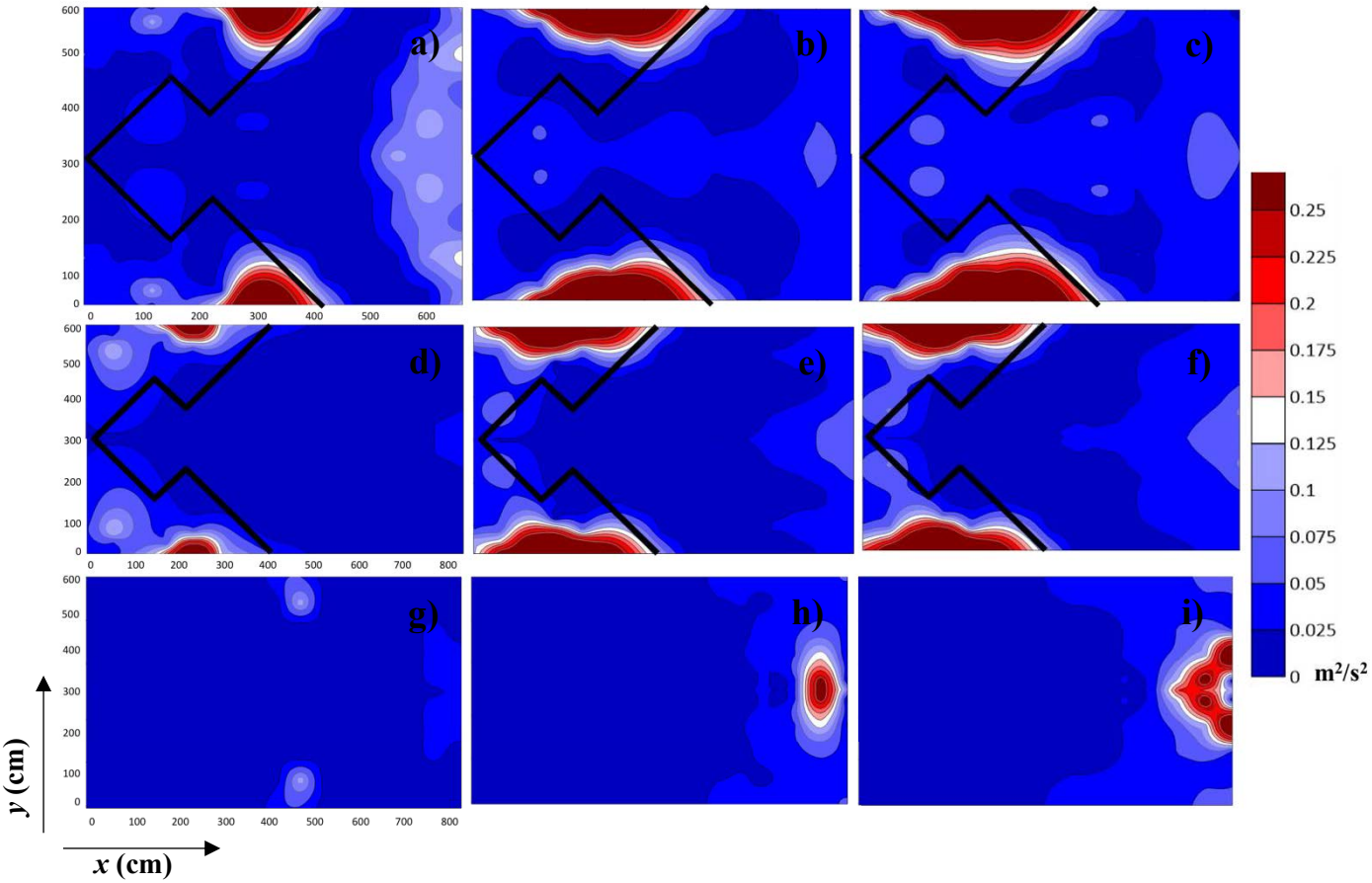


**Figure 4-14:** Counter plot of turbulent kinetic energy $0.5(u'^2+v'^2+w'^2)$ for fishway with labyrinth weir with a downstream pool; a) $D$=0.75$m$, $Q$=19 $L/s$; b) $D$=0.75$m$, $Q$=25 $L/s$; c) $D$=0.75$m$, $Q$=32 $L/s$; d) $D$=1$m$, $Q$=19 $L/s$; e) $D$=1$m$, $Q$=25 $L/s$; f) $D$=1$m$, $Q$=32 $L/s$; g) $D$=1.5$m$, $Q$=19 $L/s$; h) $D$=1.5$m$, $Q$=25 $L/s$; i) $D$=1.5$m$, $Q$=32 $L/s$.

Figure 4-15 presents spatial distribution of sweep and ejection events for fishway with upstream pool weir presented as the vertical Reynolds shear stress for those locations where sweep and ejection events are predominant. It can be observed like the downstream pool weirs ejection events are more frequent than sweep events for 0.75 m distance with medium and high flow discharges. For the other conditions sweep and ejection events were observed in downstream side of the weir close to the flume boundary except for 1.5 m distance with medium and high flowrate which it was spread through the cross section of the flume. On the other hand, it was not observed any sweep and ejection events in 1.5 m distance with low flow discharge.

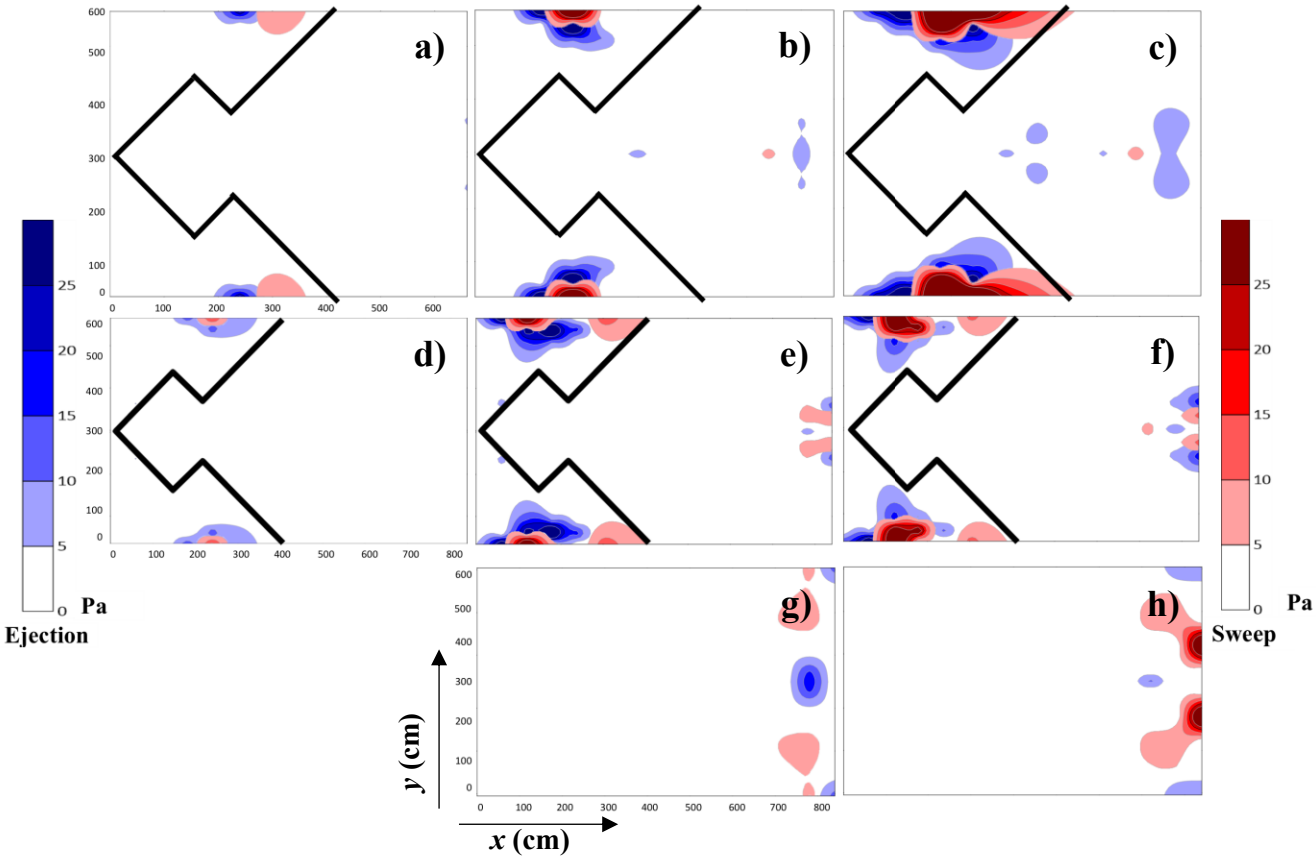


**Figure 4-15:** Predominance of sweep and ejection events presented as the vertical Reynolds shear stresses, *-pu'w'* , of series with predominance of quadrants *Q4* and *Q2* for fishway with labyrinth weir with an downstream pool; a) $D$=0.75$m$, $Q$=19 $L/s$; b) $D$=0.75$m$, $Q$=25 $L/s$; c) $D$=0.75$m$, $Q$=32 $L/s$; d) $D$=1$m$, $Q$=19 $L/s$; e) $D$=1$m$, $Q$=25 $L/s$; f) $D$=1$m$, $Q$=32 $L/s$; g) $D$=1.5$m$, $Q$=25 $L/s$; h) $D$=1.5$m$, $Q$=32 $L/s$.

### 4-3-3 Quadrant analysis

Figures 4-16 and 4-17 show the quadrant plots of the vertical versus plane normalized fluctuation velocities for fishways with a downstream and an upstream pool weirs, respectively. It was plotted for 14 points in total, 3 and 4 points for the fishway with downstream pool weir and upstream pool weir, respectively, for 0.75 m and 1 m pool distance. All velocities were normalized with the mean flow velocity. It indicates that the plots are not isotopic as fluctuating plane velocities distribution are not symmetric. Negative fluctuations that are higher in magnitude than the mean velocity, were found at location (2) for 1 m distance in the fishway with a downstream pool weirs (Figure 4-16)

and locations (1) and (4) for 0.75 m distance and location (1) for 1 m distance in the fishway with upstream pool weirs (Figure 4-17). At locations (1) and (3) positive fluctuations reached to greater than mean velocity for both conditions in the fishway with downstream pool weir, whereas, for the fishway with upstream pool weir it happened at locations (1) and (4) for 0.75 m distance and at location (1) for 1 m distance.

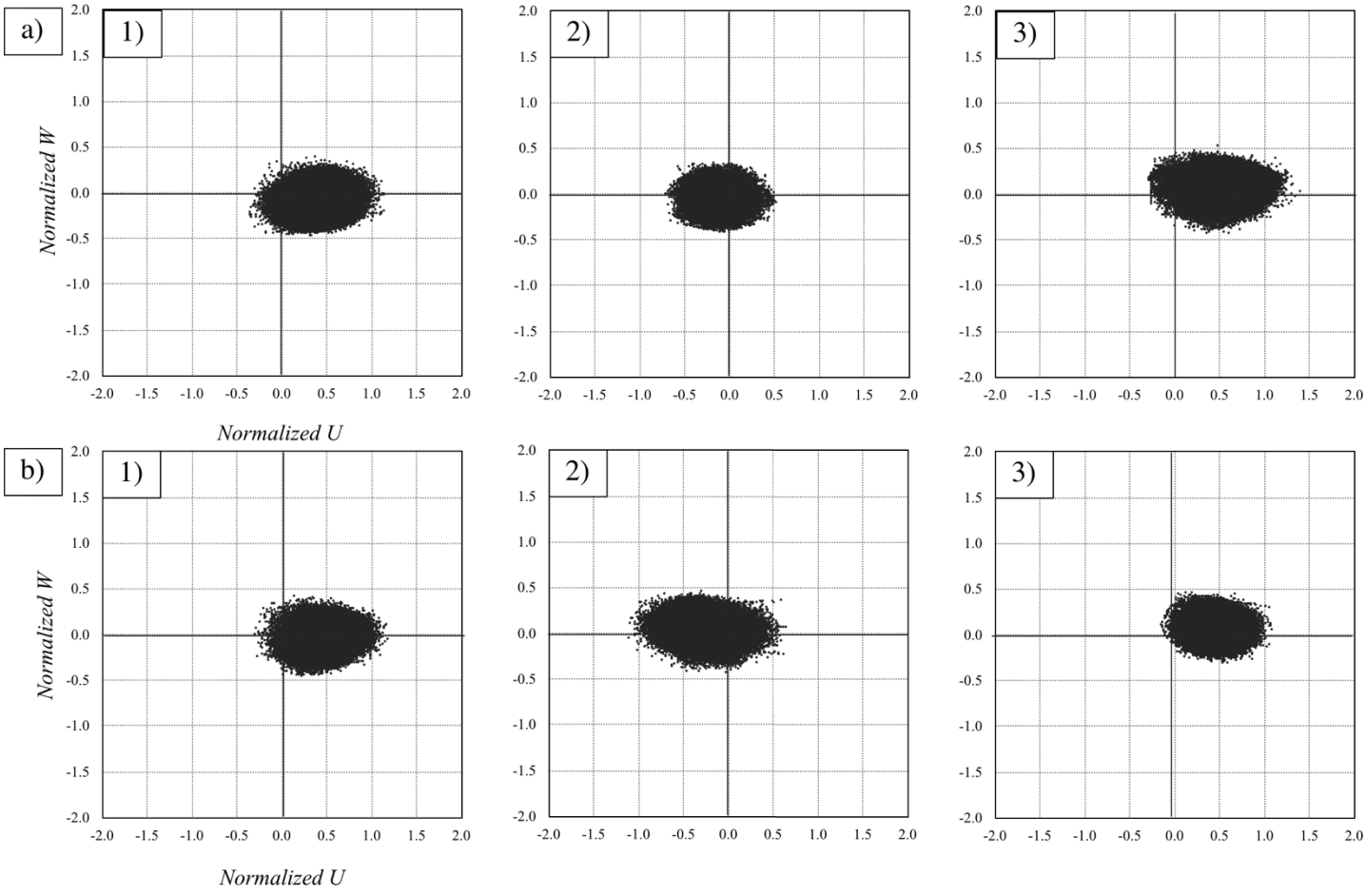


**Figure 4-16:** Quadrant plots of vertical versus plane normalized fluctuation velocity (normalized with mean velocity) for fishway with labyrinth weir with a downstream pool measured at locations (1), (2) and (3); Flow rate was 32 *L*/*s*; a) *D*=0.75*m;* b) *D*=1*m*.

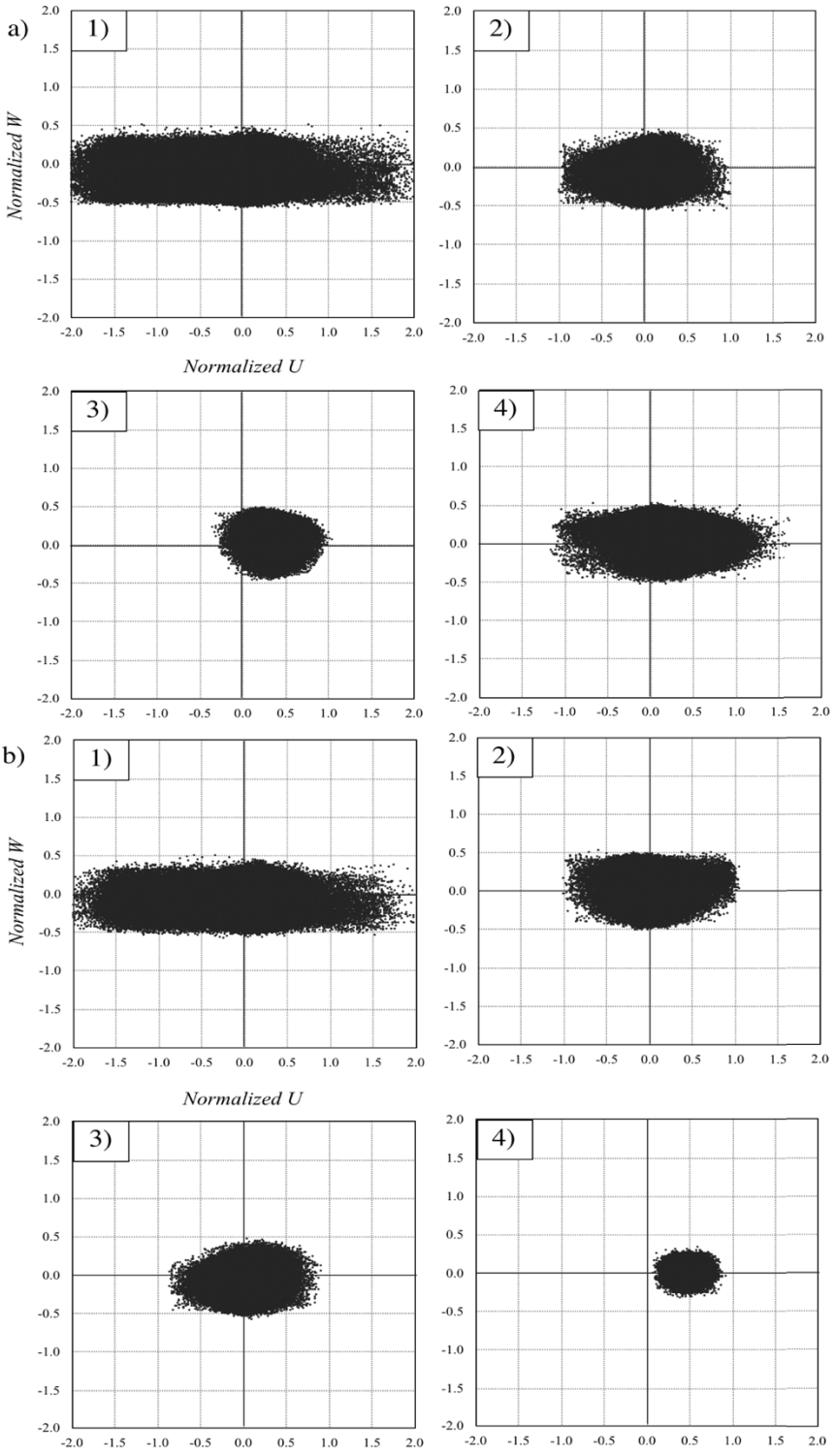


**Figure 4-17:** Quadrant plots of vertical versus plane normalized fluctuation velocity (normalized with mean velocity) for fishway with labyrinth weir with an upstream pool measured at locations (1), (2), (3) and (4); Flow rate was 32 *L*/*s*; a) *D*=0.75*m;* b) *D*=1*m*.

### 4-3-4 Spectral analysis

Power spectral density functions of velocity were calculated as proposed by Welch (1967) using a Blackman window with 50% of overlapping. A 512-window size was selected so that the random error of spectrum estimation was less than 10%. Figures 4-18 and 4-19 show power spectra of the axial, transversal, and vertical velocity for the fishway with a downstream pool weir and the fishway with an upstream pool weir, respectively. The points specified in the quadrant analysis were used for the power spectral analysis as well. The spectrum energy slopes fit relatively well with the Kolmogorov's energy cascade, enclosing the inertial sub-range up to approximately $10^0$ $H_z$. The plot worked on nature-like fishway. It can be observed that for frequency more than 1 $H_z$, location (2) has the lower energy than the other locations and almost for all the frequency, location (3) has the higher energy than the other locations for the fishway with downstream pool weir. It shows that the turbulent in the corner of the weir and the flume has the highest energy magnitude. Location (1) in the fishway with upstream pool weir has the highest energy at frequency around 10 $H_z$ for all the velocity direction, while, the same location in vertical velocity direction for 0.75 m distance almost for all frequency has the highest energy magnitude. The lowest energy magnitude is related to the location (4) at the frequency around 10 $H_z$ except for 1 m distance in vertical velocity direction that the lowest energy magnitude related to the location (3). Probably these phenomena arise from vortex stretching, the main mechanism of energy transfer.

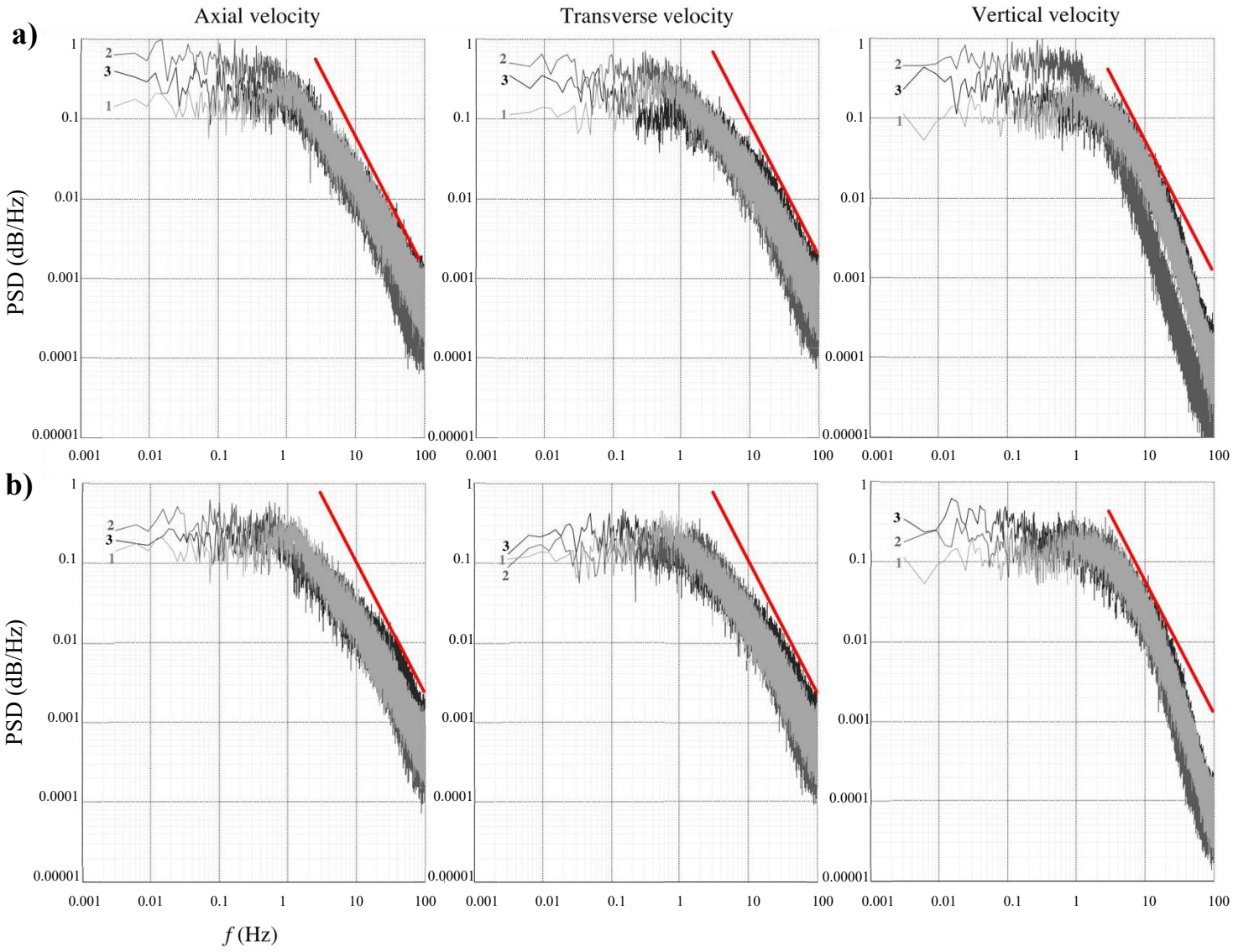


**Figure 4-18:** Power spectra of axial, transverse and vertical velocity for fishway with labyrinth weir with a downstream pool for locations (1), (2) and (3); a) $D$=0.75; b) $D$=1.

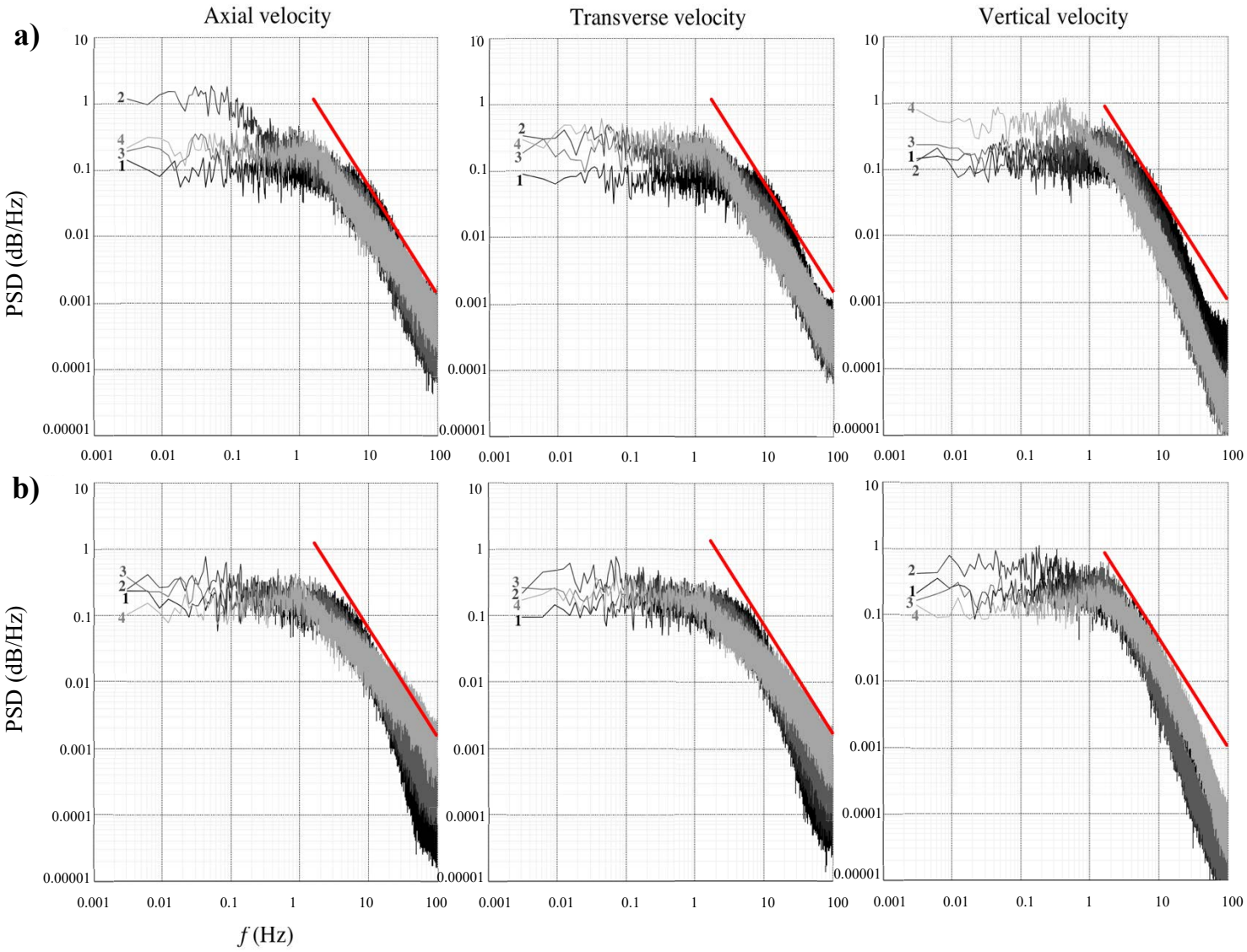


**Figure 4-19:** Power spectra of axial, transverse and vertical velocity for fishway with labyrinth weir with an upstream pool for locations (1), (2), (3) and (4); a) $D$=0.75; b) $D$=1.

# Chapter 5

# General Conclusions and Recommendations for Future Research

## 5.1 Sharp-Crested Weirs

The present laboratory experiments examined the dynamics of water flow over the upstream of two newly designed triangular labyrinth sharp-crested weirs, one with a downstream square pool and the other one with an upstream square pool. Experiments were conducted in two different hydraulic conditions of free and submerged flows. The *x, y* and *z* components of velocity and turbulent kinetic energy were measured using an Acoustic Doppler Velocitymeter (ADV). The highest values of *u* for the triangular labyrinth weir with a downstream pool occurred in the vicinity of the vertex angle between the main sidewall of the weir and the pool's sidewall and the lowest values occurred in the vicinity of the apex of the weir in $z<0.7(h_o+P)$. While, for the higher elevations the lowest amounts happened far from the apex of the weir (for distance more than 1/3 of longitudinal length of the weir). The highest values of *v* and *w* for the triangular labyrinth weir with downstream pool observed in the same area as for *u* (in the vicinity of the vertex angle between the main sidewall of the weir and the pool's sidewall) in the elevations lower than $0.85(h_o+P)$ (for higher elevations *w* had its maximum values in the corner of the weir and the flume's side wall), that it can be demonstrated that most of the flow passed through this area. Also, for this weir, lateral velocity direction changed in the vicinity of the vertex angel between the small pool sidewall and the large pool sidewall for $z<0.7(h_o+P)$. The maximum values of TKE occurred in the area between main sidewall of the weir and the pool's sidewall in elevations lower than $0.85(h_o+P)$. for higher elevations the maximum TKE happened in the corner of the weir and the flume's sidewall. Also, in the lateral plane at the corner of the pool's sidewall and the weir's

sidewall the significant sweep and ejection events have been observed while for the submerged condition these events are greater in the near flume's floor as well as the near weir's wall. For triangular labyrinth weir with upstream pool, the highest of the $u$ occurred in the pool for all elevations and the lowest happened in the vicinity of the main sidewall of the weir for the planes with elevation lower than $0.75(h_o+P)$. The highest values of the $w$ occurred in the pool for all planes and the maximum amount of that happened in the plane $z=0.7(h_o+P)$ in the pool and in the vicinity of the main sidewall of the weir. Additionally, the highest value of the $v$ occurred in the vicinity of the main sidewall of the weir and the direction of the lateral velocity changed in the elevations limited to $0.35(h_o+P)<z<0.7(h_o+P)$. The maximum amount of the TKE occurred in the pool.

**5.2 Fishways**

The results of laboratory measurements of the flow field and hydraulic properties in a weir-pool fishway using an ADV probe were presented. The turbulent flow field was specified by applying the spatial and point analysis techniques and its relation to fish behavior was discussed. The flow field indicated a high spatial variability controlled by the geometry of the weir arrangement. Mean velocity ranged from 5 to 82 cm/s and 5 to 95 cm/s for the fishway with a downstream pool and an upstream pool weir, respectively, representing longitudinal paths with relative rapid currents (with velocities more than 20 cm/s) that may be followed by fish, and slow flow regions (with velocities less than 20 cm/s) that may be used as resting areas during fish passage. A wide range of TKE magnitude with differences in space related to the position of weir was also observed. The most intense shear stress tends to occur in the middle of the flume near to the weir where ejection zones are not spread to the whole cross section. This pattern allows fish to pass through the fishway avoiding ejection zones.

Point analysis indicated that the weir to weir distance in the fishway with 0.75 m and 1 m distance was small enough to disrupt turbulent coherent structures. The areas which sweep and ejection events were not observed indicating that these zones constitute appropriate resting place for fish during their migration. TKE and Reynolds shear stress distribution indicated high spatial variation in the fishway and demonstrated that a weir-pool fishway with labyrinth weir with downstream pool and upstream pool suggested a diversity of flow conditions that let a variety of fish to choose their preferred path specified by flow properties with different values depending on the particular species.

### 5.3 Future Research Studies

Since hydraulic and dynamic design procedures of weir-pool fishways is complex, essential research can build up our understanding about the influence of various geometric variables which effect the hydraulic and dynamic performance of a weir-pool fishways. This prepares detailed information about the design procedures of weir-pool fishways and can be used to enhance and suggest applied research topics. The fishway with labyrinth sharp-crested weir shows that it is a very fascinating project due to its efficient behaviour as it can cover different species compare with the linear weirs used in fishway. Even though, the physical understanding and detailed measurements of the effect of weir's geometry and the length of the pool on the dynamic behavior of fishway are available, however, the influence of the orifice and its position on this kind of weir-pool fishway needs to be investigated since an orifice offers passage of certain fish species in which swimming or leaping against overflow weirs may not be possible. As well as, effective notches can increase the ability of the fishway to cover more species. Also, modification on slope can provide different value of turbulent kinetic energy so consequently can increase productivity of the fishway.

## Appendix 1

### Top view images of tested fishway with downstream pool at various flowrate and distance

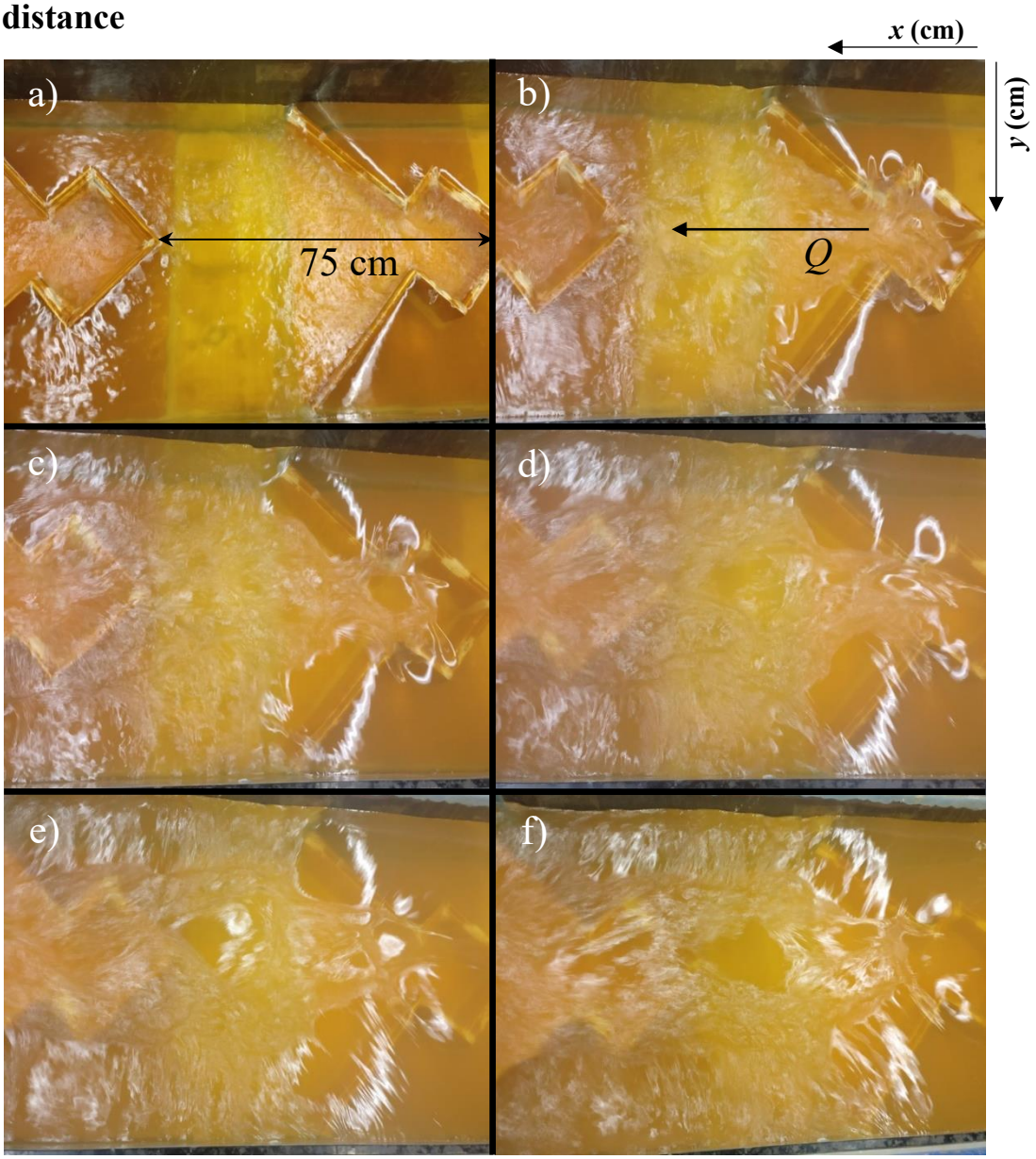


**Figure A1-1:** Top view of fishway with downstream pool and 0.75 *m* distance at flowrate: (a) *Q*= 24.8 L/s ; (b) *Q*= 31.08 L/s; (c) *Q*= 35.4 L/s; (d) *Q*= 42.39 L/s; (e) *Q*= 47.24 L/s; (f) *Q*= 51.06 L/s.

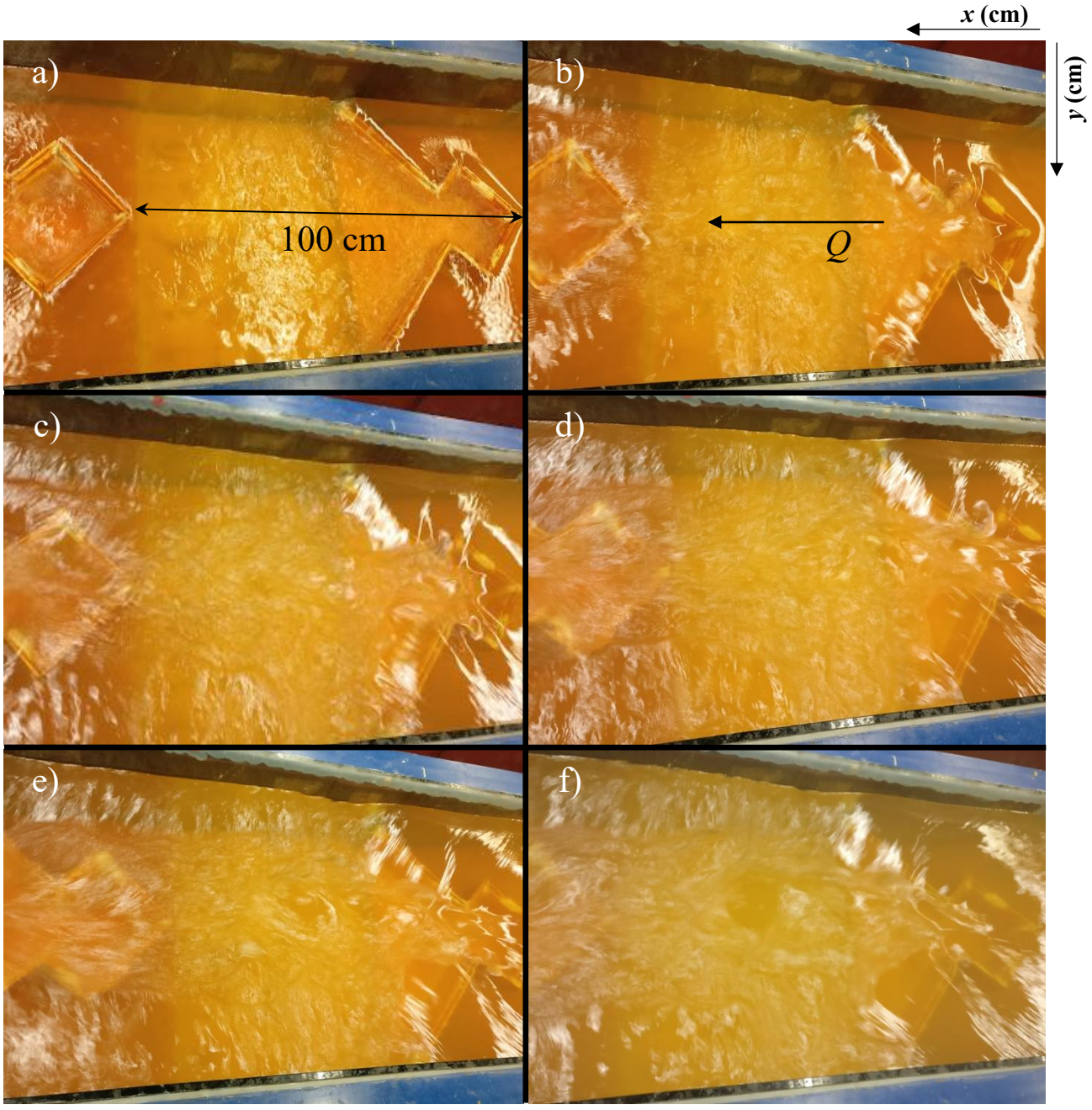


**Figure A1-2:** Top view of fishway with downstream pool and 1 *m* distance at flowrate: (a) *Q*= 24.8 L/s ; (b) *Q*= 31.08 L/s; (c) *Q*= 35.4 L/s; (d) *Q*= 42.39 L/s; (e) *Q*= 47.24 L/s; (f) *Q*= 51.06 L/s.

**Appendix 2**

## Top view images of tested fishway with upstream pool at various flowrate and distance

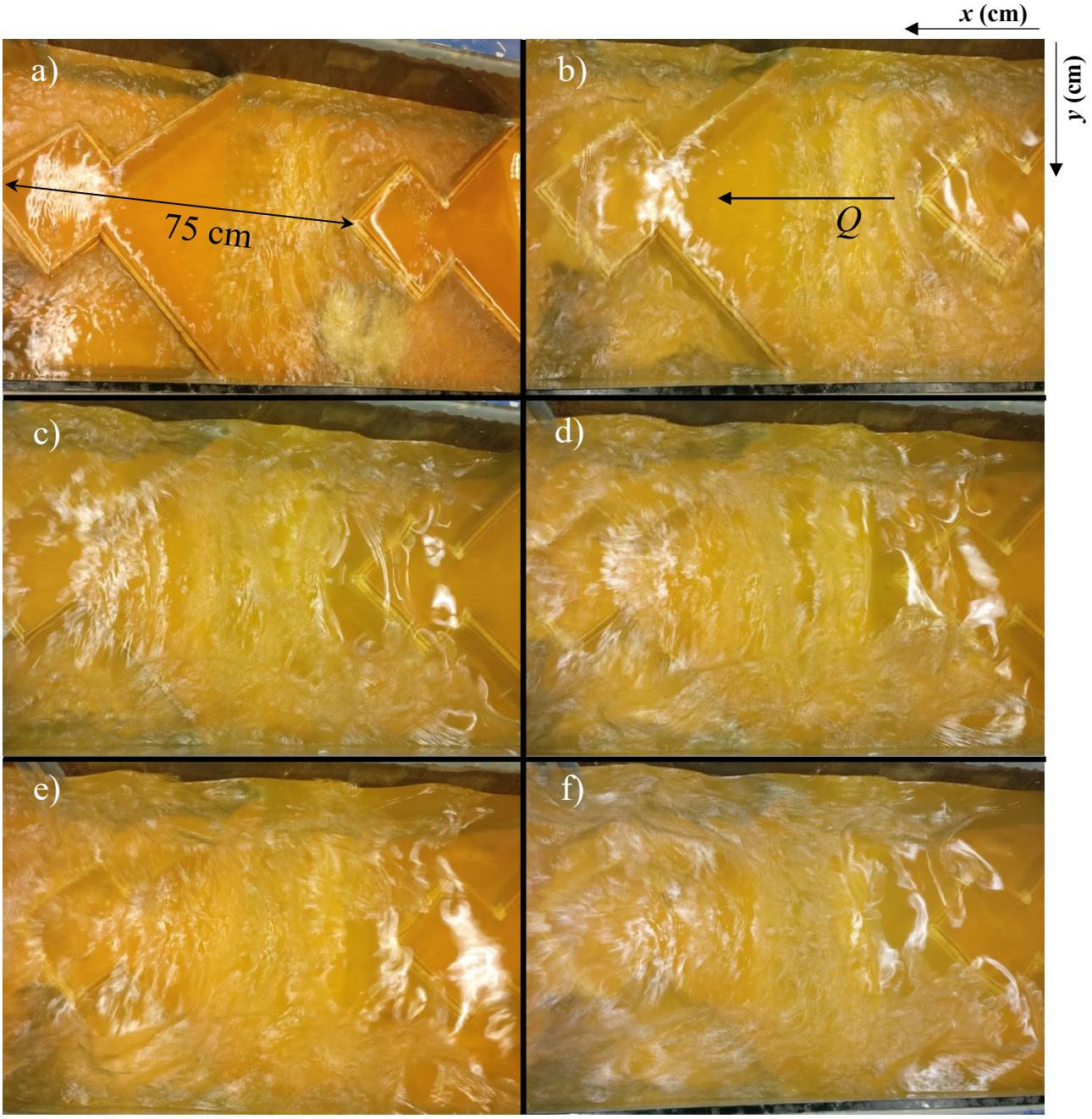


**Figure A2-1:** Top view of fishway with upstream pool and 0.75 *m* distance at flowrate: (a) *Q*= 24.8 L/s ; (b) *Q*= 31.08 L/s; (c) *Q*= 35.4 L/s; (d) *Q*= 42.39 L/s; (e) *Q*= 47.24 L/s; (f) *Q*= 51.06 L/s.

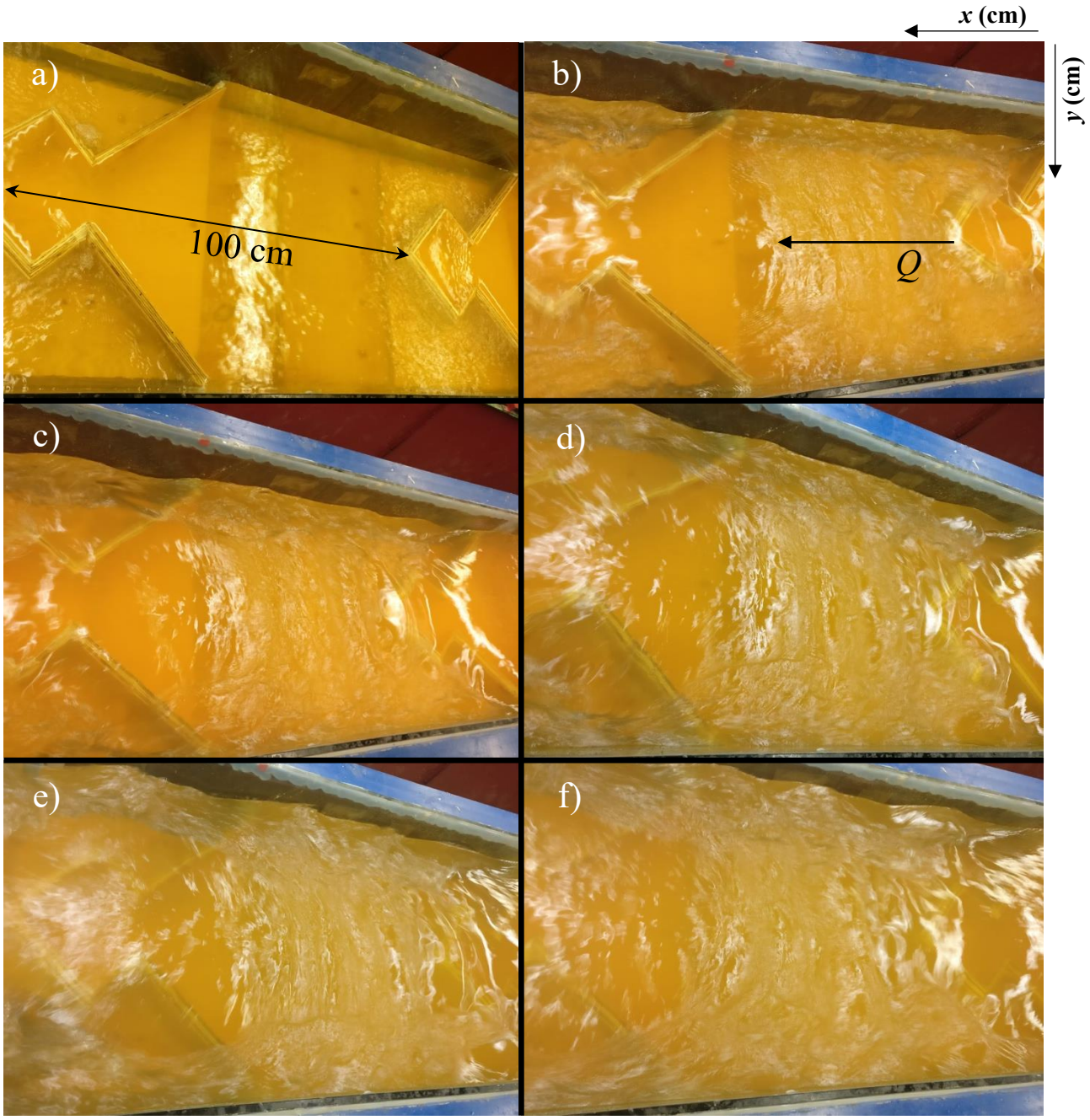


**Figure A2-2:** Top view of fishway with upstream pool and 0.75 *m* distance at flowrate: (a) *Q*= 24.8 L/s ; (b) *Q*= 31.08 L/s; (c) *Q*= 35.4 L/s; (d) *Q*= 42.39 L/s; (e) *Q*= 47.24 L/s; (f) *Q*= 51.06 L/s..

**Notation**

$a$ = Apex angle of the weir;

$b$ = The width of a one-cycle labyrinth weir;

$b_w$ = Width of the fishway;

$B$ = Width of the channel;

$C_d$ = Discharge coefficient in free flow condition;

$C_f$ = The coefficient of fluid friction;

$C_p$ = Discharge coefficient in plunging mode;

$d$ = Length of the surface stream;

$g$ = The acceleration due to gravity;

$h$ = The head over the weir;

$H$ = Total head;

$k$ = Energy dissipation;

$L$ = Length of the weir;

$L_p$ = Length of the larger side of the weir's pool;

$L_w$ = Length of the weir's crest;

$n$ = Number of cycles;

$p$ = Height of the weir;

$P$ = Pressure;

$Q$ = Flow discharge;

$Q_*$ = Dimensionless flow discharge in the streaming mode;

$Q_+$ = Dimensionless flow discharge in the plunging mode;

$Q_f$ = Discharge for free flow condition ($m^3/s$);

$S$ = Slope of the flume;

$U$ = Mean velocity;

$u$ = Longitudinal velocity;

$v$ = Lateral velocity;

$w$ = Vertical velocity;

$u'$ = Fluctuation in longitudinal direction;

$v'$ = Fluctuation in lateral direction;

$w'$ = Fluctuation in vertical direction;

$V$ = Velocity;

$W$ = The width of the pool;

$Y$ = Average height of the pool;

$Z$ = Potential head;

$\rho$ = Density of water;

$\gamma$ = Specific weight of water;

**References**


1. Ackers, P., White, W. R., Perkins, J. A., and Harrison, A. J. (1978). *Weirs and flumes for flow measurements*, Wiley, Chichester, U.K, 327 p.
2. Aydin, M. C., & Emiroglu, M. E. (2013). Determination of capacity of labyrinth side weir by CFD. *Flow Measurement and Instrumentation*, 29, 1-8.
3. Azimi, A. H., Rajaratnam, N., & Zhu, D. Z. (2014). Submerged flows over rectangular weirs of finite crest length. *Journal of Irrigation and Drainage Engineering*, 140(5), 06014001.
4. Azimi, A. H., Rajaratnam, N., & Zhu, D. Z. (2016). Water surface characteristics of submerged rectangular sharp-crested weirs. *Journal of Hydraulic Engineering*, 142(5), 06016001.
5. Azimi, A. H. (2018). Flume experiments on baffle-posts for retarding open channel flow By Caroline Ubing, Robert Ettema and Christopher I. Thornton. *Journal of Hydraulic Research*, 56(3), 431-433.
6. Bagheri, S., & Heidarpour, M. (2010). Application of free vortex theory to estimating discharge coefficient for sharp-crested weirs. *Biosystems engineering*, 105(3), 423-427.
7. Baki, A. B. M., Zhang, W., Zhu, D. Z., & Rajaratnam, N. (2016). Flow structures in the vicinity of a submerged boulder within a boulder array. *Journal of Hydraulic Engineering*, 143(5), 04016104.
8. Baki, A. B. M., Zhu, D. Z., Harwood, A., Lewis, A., & Healey, K. (2017). Rock-weir fishway II: design evaluation and considerations. *Journal of Ecohydraulics*, 2(2), 142-152.
9. Bates, K., & Whiley, A. J. (2000). *Fishway Guidelines for Washington State: Draft*. Washington Department of Fish and Wildlife, 57 p.

10. Bates, K., Bernard, B., Heiner, B. A., Klavas, J. P., & Powers, P. D. (2003). Design of road culverts for fish passage, 110 p.
11. Barrett, J., & Mallen-Cooper, M. (2006). The Murray River's 'Sea to Hume Dam'fish passage program: progress to date and lessons learned. *Ecological Management & Restoration*, 7(3), 173-183.
12. Beach, M. H. (1984). Fish pass design-criteria for the design and approval of fish passes and other structures to facilitate the passage of migratory fish in rivers, 46 p.
13. Behlke, C. E., Kane, D. L., McLean, R. F., & Travis, M. D. (1991). *Fundamentals of Culvert Design for Passage of Weak-Swimming Fish. Final Report* (No. FHWA-AK-RD-90-10).
14. Bell, M. C. (1990). *Fisheries handbook of engineering requirements and biological criteria*. CORPS OF ENGINEERS PORTLAND OR NORTH PACIFIC DIV, 353 p.
15. Bermúdez, M., Puertas, J., Cea, L., Pena, L., & Balairón, L. (2010). Influence of pool geometry on the biological efficiency of vertical slot fishways. *Ecological Engineering*, 36(10), 1355-1364.
16. Bijankhan, M., & Kouchakzadeh, S. (2017). Unified discharge coefficient formula for free and submerged triangular labyrinth weirs. *Flow Measurement and Instrumentation*, 57, 46-56.
17. Bilhan, O., Emiroglu, E., & Miller, C. J. (2016). Experimental investigation of discharge capacity of labyrinth weirs with and without nappe breakers. *Civil and Environmental Engineering Faculty Research Publications*, 32.
18. Blanckaert, K., & Lemmin, U. (2006). Means of noise reduction in acoustic turbulence measurements. *Journal of hydraulic Research*, 44(1), 3-17.

19. Borghei, S. M., Vatannia, Z., Ghodsian, M., & Jalili, M. R. (2003, June). Oblique rectangular sharp-crested weir. *In Proceedings of the Institution of Civil Engineers-Water and Maritime Engineering* (Vol. 156, No. 2, pp. 185-191). Thomas Telford Ltd.
20. Borghei, Borghei, S. M., Kabiri-Samani, A. R., & Nekoee, N. (2006). Oblique weir equation using incomplete self-similarity. *Canadian Journal of Civil Engineering*, 33(10), 1241-1250.
21. Branco, P., Branco, P., Santos, J. M., Katopodis, C., Pinheiro, A., & Ferreira, M. T. (2013). Pool-type fishways: two different morpho-ecological cyprinid species facing plunging and streaming flows. *PloS one*, 8(5), e65089.
22. Bretón, F., Baki, A. B. M., Link, O., Zhu, D. Z., & Rajaratnam, N. (2013). Flow in nature-like fishway and its relation to fish behaviour. *Canadian Journal of Civil Engineering*, 40(6), 567-573.
23. Buffin-Bélanger, Buffin-Bélanger, T., & Roy, A. G. (2005). 1 min in the life of a river: Selecting the optimal record length for the measurement of turbulence in fluvial boundary layers. *Geomorphology*, 68(1-2), 77-94.
24. Carollo, F. G., Ferro, V., & Pampalone, V. (2011). Experimental investigation of the outflow process over a triangular labyrinth-weir. *Journal of Irrigation and Drainage Engineering*, 138(1), 73-79.
25. Castro-Santos, T., & Haro, A. (2005). Biomechanics and fisheries conservation. *Fish physiology*, 23, 469-523.
26. Cea, L., Puertas, J., & Pena, L. (2007). Velocity measurements on highly turbulent free surface flow using ADV. *Experiments in fluids*, 42(3), 333-348.
27. Clay, C. H. (1961). Design of fishways and other facilities, 15 p.

*28.* Clay, C. H. (1995). Design of Fishways and Other Fish Facilities, Lewis Publish-ers. *Ann Arbor, MI*, 256 p.

29. Coutant, C. C. (1998). *Turbulent attraction flows for juvenile salmonid passage at dams*. Environmental Sciences Division, Oak Ridge National Laboratory, 247 p.

30. Cotel, A. J., Webb, P. W., & Tritico, H. (2006). Do brown trout choose locations with reduced turbulence?. *Transactions of the American Fisheries Society*, 135(3), 610-619.

31. Crookston, B. M., & Tullis, B. P. (2012). Arced labyrinth weirs. *Journal of Hydraulic Engineering*, 138(6), 555-562.

32. Crookston, B. M., & Tullis, B. P. (2011). Discharge efficiency of reservoir-application-specific labyrinth weirs. *Journal of Irrigation and Drainage Engineering*, 138(6), 564-568.

33. Dabling, M. R., & Crookston, B. M. (2012). Staged and notched Labyrinth weir hydraulics, 35 p.

34. Dabling Dabling, M. R., Tullis, B. P., & Crookston, B. M. (2013). Staged labyrinth weir hydraulics. *Journal of Irrigation and Drainage Engineering*, 139(11), 955-960.

35. Decker, L. F. (1967). *Fishways in Maine.* Maine Dept. of Inland Fisheries and Game, 47 p.

36. Doroudian, B., Bagherimiyab, F., & Lemmin, U. (2010). Improving the accuracy of four-receiver acoustic Doppler velocimeter (ADV) measurements in turbulent boundary layer flows. *Limnology and Oceanography: Methods*, 8(11), 575-591.

37. Ead, S. A., Katopodis, C., Sikora, G. J., & Rajaratnam, N. (2004). Flow regimes and structure in pool and weir fishways. *Journal of environmental engineering and science*, 3(5), 379-390.

38. Emin Emiroglu, M., & Baylar, A. (2005). Influence of included angle and sill slope on air entrainment of triangular planform labyrinth weirs. *Journal of hydraulic engineering*, 131(3), 184-189.

39. Enders, E. C., Boisclair, D., & Roy, A. G. (2003). The effect of turbulence on the cost of swimming for juvenile Atlantic salmon (Salmo salar). *Canadian Journal of Fisheries and Aquatic Sciences*, 60(9), 1149-1160.

40. Enders, E. C., Boisclair, D., & Roy, A. G. (2005). A model of total swimming costs in turbulent flow for juvenile Atlantic salmon (Salmo salar). *Canadian Journal of Fisheries and Aquatic Sciences*, 62(5), 1079-1089.

41. Enders, E. C., Castro-Santos, T., & Lacey, R. J. (2017). The effects of horizontally and vertically oriented baffles on flow structure and ascent performance of upstream-migrating fish. *Journal of Ecohydraulics*, 2(1), 38-52.

42. Everest, F. H., & Chapman, D. W. (1972). Habitat selection and spatial interaction by juvenile chinook salmon and steelhead trout in two Idaho streams. *Journal of the Fisheries Board of Canada*, 29(1), 91-100.

43. Falvey, H. T. (2003). *Hydraulic design of labyrinth weirs*. Reston, VA: ASCE Press (American Society of Civil Engineers), 161 p.

44. Fuentes-Pérez, J. F., Sanz-Ronda, F. J., de Azagra, A. M., & García-Vega, A. (2016). Non-uniform hydraulic behavior of pool-weir fishways: A tool to optimize its design and performance. *Ecological engineering*, 86, 5-12.

45. Fuentes-Pérez, J. F., Sanz-Ronda, F. J., Martínez de Azagra Paredes, A., & García-Vega, A. (2014). Modeling water-depth distribution in vertical-slot fishways under uniform and nonuniform scenarios. *Journal of Hydraulic Engineering*, 140(10), 06014016.

46. Gibson, R. J., Haedrich, R. L., & Wernerheim, C. M. (2005). Loss of fish habitat as a consequence of inappropriately constructed stream crossings. *Fisheries*, 30(1), 10-17.
47. Goring, D. G., & Nikora, V. I. (2002). Despiking acoustic Doppler velocimeter data. *Journal of hydraulic engineering*, 128(1), 117-126.
48. Guiny, E., Ervine, D. A., & Armstrong, J. D. (2005). Hydraulic and biological aspects of fish passes for Atlantic salmon. *Journal of Hydraulic Engineering*, 131(7), 542-553.
49. Gupta, S. K., & Singh, V. P. (2013). Discussion of "Experimental studies on flow over labyrinth weir" by BV Khode, AR Tembhurkar, PD Porey, and RN Ingle. *Journal of Irrigation and Drainage Engineering*, 139(12), 1048-1051.
50. Hakim, S. S., & Azimi, A. H. (2017). Hydraulics of submerged triangular weirs and weirs of finite-crest length with upstream and downstream ramps. *Journal of Irrigation and Drainage Engineering*, 143(8), 06017008.
51. Hard, A., & Kynard, B. (1997). Video evaluation of passage efficiency of American shad and sea lamprey in a modified Ice Harbor fishway. *North American Journal of Fisheries Management*, 17(4), 981-987.
52. Haro, A., Castro-Santos, T., Noreika, J., & Odeh, M. (2004). Swimming performance of upstream migrant fish in open-channel flow: a new approach to predicting passage through velocity barriers. *Canadian Journal of Fisheries and Aquatic Sciences*, 61(9), 1590-1601.
53. Hatry, C., Binder, T. R., Thiem, J. D., Hasler, C. T., Smokorowski, K. E., Clarke, K. D., ... & Cooke, S. J. (2013). The status of fishways in Canada: trends identified using the national CanFishPass database. *Reviews in Fish Biology and Fisheries*, 23(3), 271-281.
54. Hay, N., & Taylor, G. (1970). Performance and design of labyrinth weirs. *Journal of the Hydraulics Division*, 96(11), 2337-2357.

55. Hinch, S. G., & Rand, P. S. (2000). Optimal swimming speeds and forward-assisted propulsion: energy-conserving behaviours of upriver-migrating adult salmon. *Canadian Journal of Fisheries and Aquatic Sciences*, 57(12), 2470-2478.

56. Hurther, D., & Lemmin, U. (2001). A correction method for turbulence measurements with a 3D acoustic Doppler velocity profiler. *Journal of Atmospheric and Oceanic Technology*, 18(3), 446-458.

57. Jones, D. R., Kiceniuk, J. W., & Bamford, O. S. (1974). Evaluation of the swimming performance of several fish species from the Mackenzie River. *Journal of the Fisheries Board of Canada*, 31(10), 1641-1647.

58. Kabiri-Samani, A., Ansari, A., & Borghei, S. M. (2010). Hydraulic behaviour of flow over an oblique weir. *Journal of Hydraulic Research*, 48(5), 669-673.

59. Katopodis, C. (1992). Introduction to fishway design, working document. *Freshwater Institute, Central and Arctic Region, Department of Fisheries and Oceans*, 70 p.

60. Khorsandi, B., Mydlarski, L., & Gaskin, S. (2012). Noise in turbulence measurements using acoustic Doppler velocimetry. *Journal of Hydraulic Engineering*, 138(10), 829-838.

61. Kim, J. H. (2001). Hydraulic characteristics by weir type in a pool-weir fishway. *Ecological Engineering*, 16(3), 425-433.

62. Kim, H., Kline, S. J., & Reynolds, W. C. (1971). The production of turbulence near a smooth wall in a turbulent boundary layer. *Journal of Fluid Mechanics*, 50(1), 133-160.

63. Kline, S. J., Reynolds, W. C., Schraub, F. A., & Runstadler, P. W. (1967). The structure of turbulent boundary layers. *Journal of Fluid Mechanics*, 30(4), 741-773.

64. Kumar, S., Ahmad, Z., & Mansoor, T. (2011). A new approach to improve the discharging capacity of sharp-crested triangular plan form weirs. *Flow Measurement and Instrumentation*, 22(3), 175-180.

65. Katopodis, C., & Rajaratnam, N. (1983). A review and laboratory study of the hydraulics of Denil fishways, 181 p.

66. Katopodis, C., Kells, J. A., & Acharya, M. (2001). Nature-like and conventional fishways: alternative concepts?. *Canadian Water Resources Journal*, 26(2), 211-232.

67. Katopodis, C. (2005). Developing a toolkit for fish passage, ecological flow management and fish habitat works. *Journal of Hydraulic Research*, 43(5), 451-467.

68. Katopodis, C., & Gervais, R. (2012). Ecohydraulic analysis of fish fatigue data. *River Research and Applications*, 28(4), 444-456.

69. Kupferschmidt, C., & Zhu, D. Z. (2017). Physical modelling of pool and weir fishways with rock weirs. *River Research and Applications*, 33(7), 1130-1142.

70. Lacey, R. J., Neary, V. S., Liao, J. C., Enders, E. C., & Tritico, H. M. (2012). The IPOS framework: linking fish swimming performance in altered flows from laboratory experiments to rivers. *River Research and Applications*, 28(4), 429-443.

71. Lacey, R. J., & Rennie, C. D. (2011). Laboratory investigation of turbulent flow structure around a bed-mounted cube at multiple flow stages. *Journal of Hydraulic Engineering*, 138(1), 71-84.

72. Larinier, M. (1992). Passes à bassins successifs, prébarrages et rivières artificielles. *Bulletin Français de la Pêche et de la Pisciculture*, (326-327), 45-72.

73. Larinier, M. (2002). Biological factors to be taken into account in the design of fishways, the concept of obstructions to upstream migration. *Bulletin Français de la Pêche et de la Pisciculture*, (364), 28-38.

74. Larinier, M., & Marmulla, G. (2004). Fish passes: types, principles and geographical distribution–an overview. *In Proceedings of the second international symposium on the management of large rivers for fisheries* (Vol. 2, pp. 183-206). RAP Publication.

75. Liao, J. C., Beal, D. N., Lauder, G. V., & Triantafyllou, M. S. (2003). Fish exploiting vortices decrease muscle activity. *Science*, 302(5650), 1566-1569.

76. Liu, M., Rajaratnam, N., & Zhu, D. Z. (2006). Mean flow and turbulence structure in vertical slot fishways. *Journal of Hydraulic Engineering*, 132(8), 765-777.

77. Lux III, F. (1984). Discharge characteristics of labyrinth weirs. *In Water for Resource Development* (pp. 385-389). ASCE.

78. McKinnon, G. A., & Hnytka, F. N. (1985). Fish passage assessment of culverts constructed to simulate stream conditions on Liard River tributaries, 121 p.

79. Morantz, D. L., Sweeney, R. K., Shirvell, C. S., & Longard, D. A. (1987). Selection of microhabitat in summer by juvenile Atlantic salmon (Salmo salar). *Canadian Journal of Fisheries and Aquatic Sciences*, 44(1), 120-129.

80. Nilsson, C., Reidy, C. A., Dynesius, M., & Revenga, C. (2005). Fragmentation and flow regulation of the world's large river systems. *Science*, 308(5720), 405-408.

81. Odeh, M., Noreika, J. F., Haro, A., Maynard, A., Castro-Santos, T., & Cada, G. F. (2002). Evaluation of the effects of turbulence on the behavior of migratory fish. *Final Report to the Bonneville Power Administration, Contract*, 22.

82. Parsheh, M., Sotiropoulos, F., & Porté-Agel, F. (2010). Estimation of power spectra of acoustic-doppler velocimetry data contaminated with intermittent spikes. *Journal of Hydraulic Engineering*, 136(6), 368-378.

83. Paxson, G., & Savage, B. (2006). Labyrinth spillways: comparison of two popular USA design methods and consideration of non-standard approach conditions and geometries. *In International Junior Researcher and Engineer Workshop on Hydraulic Structures, Report CH61/06, Brisbane, Australia.*

84. Paxson, G., Campbell, D., & Monroe, J. (2011). Evolving design approaches and considerations for labyrinth spillways. *In USSD Conference* (pp. 1645-1666).

85. Porcher, J. P., & Travade, F. (2002). Fishways: biological basis, limits and legal considerations. *Bulletin Français de la Pêche et de la Pisciculture*, (364), 9-20.

86. Quaresma, A. L., Ferreira, R. M., & Pinheiro, A. N. (2017). Comparative analysis of particle image velocimetry and acoustic doppler velocimetry in relation to a pool-type fishway flow. *Journal of Hydraulic Research*, 55(4), 582-591.

87. Rajaratnam, N., Van der Vinne, G., & Katopodis, C. (1986). Hydraulics of vertical slot fishways. *Journal of Hydraulic Engineering*, 112(10), 909-927.

88. Rajaratnam, N., Katopodis, C., & Mainali, A. (1988). Plunging and streaming flows in pool and weir fishways. *Journal of Hydraulic Engineering*, 114(8), 939-944.

89. Rajaratnam, N., Katopodis, C., & Fairbairn, M. A. (1990). Hydraulics of culvert fishways V: Alberta fish weirs and baffles. *Canadian Journal of Civil Engineering*, 17(6), 1015-1021.

90. Rajaratnam, N., Katopodis, C., & Solanki, S. (1992). New designs for vertical slot fishways. *Canadian Journal of Civil Engineering*, 19(3), 402-414.

91. Sanz-Ronda, F. J., Ruiz-Legazpi, J., Bravo-Córdoba, F. J., Makrakis, S., & Castro-Santos, T. (2015). Sprinting performance of two Iberian fish: Luciobarbus bocagei and Pseudochondrostoma duriense in an open channel flume. *Ecological Engineering*, 83, 61-70.

92. Sanz-Ronda, F. J., Bravo-Córdoba, F. J., Ruiz-Legazpi, J., & Fuentes-Pérez, J. F. (2015). The most evaluated fishway in Spain: a new lesson every year. In Fish Passage 2015. *Internationl Conference on River Connectivity Best Practices and Innovations. Groningen, The Netherlands* (pp. 146-147).

93. Silva, A. T., Santos, J. M., Franco, A. C., Ferreira, M. T., & Pinheiro, A. N. (2009). Selection of Iberian barbel Barbus bocagei (Steindachner, 1864) for orifices and notches upon different hydraulic configurations in an experimental pool-type fishway. *Journal of Applied Ichthyology*, 25(2), 173-177.

94. Silva, A. T., Santos, J. M., Ferreira, M. T., Pinheiro, A. N., & Katopodis, C. (2011). Effects of water velocity and turbulence on the behaviour of Iberian barbel (Luciobarbus bocagei, Steindachner 1864) in an experimental pool-type fishway. *River Research and Applications*, 27(3), 360-373.

95. Silva, A. T., Santos, J. M., Ferreira, M. T., Pinheiro, A. N., & Katopodis, C. (2012). Passage efficiency of offset and straight orifices for upstream movements of Iberian barbel in a pool-type fishway. *River Research and Applications*, 28(5), 529-542.

96. Sitompul, A. T. (1993). *Hydraulic modelling of a sharp crested labyrinth weir* (Doctoral dissertation, Memorial University of Newfoundland), 214 p.

97. Smith, D. L., Brannon, E. L., Shafii, B., & Odeh, M. (2006). Use of the average and fluctuating velocity components for estimation of volitional rainbow trout density. *Transactions of the American Fisheries Society*, 135(2), 431-441.

98. Stuart, I. G., Zampatti, B. P., & Baumgartner, L. J. (2008). Can a low-gradient vertical-slot fishway provide passage for a lowland river fish community?. *Marine and Freshwater Research*, 59(4), 332-346.

99. Tingey, S. E. (2011). *Discharge characteristics of oblique weirs*. Utah State University.

100. Triantafyllou, M. S., Triantafyllou, G. S., & Yue, D. K. P. (2000). Hydrodynamics of fishlike swimming. *Annual review of fluid mechanics*, 32(1), 33-53.

101. Tritico, H. M., & Cotel, A. J. (2010). The effects of turbulent eddies on the stability and critical swimming speed of creek chub (Semotilus atromaculatus). *Journal of Experimental Biology*, 213(13), 2284-2293.

102. Tullis, J. P., Amanian, N., & Waldron, D. (1995). Design of labyrinth spillways. *Journal of hydraulic engineering*, 121(3), 247-255.

103. Tullis, B. P., Young, J. C., & Chandler, M. A. (2007). Head-discharge relationships for submerged labyrinth weirs. *Journal of Hydraulic Engineering*, 133(3), 248-254.

104. Villemonte, J. R. (1947). Submerged weir discharge studies. *Engineering news record*, 866, 54-57.

105. Wahl, T. L. (2000). Analyzing ADV data using WinADV. *In Building partnerships* (pp. 1-10).

106. Welch, P. (1967). The use of fast Fourier transform for the estimation of power spectra: a method based on time averaging over short, modified periodograms. *IEEE Transactions on audio and electroacoustics*, 15(2), 70-73.

107. Wormleaton, Wormleaton, P. R., & Soufiani, E. (1998). Aeration performance of triangular planform labyrinth weirs. *Journal of environmental engineering*, 124(8), 709-719.

108. Wu, S., & Rajaratnam, N. (1996). Submerged flow regimes of rectangular sharp-crested weirs. *Journal of Hydraulic Engineering*, 122(7), 412-414.

109. Wu, S., Rajaratnam, N., & Katopodis, C. (1999). Structure of flow in vertical slot fishway. *Journal of Hydraulic Engineering*, 125(4), 351-360.

110. Yagci, O. (2010). Hydraulic aspects of pool-weir fishways as ecologically friendly water structure. *Ecological Engineering*, 36(1), 36-46.